AN APPROACH FOR THE DEVELOPMENT AND VALIDATION OF PHYSICALLY-BASED MODELS FOR RAINFALL-INDUCED SHALLOW LANDSLIDES AND THEIR APPLICATION TO UNDERSTAND KEY INITIATION MECHANISMS

Brunella Balzano

Thesis submitted to the Department of Civil and Environmental Engineering, University of Strathclyde, Glasgow, in fulfilment of the requirements for the degree of

Doctor of Philosophy

in

Civil and Environmental Engineering

June 2018,

Glasgow, UK

Declaration of authenticity and author’s right

This thesis is the result of the author’s original research. It has been composed by the author and has not been previously submitted for examination which has led to the award of a degree.

Signed:

Date: June 2018

To Alessia and Gea, my adventure companions.

To Gianfranco and Sasha, the younger and the older brother.

A mia madre a mio padre, i modelli.

ACKNOWLEDGEMENTS

This Thesis has been one of the hardest and most satisfying experiences of my life. I could have never made it through this trip if it was not for the help of great people who I was lucky enough to meet.

I wish to thank my supervisor, Professor Alessandro Tarantino, for giving me the chance to discover the amazing world of the Research. Thank you for the patience, the advices and for being present always.

I wish to thank the Department of Civil Engineering of Strathclyde University for giving a “home” where to pursue my research. Thank you to all the staff for the support.

I wish to thank my family who has always supported me and my decisions even and especially when they turned out to be wrong. Thank you, mum and dad for teaching me the hardest of the lessons, life. You are and always be my inspiration and my model. Thank you Gianfri, for being the best brother ever, for listening and advising.

I wish to thank the two people who were capable to make this trip as nice as a walk on a beach at the sunset: Alessia and Gea. To you, who are the only two people who I wanted to share my mind and my soul with. To you who were always next to me laughing, crying and arguing. Thank you for being my best friends and my family. Sharing this experience with you was the best gift a person could ask for. Thank you girls.

Thanks to all my amazing friends in Glasgow. Thank you to Carolina and Elena, for being so special. Thank you for bringing a whole new set of sounds’ frequencies into my life with your “not-so-quiet” tones.

Thank you, Riccardo for being the best supportive, my “alter-ego”, easy-going friend. I have never been so happy to argue with a person like I do with you.

Thank you, Sara for boosting the artistic side of me. Thank you for tall the evenings spent together, watching movies, playing games, drawing or simply chatting.

Thank you Michela, Livia and Silvia for the for being the best sport mates ever. Thank you for never letting me win. Thank you for the “breaks” from the PhD life. The whole trip was much lighter with you all.

Thank you Matteo, for being the “wise” friend and for sharing your experience and advising me when I was lost.

Thank you Andrea, one of the first people I met during this Scottish adventure. Thank you for making me feel at home always. Thank you for all the amazing weekends spent together. Thank you for being the wonderful friend you are.

Thank you all, guys for being the amazing people you are. Thank you for deciding to come to the “cold” Glasgow, which for me was not so cold after all, just because I met all of you. I couldn’t ask for better mates for this trip. Thank you for being my family.

Thank you, Hilde, for being the best friend ever, for never letting me go. Thank you for being there for so long and have saved the same enthusiasm you had when I first met you.

Thank you to Chiara and Milly the life-long friends. We lasted more than many weddings do, and still I love you like the first time.

Thank you Jareth, for being my partner and my friend. Thank you for being the wonderful person you are and thank you for coming into my life. Thank you for supporting my crazy dreams, and helping me in pursuing them. You have made me the happiest woman, and I promise I’ll work hard everyday “trying to make you feel the same way”. I love you so much.

Finally, I‘d like to thank myself. It was hard, very. Many have been the times in these years

I thought I was not the right person, I didn’t have the right attitude, I would have never made it. In the end I proved myself wrong. I am the right person, I have the right attitude and I made it. I was strong enough to not quit, I was wise enough to use my errors to learn and not be overwhelmed by them.

Hence a big thank you to all the mistakes I made, because they turned to be the best book of learning.

Brunella

ABSTRACT

Rainfall-induced shallow landslides are one of the major natural hazards and have a significant impact on society and economy. The areas affected by this phenomenon are often very extended and unfortunately, sometimes, crossing human activities. Hence, the hazard to people and infrastructures might be significantly high.

Landslides initiate with the failure of sloping earth materials which happens when forces or stresses overcome the strength of the soil cover. Shallow landslides usually involve the first few meters of soils and are mainly characterized by a translational movement on a failure surface parallel to the undisturbed ground.

One of the main landslides triggering factors is heavy and/or prolonged rainfall events. As rainwater infiltrates into the slope, the pore-water pressure increases resulting in a decrease of the shear strength of the soil eventually triggering the slope instability.

The destructiveness of rainfall-induced shallow landslides may increase when, in adverse weather conditions, rainwater may saturate the soil leading to a flow slides or debris flow. Flow slides and/or debris flow are characterized by a fluid mass of a mixture of soil and fragments of rocks, flowing down the slope at very high velocities.

Landslides risk is defined as the likelihood of a slope failure to happen and adversely impact the society. It is the result of the combination between the hazard, i.e. the likelihood of landslide occurrence, and vulnerability, i.e. the degree of loss of one or more elements at risk, resulting from the landslides occurrence. Risk, hazard and vulnerability are human concepts. Indeed, they can be only applied in those instances where human beings and goods could be adversely impacted by the landslides. The landslides risk assessment consists of a series of

procedures aiming to quantify the possible consequences related to the landslides phenomena, to assess their probability of occurrence and, finally, what can be done to mitigate them. The first step of a landslides risk assessment consists of the evaluation of the hazard.

Landslide hazard can be quantified using several approaches. A well-known method is the use of hazard maps, also known as landslides potential or susceptibility maps. They are built by combining the study of past landslides events and the identification of controlling factors over the territory, i.e. slope inclinations, soil profiles, past landslides. They divide a region into zones reflecting the intensity of landslide hazard. The hazard zones are usually classified into at least four categories, for example high, moderate, low and no susceptibility. Landslide hazard maps are a very useful tool for the development planning. Their potential to illustrate regional area with different level of potential landslides hazard may help decisions about the appropriate land-use, building regulation and engineering practice.

Landslide hazard maps, together with information on existing or expected vulnerability, can be used to estimate the risk associated with critical facilities like road and rail networks, hospitals, or water pipelines. Such information may be used to make decisions regarding the 'acceptable risk' for one or more facilities, the need for relocation or the application of appropriate remedial measures.

However, landslide hazard maps are not able to predict when or exactly where landslides will occur during a specific triggering event. They don't take into account the physics related to the phenomenon. Moreover, they are implicitly based on the assumptions that geomorphological and meteorological conditions causing failure in the past will not change in the future. This assumption may not hold for the case where climate pattern is expected to change.

Another class of approaches aiming to quantify the landslides hazard are based on the use of physically-based models. They mainly attempt to extend spatially the slope stability theories. Physically-based models can potentially estimate the rainfall event which is likely to trigger slope failures, the location and the time of occurrence of the event. They usually combine a mechanical model for landslide initiation and a hydraulic model for rainwater infiltration.

However, physically-based models require detail spatial information about the hydrological and mechanical properties of the soils and about the morphology of the slopes. Furthermore, physically-based models are calibrated using rainfall events registered at the time and the location of the landslides event. This information might not be always available and it can be expensive to obtain.

When Hazard assessment is combined with vulnerability assessment, i.e. the assessment of losses that may be incurred through the impact of landslides hazards on vulnerable elements, it is hence possible to assess the risk. The last step of the risk assessment procedure consists in design procedures and methodologies with the aim of reducing the risk associated with rainfall-induced shallow landslides. The risk can be mitigated by either reducing the hazard or the vulnerability.

The hazard can be mitigated by acting on those factors which make the slopes susceptible to fail and/or enhancing mechanisms which would lead the slope to remain stable. With this aim, vegetation is often seen as one of the few practicable solutions to mitigate landslide hazard at the catchment scale. It’s well established in literature how the vegetation may positively contribute to the slope stability by reinforcing the slope thanks to the anchoring of the root systems. It is also well known how plants can give a hydrological contribution too, by promoting low pore water pressures via the transpiration process. However, there is an other hydrological effect which the plants are responsible for and it consists in the rhizosphere hydrological contribution. The rhizosphere may have beneficial effects on slope stability by preventing downward rainwater infiltration. Indeed, the rhizosphere acts as a natural lateral drainage. In turn, this implies that shallow landslide hazard can be potentially mitigated by promoting plants with root-system architecture that enhances lateral subsurface flow as a remedial measure.

The vulnerability of landslides affected area can be mitigated via early-warning systems. They are usually based on threshold values of rainfall, which is the most ‘accessible’ and frequently used as landslide precursors. Empirical rainfall thresholds are defined through the study of rainfall events registered at the occurrence of landslides phenomena.

The thresholds curves are usually obtained by drawing lower-bound lines to the rainfall conditions that resulted in landslides plotted in Cartesian, semilogarithmic, or logarithmic coordinates. They usually build correlation between either the intensity and duration of the rain event registered at the slope failure or between the cumulated rain in the period antecedent the day of the landslides and the daily event at the failure.

For a reliable early warning system, a significant amount of data on past failure is needed. Threshold curves are usually defined as a lower bound of the registered critical rainfalls. Unfortunately, this approach often leads to over-conservative thresholds, resulting in false alerts and therefore a malfunctioning of the early warning system.

This thesis work proposes a methodology for the study of rainfall-induced shallow landslides, with the aim to gain a deep understanding of the processes related to their triggering mechanisms and provide a reliable tool to improve the landslides risk assessment procedures.

List of Journal Papers:

‘Building physically-based model for rainfall-induced shallow landslide from geological survey and geotechnical investigation: the case study of the Sorrento Peninsula (Italy)’, *B. Balzano, A. Tarantino, M. V. Nicotera, G. Forte, M. de Falco, A. Santo* – Submitted for publication to Canadian Geotechnical Journal (under review).

‘The hydraulic control of the rhizosphere on rainfall-induced shallow landslides: the lesson learned from a case study in Scotland.’, *B. Balzano, A. Tarantino* – To be submitted to Landslides.

‘Criteria to identify rainfall thresholds for the triggering of rainfall-induced shallow landslides’, *B. Balzano, A. Tarantino, M.V. Nicotera* – To be submitted to Canadian Geotechnical Journal.

TABLE OF CONTENTS

1 BACKGROUND

1.1 LITERATURE REVIEW

1.1.1 Landslides Hazard

Landslides are considered one of the most common agents sculpting the earth’s surface. They are very frequent in mountainous contexts all over the world and they play an important role in moving earth materials from uplands to the rivers.

The general term “landslides” is used to describe a wide range of gravity-driven mass movements (Lu et al., 2013). They can include several slope movements from rock fall to debris flows. Landslides are caused by the failure of sloping earth materials and happen when forces or stresses overcome the strength of the soil cover. The destructiveness or hazard associated with landslides is proportional to their velocity (Lu et al., 2013).

The great danger associated with the landslides is related to the fact that they may unpredictably evolve in even more catastrophic phenomena. Indeed, in adverse weather conditions, a simple translational slope failure may dangerously evolve into a debris flow. This phenomenon usually occurs in heavy rain conditions, as the rainwater may completely saturate the slope material. Consequently, a fluid mass of a mixture of soil and fragments of rocks may start flowing down the slope at very high speed (sometimes it can reach more than 10m/s).

One of the most common landslides (or debris flow) triggering factors is heavy precipitation, either rainfall or melting snow. Prolonged rainfall events can generate landslide over broad geographic areas, often causing tremendous loss of life and property. Rainfall-induced landslides are typically shallow, mainly characterized by translational slope failures. They may occur wholly or partly in the unsaturated zone and may dominate mass movement processes in hillslope environments (Campbell, 1975; Wilson, 1989).

Rainfall-induced landslides are classified as one of the major natural hazards and account for significant economic and social disasters. The evaluation of spatial and temporal landslide risk is key to developing mitigation measures. The risk related to landslides can be seen as the combination of hazard, i.e. the likelihood of landslide occurrence, and vulnerability, i.e. the consequences in terms of expected number of lives lost, persons injured, damage to property, and disruption of economic activity (Varnes, 1984).

1.1.2 Empirical approaches for the landslides hazard evaluation

Landslide hazard can be quantified using empirical approaches. Some of them are based on the correlation of historical records of landslide occurrence with predisposition factors. This approach may lead to the building of susceptibility maps. Those maps are usually the result of an overlapping of more maps, each of one is related to a factor considered influent in making a slope keen to landslide. According to the literature, those factors are mainly related to the geometry of the basin. They are usually assessed after a statistical analysis over a wide range of past case studies. Wang et al. (2009) studied the case of landslides in GuiZhou, south-west China; in this study, slope, lithology, landslide inventory, tectonic activity, drainage distribution and annual precipitation were taken as independent causal factors. They were used to build several casual factors maps and then combine them together in a general susceptibility map. Di Crescenzo et al. (2008) used this approach to evaluate the flow-slides susceptibility in the Campania region, in Southern Italy.

Another empirical approach often used to assess the rainfall-induced landslides hazard is by determining the rainfall thresholds. A threshold is the minimum or maximum level of some quantity needed for a process to take place or a state to change (White et al., 1996). For rainfall-induced landslides a threshold may define the rainfall events that, when reached or exceeded, are likely to trigger landslides (Guzzetti et al., 2007).

Rainfall thresholds are defined through the study of rainfall events registered at the occurrence of landslides phenomena. In order to obtain a reliable study, a large data-set of historical landslides. The thresholds curves are usually obtained by drawing lower-bound lines to the rainfall conditions that resulted in landslides plotted in Cartesian, semilogarithmic, or logarithmic coordinates (Guzzetti et al., 2007).

Threshold curves aim to separate the rainfall condition that resulted in slope instability from the ones that didn’t trigger any. A key factor in the construction of a reliable empirical model to forecast the possible occurrence of rainfall-induced landslides is the definition of the intensity of the rainfall. Rainfall intensity can be defined as the amount of precipitation cumulated over a period of time. If the length of the observation period is relatively short, the rainfall intensity may represent an “instantaneous” measure of the rainfall rate, or an average value over the observation period (i.e. hourly intensity, daily intensity). For longer periods, rainfall intensity represents an ‘‘average’’ value over the observation time-frame. This may result in underestimating the peak (maximum) rainfall rate occurred during the observation period.

Based on the considered rainfall measurements, thresholds curves can link the measurements of the event and the antecedent rainfall to the landslides or the intensity and the duration of the event which triggered the landslide phenomenon.

Within the Intensity Duration (ID) approach (IRPI, 2008) rainfall intensity is plotted against rainfall duration. ID thresholding generally has the form, $I = c + \alpha D^{\beta}$, where I is rainfall intensity, D is rainfall duration, and $c>0$, $\alpha>0$, $\beta>0$ are parameters. Although this approach has been widely used both at regional and local scale, there are some limitations that should be taken into account. A first limit is related to the fact that ID thresholds defined for a specific region or area cannot be easily exported to neighbouring regions or similar areas (Crosta, 1989). Moreover, ID thresholds do not take into account morphological and lithological differences and climate variability.

With the antecedent rainfall approach, on the other hand, the threshold is obtained with the correlation between the amount of antecedent precipitation prior the landslides occurrence and the rainfall intensity registered in the day of the event. Antecedent precipitation influences groundwater levels and soil moisture and can be used to determine when landslides are likely to occur (Guzzetti et al., 2007). The main difficulty related to this approach consist in the definition of the antecedent period. Several authors experienced that the amount of daily rainfall needed to trigger landslides decreased when a longer period is considered to evaluate the antecedent rainfall. De Vita (2000) used antecedent periods from 1 to 59 days. Pasuto et al. (1998) tested rainfall periods from 1 to 120 days and found best correlation with landslide occurrence for the 15-day antecedent rainfall. Cardinali et al. (2006) found a correlation between landslide occurrence and the 3-month and the 4-month antecedent rainfall. The large variability can depend on several factors such as morphology, vegetation, climatic regimes and so on. On the other hand, there are also authors who didn’t find any correlation between the critical and the cumulative rainfall and the occurrence of landslide (Aleotti, 2004; Brand et al., 1984). Corominas (2000) and Corominas et al. (1999), observed that slopes exhibiting large macropores were likely to show instability without any significant antecedent rainfall.

1.1.2.1 Discussion

Generally, empirical approaches are implicitly based on the assumptions that geomorphological and meteorological conditions causing failure in the past will not change in the future. This assumption may not hold for the case where climate pattern is expected to change. It has been widely recognized by the academic world that global precipitation patterns are being moved in new directions by climate change. Climate models predict that the addition of heat-trapping gases in the atmosphere will shift precipitation. They expect a strengthening of existing precipitation patterns. Warmer air traps more water vapour, and scientists expect that additional water to fall in already wet parts of the Earth.

Furthermore, empirical models tend to neglect the theoretical laws governing the hydrological processes within the slopes. This may lead to some critical factors to be missed, which could be instead captured by physically-based models for the landslide mechanism. A physically based landslide model considers the physical mechanisms influencing slope instability using a range of topographic, geologic, geotechnical, and hydrological parameters.

1.1.3 Physically-based models for the landslides hazard evaluation

Physically-based models attempt to extend spatially the slope stability theories (i.e., the infinite slope method) widely adopted in geotechnical engineering. To link rainfall pattern and its history to slope stability/instability conditions, physically-based models incorporate infiltration models as well.

Several approaches have been developed to quantify landslide hazard at the temporal and spatial scale based on physically-based models. They usually combine a mechanical model for landslide initiation and a hydraulic model for rainwater infiltration.

The 1-D infinite slope is commonly adopted for the mechanical modelling of the slope failure. This consists in assuming the slopes to be indefinitely wide and considering a translation along the sliding surface as failure mechanism. A factor of safety is determined by relating the destabilizing forces and the resistance of the soil. To define the factor of safety of an infinite unsaturated slope, it is first necessary to introduce an equation for the shear strength of the soil.

A common equation used to define the shear strength in the unsaturated range is the following, suggested by Nicotera et al. (2015):

$$\tau = c' + (\sigma + s \cdot S_r) \cdot tan\phi'$$

where c' is the cohesion, σ is the normal total stress, s is the suction, S_r is the degree of saturation, and ϕ' is the friction angle.

The water flow within the slope can be modelled via the Richards’ equation (Richards, 1931). This is a general 3D partial differential equation describing water movement in unsaturated soils. It is derived by combining the Darcy’s law extended to the case of unsaturated soils and the mass balance equation of liquid water. The full Richards’ equation can be written as follows

$$C\frac{\partial \Psi}{\partial t} = div[Kgrad(\Psi)]$$

where Ψ= piezometric head; K = hydraulic conductivity; $C = (\partial\theta/\partial\Psi)$, referred to as water capacity of the soil and where θ is the volumetric water content (function of Ψ). The hydraulic conductivity K depends on the degree of saturation, which in turn depends on pore water pressure. In the original 3D form of Richards’ equation, the hydraulic conductivity K should be considered as a vector and characterized by three components along the three flow directions [Kx Ky Kz]. However, it is a common practice to assume the soil as an isotropic material, hence the following assumption can be made:

$K_x=K_y=K_z=K$

Depending on the cases, Richards’ equation can be simplified in its 1D or 2D form. However, Richards’ equation does not have a closed-form analytical solution, hence the problem has to be solved numerically.

Various approaches are considered to model rainwater infiltration and lateral flow. In principle, a full 3-D water flow numerical model (based on either finite difference or finite element methods) should be implemented at the catchment scale. However, this would involve a prohibitive computational burden and for this reason, many of the models in literature have introduced some simplifications.

Montgomery and Dietrich (1994) developed The Shallow Landslide Stability Model (SHALSTAB), a digital terrain model which aims to map the pattern of potential shallow slope instability. The model is a deterministic and distributed model based on a combination of infinite slope and steady-state hydrological models and relies on the concept that typically the boundary between the soil and the underlying bedrock is abrupt. SHALSTAB is integrated into a GIS (ArcView 3.2) through which the upslope drainage area, elevation and slope values are calculated by using a digital elevation model (DEM), and these values are assigned to each pixel.

A very similar model is the SHIA_Landslides developed by Aristizabal et al. (2015). The model is supported by geotechnical and hydrological features occurring on a basin scale in tropical and mountainous terrains. SHIA_Landslides incorporates a distributed hydrological tank model that includes water storage in the soil coupled with a classical analysis of infinite slope stability under saturated conditions.

Baum, et al. (2002) developed the Transient Rainfall Infiltration and Grid-Based Regional

Slope-Stability Model (TRIGRS), a Fortran program designed for modelling the timing and distribution of shallow, rainfall-induced landslides. The software performs a time- dependent analysis, showing the changing in pore water pressure and consequently the Factor of Safety due to rainwater infiltration. The program adopts a one-dimensional vertical flow in isotropic, homogeneous materials for either saturated or unsaturated conditions. Unfortunately, the model seems to be very sensitive to the initial conditions. Therefore, the model’s results may be questionable where the initial water table depth is poorly estimated.

GEOtop, first developed by Rigon et al. (1997), considers a 3-D water flow model by uncoupling lateral from vertical flow. It is a terrain-based model; it simulates the fluxes and budgets of energy and water on a landscape defined by three-dimensional grid boxes, whose surfaces come from a digital elevation model (DEM) and whose lower boundaries are located at some specified spatially varying depth. GEOtop was later coupled with an infinite slope mechanical model, giving birth to the version GEOtop-FS, which simulates the probability of occurrence of shallow landslides and debris flows. Although the extreme precision achieved by this model, it is still a very computationally expensive. Nonetheless, the model seems to be quite sensible from the chosen DEM. The DEM, indeed, influences directly the precision of the discretization of the domains. Like many other examples in literature, GEOtop results are affected by the choice of the initial condition, which should be derived by an appropriate calibration.

Many authors use as rule of thumb for the initial soil moisture distribution, an equilibrium condition which implies hydrostatic distribution of pressure in both the vadose and saturated zones. This implies that an initial position of the water table must be guessed. The initial condition has a considerable influence on the numerical results, i.e. the slope may or may not experience failure in the numerical simulation. A good approach would be to assume an arbitrary initial condition and perform an analysis sufficiently long to cancel it. Nonetheless, this may be also a way to validate the hydrological model. One would expect that a hydrological balance is accomplished over a relatively long period. If the hydraulic model had not been set properly, it would occur that the slope could become either oversaturated or entirely dry over a relatively long period of time.

1.1.3.1 Discussion

Physically-based models can potentially estimate the rainfall event which is likely to trigger slope failures, the location and the time of occurrence of the event. However, there are limitations related to this methodology too. Physically-based models require detailed spatial information about the hydrological and mechanical properties of the soils and about the morphology of the slopes. Furthermore, physically-based models are calibrated using rainfall events registered at the time and the location of the landslides event. This information might not be always available and it can be expensive to obtain.

1.1.4 The role of the rhizosphere in slope hydrology and stability

It is widely recognized how vegetation can influence landslide occurrence. Plants can significantly enhance slope stability by reinforcing the soil due to root anchoring effects and/or increasing its shear strength via the particle bonding associated with root exudates and microbiological activity. Plant roots can help stabilizing slopes by anchoring a weak soil mass to fractures in bedrock, by crossing zones of weakness to more stable soil, and by providing long fibrous binders within a weak soil mass. In deep soil, anchoring to bedrock becomes negligible and the other two conditions predominate (Noroozi et al., 2015).

On the other hand, vegetation can also significantly affect soil moisture, promoting soil water extraction via the transpiration process (soil water is driven from the soil through the plant to the atmosphere). This mechanism helps keeping the soil in an unsaturated state thus enhancing the shear strength of the slopes. There is indeed a third behaviour that can affect the hydrology of the hillslope. The root system can promote subsurface lateral flow in the top horizon of the hillslope: the rhizosphere.

In 1904 the German agronomist Lorentz Hiltner first coined the term “rhizosphere” to describe the area around the plant root that is inhabited by a unique population of microorganisms influenced by chemicals released from plant roots. In the years since, the definition of the rhizosphere has been revised and refined. Many authors seem to agree with the idea that the rhizosphere is a region with a not clearly defined size or shape but, instead, consists of a gradient in chemical, biological and physical properties which changes along the root (McNear, 2013).

The spatial extension of the rhizosphere is closely related to the root system architecture. The root system of plants is a branched network and its architecture is highly influenced by changing climatic and biological condition. The root system grows solely through reiteration and elongation of root organs (Malamy, 2005). During the primary growth stage, fine roots grow in length, then, gradually, in diameter to facilitate their penetration through soil material.

Water availability is known to impact root physiology and growth (Bao et al., 2014). There is evidence that plants can “sense” the presence of water and nutrients in the soil around them; therefore, they tend to grow towards and/or within the areas where the nutrients are. During this process, soil particles may reorganize around the root surface. For this reason, the structure of the rhizosphere is substantially different from the one of rootless soils.

Together with other natural agents (i.e. presence of worm, insects and other animals, freeze–thaw and wetting–drying cycles, erosion), roots activity is responsible of the typically high porosity and the sponge-like aspect of the rhizosphere. In particular, all these activities promote the formation of a network of interconnected macropores. A macropore is a large pore, cavity, passageway, channel, tunnel, or void in the soil, through which water usually drains freely (Aubertin, 1971). They can show different shape, depending on the process responsible of their formation: from planar slits (cracks or fissures) through voids of irregular cross section (vughs), to cylindrical pipes.

Many authors studied the nature of the macropores in rooted soils and observed their capability to provide pathways or conduits for the rapid movement of free water into and through the soil profile.

Noguchi et al. (1997) highlighted the similarity between the direction of subsurface flow and the direction of root growth in the upper layers. Indeed, the root system can alter subsurface flow. Plant roots, alive or dead, can promote slope drainage by functioning as hillslope-scale preferential flow paths that drain subsurface water away from potentially unstable sites (Ghestem et al., 2011). This hydrological mechanism may help to ‘preserve’ low pore-water pressures in potentially unstable layers thus reducing the susceptibility of slopes to landsliding.

Aubertin (1971) conducted an intense site campaign, observing the significant difference in terms of hydraulic conductivity between the rhizosphere and the deeper horizons. Therefore, when rainwater falls in the rhizosphere, is prevented from vertical infiltration. Because of the high hydraulic conductivity of the rhizosphere, the water is instead driven horizontally, promoting lower pore water pressures in the weaker deep horizons. Of course, this mechanism is particularly dependent on the nature of the vegetation present on the slope (Ghestem et al., 2011), and on the type of root architecture. Plants exhibit many different forms and structures and, indeed, some root orientations may be more efficient than others. Some systems may be oriented in such a way to facilitate the water drainage along the slope. On the other hand, there could be scenarios, like the case of large root extremities, which are more likely to promote accumulation of water in the deeper horizons. There are also some roots systems, of which effects are still unclear, as for the case of tuft root system, typical of herbs species (Ghestem et al., 2011).

Topography plays also a role with regards to subsurface water movement, roots growth and therefore slope stability. For example, concave slopes tend to converge the water flow. Some studies showed that in the gullies, roots are more uniformly distributed in the column of soil, while in convex slopes they are concentrated on the upper horizons.

It is evident how all these elements bring the structure of the soil to show a considerable heterogeneity, especially with regards to the hydraulic conductivity, between the top and sub soils. These variations in hydraulic conductivity can influence the hydraulic gradients and seepage forces (Reid et al., 1992), the surficial pattern of recharge and discharge areas, and the quantities of discharge (Freeze et al., 1979).

1.1.4.1 Discussion

The ability of the root system to create preferential flow paths and, thus, promote water discharge, is a key factor when it comes to study the rainfall-induced landslides phenomenon and its mitigation.

Environmental considerations have increasingly become an important factor in the choice of suitable remedial measures (Popescu, 2015). For this reason, the use of vegetation is a more and more frequent solution for the stabilization of the slopes. Its capacity to offer a ‘diffuse’ mitigation and for its environmental friendly aspect, makes the vegetation one of the few practicable solutions to mitigate the landslides risk.

Any reliable design of a mitigation measure cannot be done without a comprehensive understanding of the mechanisms involved. This is why more studies with the aim of better understanding the preferential flow processes should be promoted.

1.2 OBJECTIVES

The main objectives of this wok can be summarized as follows:

1. The development of a physically-based model for the study of shallow landslides at the catchment scale using a bottom-up approach. The physically-based model is initially set as simple as possible and then moved to a higher level of complexity if the model is not capable of simulating past landslide events. The procedure has been tested against the case study of the Sorrento Peninsula catchment.

2. Highlight the hydrological effect of the vegetation on the slope stability, focusing on the beneficial action of the rhizosphere. A physically-based model is developed and tested against the case study of Rest and Be Thankful in Scotland, with the aim to prove the effect of the lateral drainage promoted by the rhizosphere.

3. Present an approach based on the use of a physically –based model to overcome the limitations of antecedent daily rainfall model for landslides hydrological thresholds. Again, the case study of the Sorrento Peninsula catchment is considered to test and validate the proposed procedure.

1.3 THESIS OUTLINE

After providing an overview of the research background (**Chapter 1**), the present work will be structured as follows:

Chapter 2 presents an alternative 'bottom-up' approach to the modelling of a particular type of shallow landslides, i.e. flow-like landslides. The approach is based on the use of a physically-based model and have been tested against two case studies of the Sorrento Peninsula catchment. The physically-based model used to characterise shallow landslides at the catchment scale is built from geological, geomorphological, and geotechnical investigation of historic landslide events.

Chapter 3 presents a case study of shallow landslide where the rhizosphere is shown to play a major role in controlling slope stability. The case study is located in Scotland and many laboratory tests have been carried out in order to characterize the soil behaviour. The laboratory results are used to develop a physically-based model, with the aim to demonstrate the beneficial effects of the rhizosphere on slope stability.

Chapter 4 focuses on the use of antecedent daily rainfall models for the design of threshold curves. An approach for correctly selecting of the ‘antecedent’ period is presented. The approach is based on the use of the physically-based model previously discussed in Chapter 1 and is tested against the slopes of the Sorrento Peninsula.

2 BUILDING PHYSICALLY-BASED MODEL FOR RAINFALL-INDUCED SHALLOW LANDSLIDE FROM GEOLOGICAL SURVEY AND GEOTECHNICAL INVESTIGATION: THE CASE STUDY OF THE SORRENTO PENINSULA (ITALY)

Submitted for publication to Canadian Geotechnical Journal - Under revision

Brunella Balzano[(1)], *Alessandro Tarantino*[(2)], *Marco Valerio Nicotera*[(3)], *Giovanni Forte*[(4)], *Melania de Falco*[(5)], *Antonio Santo*[(6)]

POSITION AND AFFILIATION:
[(1)] Phd Student, University of Strathclyde, Department of Civil and Environmental Engineering
[(2)] Professor, University of Strathclyde, Department of Civil and Environmental Engineering
[(3)] Lecturer, Università degli Studi di Napoli Federico II, Department of Civil Engineering
[(4)] Phd Student, Università degli Studi di Napoli Federico II, Department of Civil Engineering
[(5)] Researcher, Università degli Studi di Napoli Federico II, Department of Civil Engineering
[(6)] Lecturer, Università degli Studi di Napoli Federico II, Department of Civil Engineering

Candidate’s contribution: My contribution to this paper consisted in developing and validating the physically-based model for the Sorrento Peninsula Landslides. I introduced the methodology adopted for the validation of the hydrological model and further used in the following chapters. The group of the Department of Civil Engineering of the University of Naples Federico II provided all the details about the geometry and soil hydraulic and mechanical properties.

ABSTRACT

The 1996-1997 winter season recorded prolonged and intense rainfalls all over the Campania region in Italy. As a result, a large number of extremely rapid flow-like landslides were triggered. These phenomena occurred in the late Quaternary volcanoclastic deposits, mantling the carbonate slopes of Campania region. The Sorrento Peninsula- Lattari Mts. was the most affected area by this catastrophic event: some hundreds of shallow mass movements took place during January 1997.

These phenomena have been studied and monitored for several years since then. Field campaigns and investigations have been conducted in order to gain information about the stratigraphy of the areas affected by the slope instabilities and laboratory tests have been performed in order to characterise the hydro-mechanical behaviour of the soils involved in the landslides.

The aim of this work is to build reliable physically-based models for shallow landslides occurring in the Sorrento Peninsula. These models were built in a bottom-up fashion based on geological surveys and geotechnical investigation and were validated against well characterized slope failures. The physically-based models allowed identifying key stratigraphic factors affecting the susceptibility to landslide of shallow slopes and represent an essential step towards the design of early warning system in order to reduce the risk of the area.

2.1 INTRODUCTION

Rainfall-induced landslides are one of the major natural hazards and account for significant economic and social disasters. The evaluation of spatial and temporal landslide risk is the key to developing mitigation measures. The risk related to landslides can be seen as the combination of hazard, i.e. the likelihood of landslide occurrence, and vulnerability, i.e. the degree of loss of one or more elements at risk, resulting from the landslides occurrence.

Landslide hazard can be quantified using empirical approaches. These are based on the correlation of historical records of landslide occurrence with either predisposition or triggering factors, which lead to susceptibility maps (Andriola et al., 2009; Di Crescenzo et al., 2008; Godt et al., 2008; Wang et al., 2015) and rainfall thresholds respectively (De Vita et al., 2002; Guzzetti, et al., 2007).

Empirical approaches are implicitly based on the assumptions that geomorphological and meteorological conditions causing failure in the past remain unchanged in the future. This assumption may not hold for the case where climate pattern is expected to change. Susceptibility maps may be limited by the empirical identification of predisposing factors. This may lead to some critical factors to be missed, which could be instead captured by physically-based models for the landslide mechanism.

Empirical rainfall thresholds are generally based on a minimum or ‘safety’ threshold for rainfall amounts and/or or intensity-duration that have produced landslides in the past. The conservative nature of the rainfall thresholds may lead to false alarm and the consequent loss of confidence in the early warning system (Intrieri et al., 2012).

Several approaches have been developed to quantify landslide hazard at the temporal and spatial scale based on physically-based models. These combine a mechanical model for landslides initiation and a hydraulic model for rainwater infiltration.

The 1-D infinite slope is commonly adopted for the modelling of the slope failure. On the other hand, various approaches are considered to model rainwater infiltration and lateral flow. In principle, full 3-D water flow numerical models (based on either finite difference or finite element methods) should be implemented at the catchment scale. However, this would involve a prohibitive computational burden and simplifications need to be introduced. A first class of models only consider saturated flow by neglecting the effect of the unsaturated upper part of the soil profile on the water redistribution mechanisms. These include SHALSTAB (Montgomery et al., 1994) and TRIGRS (Baum et al., 2002) and SHIA_Landslide (Aristizabal et al., 2015).

A second group takes into account unsaturated flow. Montrasio et al. (2016) compared a physically-based mathematical model (SLIP) with the result of flume tests for shallow landslides. Rigon et al. (2005) consider 3-D water flow model by uncoupling lateral from vertical flow. However, the latter is modelled using a relatively coarse discretisation of the flow domain, which may not allow capturing the high pore-water pressure gradients that may develop during a rain-water infiltration process. Savage et al. (2004), Baum et al. (2010), and Papa et al. (2013) consider a 1-D vertical infiltration only but the closed-form analytical solution implemented allows accurate representation of the evolution of pore-water pressure profile.

The common thread between these approaches is that the hydraulic model at the catchment scale is set-up a priori without consideration for the specific hillslope hydrology and landslide mechanisms actually characterising a specific area. The hydraulic model is intended to be 'universal' and therefore adapted to any catchment in a 'top-down' fashion.

This paper presents an alternative 'bottom-up' approach to the modelling of a particular type of shallow landslides, i.e. flow-like landslides (Hungr et al. 2014; Santo et al. 2018). The physically-based model used to characterise shallow landslides at the catchment scale is built from geological, geomorphological, and geotechnical investigation of historic landslide events. The physically-based model is initially set as simple as possible and then moved to a higher level of complexity if the model is not capable of simulating past landslide events. In other words, a one-dimensional scheme is initially adopted for both mechanical and hydraulic component of the physically-based model. This is then tested against historic landslide events. If the test is negative, the model is scaled-up to a higher level of complexity (e.g. 2-D flow).

The approach is illustrated with reference to the case study of the Sorrento Peninsula located in the Campania region in Southern Italy. Two historic landsides representative of the most typical soil profiles have been selected. The ‘quality’ of the physically-based model has been therefore assessed against its capability to reproduce the time of failure and the location of the slip surface identified by the geological survey following the landslide event.

2.2 STUDY AREA

2.2.1 Geological setting

The study area is located on the Tyrrhenian coast of Campania. During the Plio-Quaternary times, important regional faults associated with the extension of the Tyrrhenian area generated a major tectonic depression named the Campania graben (Southern Italy). The structural horsts bounding this graben include the carbonate Sorrento Peninsula–Lattari Mountains, the Partenio Mountains, the Caserta Hills, Pizzo D’Alvano mountain, and Maggiore Mountain. These mountains consist of more than 1500-m-thick Mesozoic dolomites and limestones.

The most recent deposits on the limestone formation are quaternary continental debris and pyroclastic deposits; the latter are a few metres thick and associated with the Late Pleistocene–Holocene Plinian eruptions of the Campi Flegrei and Somma-Vesuvio volcanic areas. The fallout products of these volcanic areas were deposited mostly on the carbonate formation.

Studies of the dispersion axis of pyroclastic deposits have shown that the most superficial layers (pumices and pyroclastic cover) in the area of the Sorrento Peninsula are associated with the AD 79 eruption.

The geomorphological pattern is characterized by high relief slopes, with peaks often reaching altitudes greater than 1000 m. In most cases, these slopes have been associated with fault scarps generated by various phases of block faulting that occurred during the late Pliocene and the lower and middle Pleistocene. Slope replacement then took place, producing linear slopes characterized by a rectilinear cross profile with a medium slope angle of about 35° (Brancaccio et al., 1999). This morphological context affected the deposition of the Holocene pyroclastic fall deposits. The presence of pyroclastic covers, especially in the steeper areas, makes wide sectors of these slopes particularly susceptible to the triggering of debris slides–rapid earth flows. These are usually triggered by short duration intense meteorological events, particularly after prolonged periods of antecedent rainfall. Due to their high degree of fluidity they can travel over long distances, thereby increasing their power of destruction. Many landslides events took place in the past, very often with tragic consequences on goods and human lives.

2.2.2 The landslide events of January 1997

An intense period of precipitation occurred in Campania from January 9th to 11th, 1997. Rainfall was particularly intense in the western areas of the region, namely, the Sorrento Peninsula and the Lattari Mountains. A 3-day cumulative rainfall of about 280 mm was registered at those locations, preceded by a 4-month period of high cumulative rainfall. On the same days, several hundreds of landslides were triggered in the Campania region. Most of these landslides (about

400) occurred in the Sorrento Peninsula–Lattari Mountains. Landslides involving natural slopes were mainly superficial, sometimes turning into debris/earth flows. Small-scale falls and slides occurred on cut slopes (Di Crescenzo e Santo, 1999).

This work deals with two events occurred on the 10^{th} of January 1997: the Gragnano and Corbara's landslides (Figure 2-1).

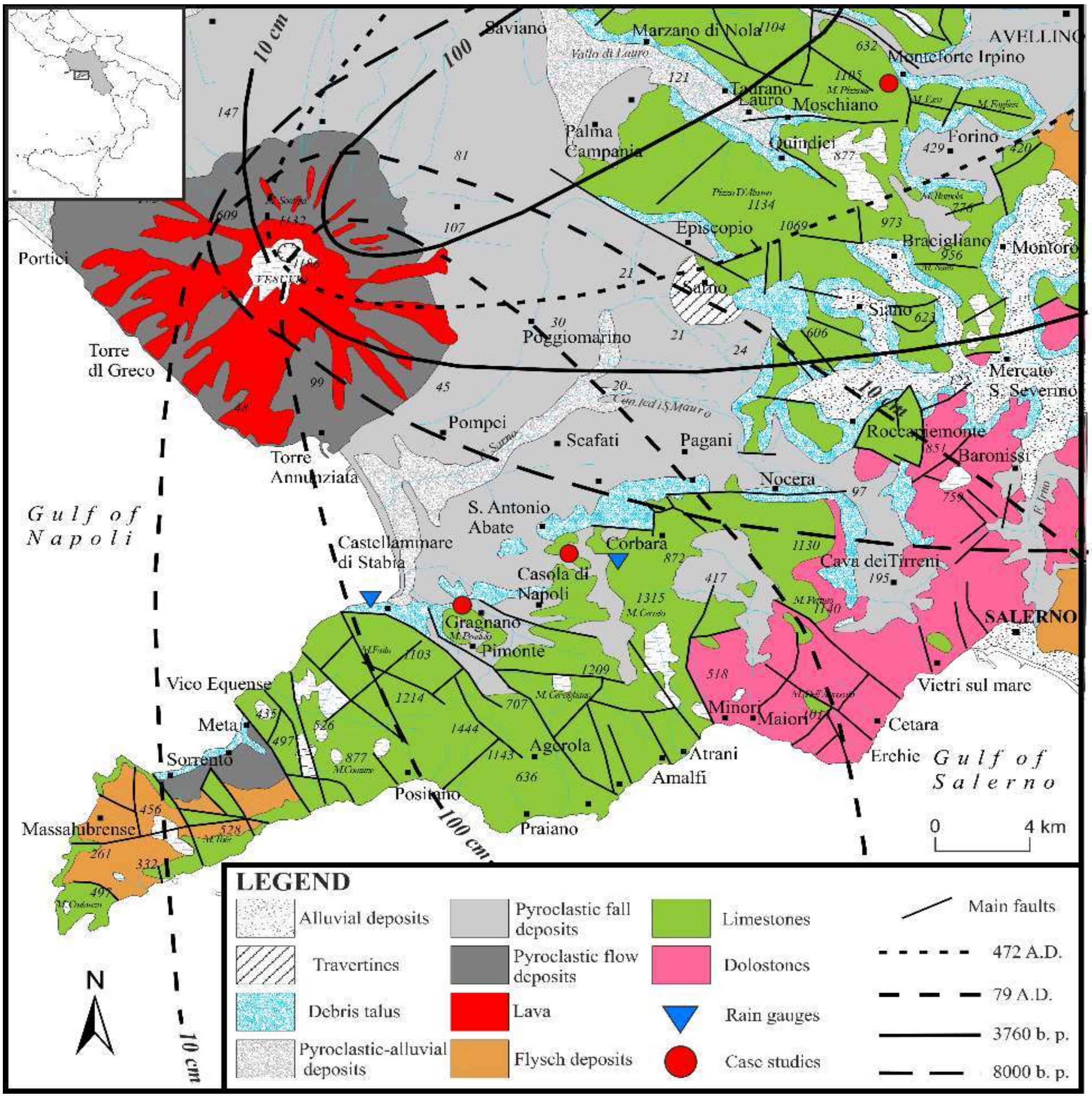

Figure 2-1. Main Somma-Vesuvio pyroclastic fall deposits. (Di Crescenzo & Santo, 2005).

2.2.2.1 Gragnano

The Gragnano (1997) landslide was triggered on the northern slope of Pendolo Mt., an area severely affected by those events in the past. The area is characterized by a high grade of susceptibility, mainly due to high values of slope angles (between 33°- 35°) and a fair continuity of the pyroclastic material between 0.5 -2.5 m thick. The carbonate bedrock in the area is strongly fractured and karstified and it is covered by an ash-fall layer characterized by a high clay content. The latter is covered by the products of 79 AD Plinian eruption, eventually modified by the presence of microbiological activities.

This landslide event occurred around 1:30pm of the 10th of January 1997 and took place in an area affected by another previous event, activated at 9 am of the very same day. It seems that before the major landslide events, the soil itself showed some premonitory cuts on its surface. The average length of the landslide is roughly 220 m, involving 4500 m^3 of material.

Figure 2-2. Structural slopes of Pendolo Mt.

2.2.2.2 Corbara

This event took place adjacent to the road that leads to the Chiunzi Pass and was characterised by a total length of 250m. It started as a translational shallow landslide that evolved into a debris flow. In this case, it was not possible to identify the soil profile at the landslide scarp due to remedial works that took place immediately after the event. The soil profile was characterised by boreholes and/or trenches out by the Geology Department of University of Naples Federico II just close to the landslide site and is shown in Figure 2-3. In this case, the bedrock appears to be covered by a very thin layer (0.3-0.4 m) of ashes, overlain by a 0.8-0.9 m layer of yellow pumices and a 0.9m layer of pedogenised pyroclastic soil.

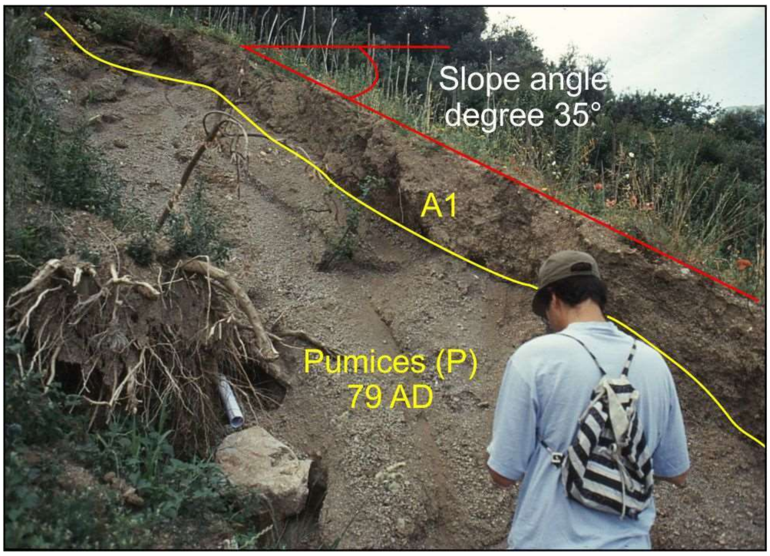

Figure 2-3. Transition zone of Corbara.

2.3 MATERIALS

Three major soil types cover the limestone bedrock (Figure 2-4):

- A top layer of pyroclastic soil, which has been affected by biogeochemical processes as a result of the direct and indirect action of microorganism and vegetation (A1). This layer originally formed during the last stage of the 79 AD eruption.
- Pumices (P). This layer was deposited during the early stage of the 79 AD eruption.
- Ashes, deriving from an ancient eruption (130000 years ago ca.) from Campi Flegrei

volcanic areas (C1 and C2).

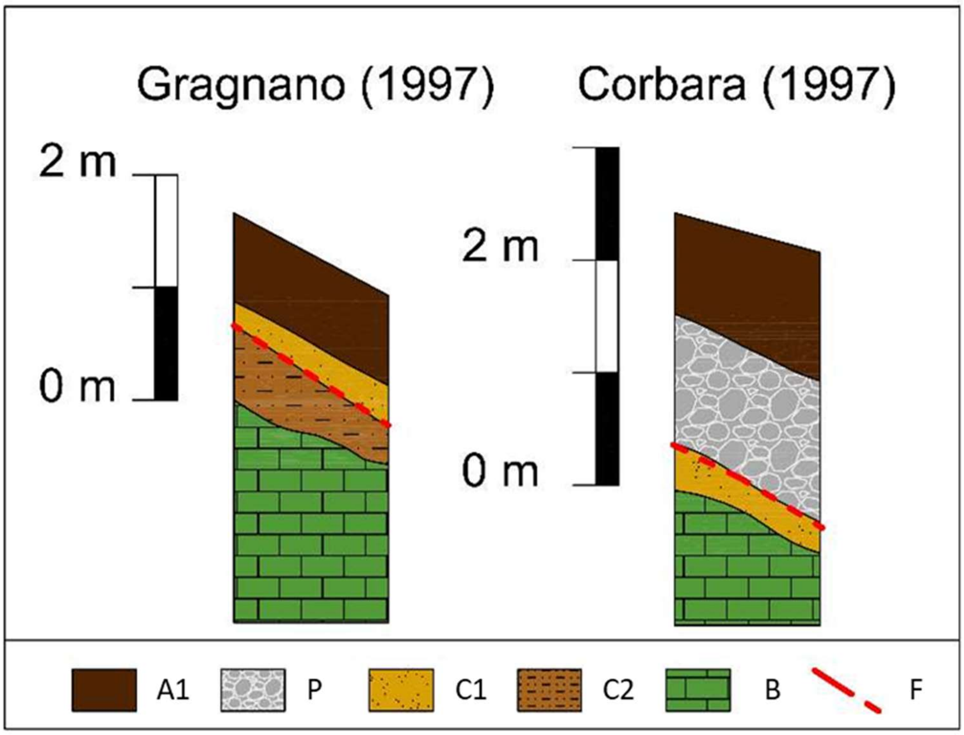

Figure 2-4. Soil profiles: A1) Pedogenized Pyroclastic Soil; P) Pumices; C1) Ashes; C2) Compacted Ashes; B) Bedrock; F) Failure Surface.

The hydro-mechanical characterisation of these soils was carried using different approaches depending on the layer in question. The choice hydro-mechanical properties of the layers A1, P, and C1 was based on the characteristics of similar soils at a site located in another area of the Campania region due to the similarity in terms of the grain-size distribution and volcanic origin (Monteforte Irpino, Figure 2-1). The hydraulic properties of the soils at the Monteforte Irpino site were indeed investigated extensively via laboratory testing and field monitoring (Pirone et al., 2015; Pirone et al. 2016). A typical soil profile at the Monteforte Irpino site is reported in Figure 2-5.

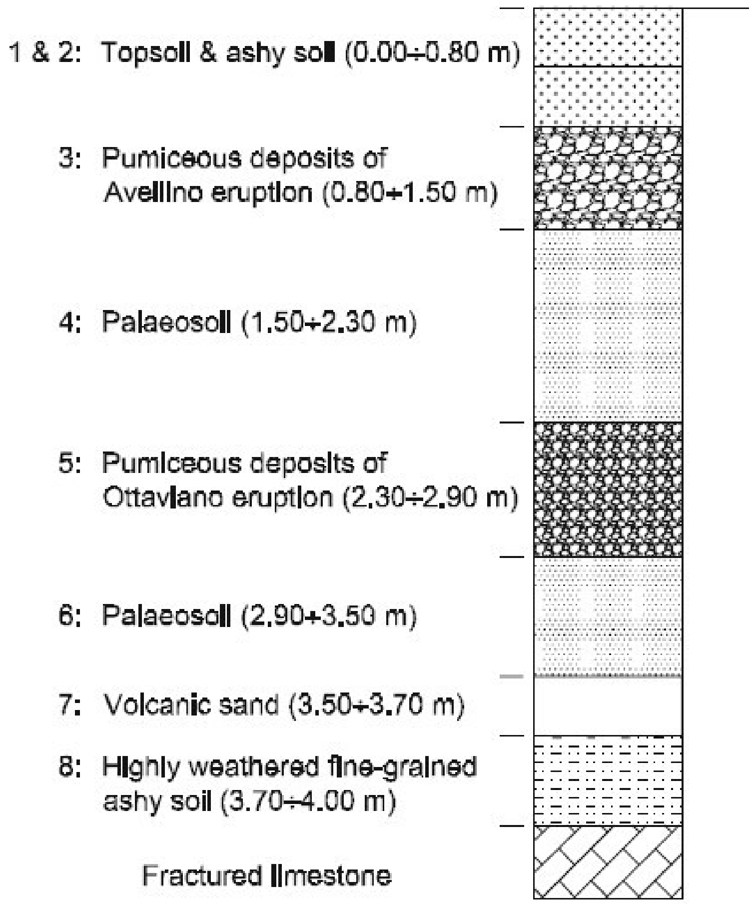

Figure 2-5.T ypical soil profile in Monteforte Irpino (Pirone, et al., 2015).

The hydraulic characterisation of soil C2 was carried out via laboratory testing of single sample taken from the C2 layer in the Sorrento Peninsula. This soil type is not present in the Monteforte Irpino soil profile and, hence, its properties could not be borrowed from any of the soils at this site.

2.3.1 Hydraulic Properties

2.3.1.1 Soil A1 and C1

Figure 2-6 shows the comparison between the grain size distributions of Soil 1 from Monteforte Irpino and Soil A1 from the Sorrento Peninsula (a) and between Soil 6 from Monteforte Irpino and Soil C1 from the Sorrento Peninsula (b). Due to the similarity of the GSD, it was assumed that hydraulic and mechanical properties are also similar.

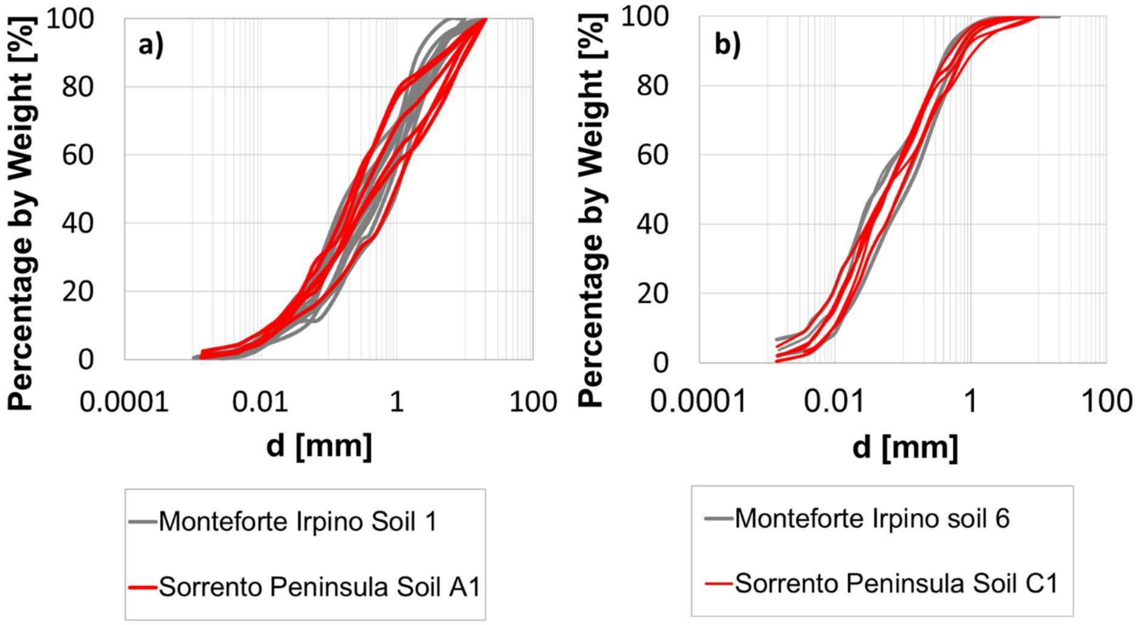

Figure 2-6. a) Grain size distribution of soil 1 from Monteforte Irpino site and soil A1 of Sorrento Peninsula. (b) Grain size distribution of soil 6 from Monteforte Irpino site and soil C1 of Sorrento Peninsula.

Figure 2-7a shows the water retention data derived from field measurements in Soil 1. The water retention curve has been represented with suction in linear scale. It represents the water retention behaviour up to saturation in the negative range of suction (positive range of pore-water pressure). The main drying and main wetting curves derived from laboratory measurements are also shown in the figure (Pirone et al., 2015). The field data lie between the main drying and main wetting curves, i.e. they appear to populate scanning paths. Since the field data tends to cover a relatively narrow region, water retention behaviour of Soil 1 was modelled via a single (scanning) curve. A modified Van Genuchten function (Van Genuchten 1980) has been used to model the water retention behaviour for Soil 1.

$$\theta = \theta_r + (\theta_s - \theta_r)(1 + \alpha(u_w^* + s)^{\,n})^{-(1-\frac{1}{n})} \qquad \textbf{[2-1]}$$

where

- θ_s is the volumetric water content at saturation
- θ_r is the residual volumetric water content
- u_w^* is the value of (positive) pore water pressure at which the degree of saturation becomes equal to 1 ($\theta = \theta_s$)
- α, *n* and *l* are fitting parameters

Figure 2-8b shows the field measurements of hydraulic conductivity for the Soil 1 (Pirone et al. 2015). For comparison, the hydraulic conductivity derived in the laboratory from undisturbed samples is also shown in the figure. The saturated hydraulic conductivity measured in the field appears to be higher than the one measured in the laboratory by one order of magnitude. This can be attributed to macro-porosities that are present in the field due to the effect of microbial activity and presence of roots in the rhizosphere. A modified Mualem-Van Genuchten function (Mualem, 1976) has been used to model the hydraulic conductivity behaviour for Soil 1.

$$k = k_s S_r^l [1 - \left(1 - S_r^{\,n/_{n-1}}\right)^{1-\frac{1}{n}}]^2 \qquad \textbf{[2-2]}$$

where k_s is the saturated hydraulic conductivity and S_r is the degree of saturation and it can be expressed as

$$S_r = \frac{\theta \quad - \theta_r}{\theta_s - \theta_r} \qquad \textbf{[2-3]}$$

.

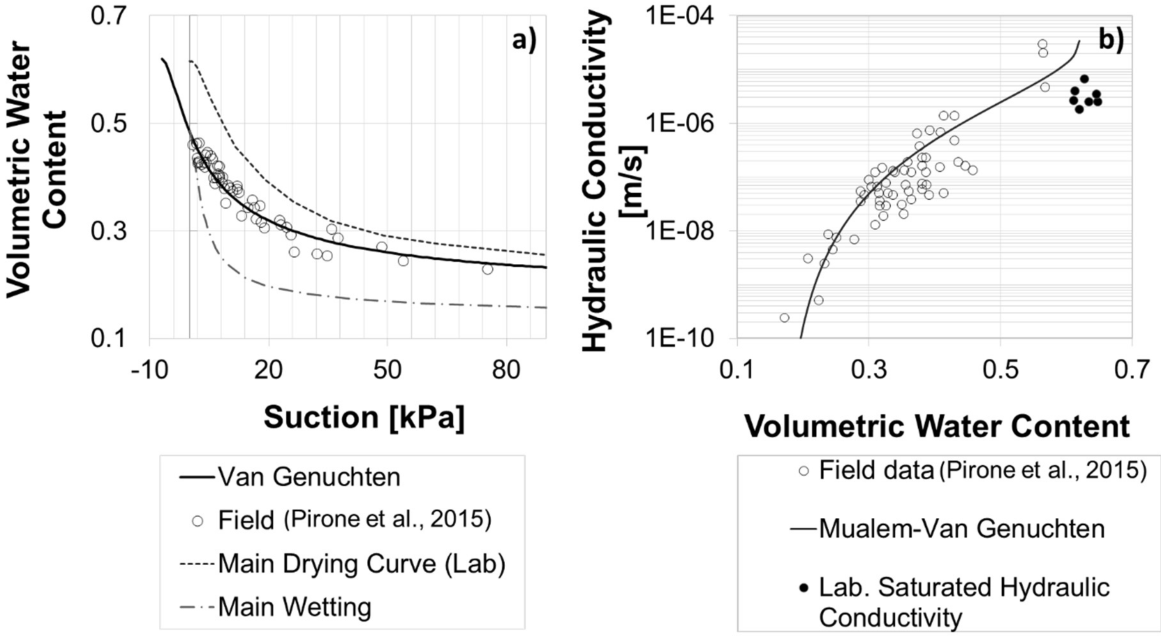

Figure 2-7. Water retention curve (a) and hydraulic conductivity (b) of the soil A1.

Figure 2-8a shows the water retention data derived from field measurements in Soil 6. The main drying curve derived from laboratory measurements is also shown in the figure (Pirone et al., 2015). By comparison with Figure 2-7a, it can be inferred that field data for Soil 6 also populate scanning paths. Equation **[2-1]** was also used to model the (scanning) water retention curve for Soil 6.

Figure 2-8b shows the unsaturated hydraulic conductivity function for Soil 6 as derived from laboratory testing on undisturbed samples (Pirone et al., 2016) and also the laboratory measurements of saturated hydraulic conductivity on a second series undisturbed samples. As field data for hydraulic conductivity of Soil 6 are not available, an assumption had to be made regarding the field scaling factor for the hydraulic conductivity (i.e. the ratio between the values of hydraulic conductivity in the field and the laboratory respectively).

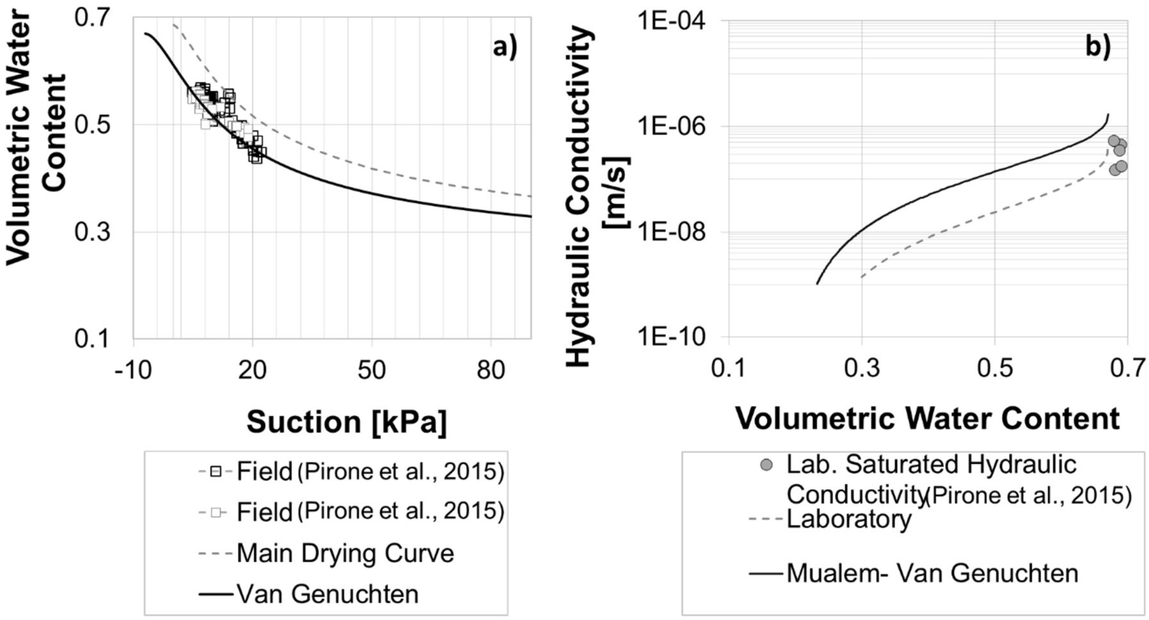

Figure 2-8. Water retention curve (a) and hydraulic conductivity (b) of the soil C1.

It can be reasonably inferred that smaller number and size of macro-pores are present in C1 as compared to A1 due to reduced microbial activity and presence of roots. A scaling factor of 5 has therefore been used for Soil C1 as compared to the scaling factor of 10 observed for Soil A1. The parameters used to model the soil A1 and C1 are reported in Table 2-1.

Table 2-1. Hydraulic Parameters for the soil A1 and C1.

Soil	$\theta_s = n^*$	$\theta_{suc=0}$	θ_r	u_w^*	α	n	l	k_s
		-	-	*kPa*	*1/kPa*	-	-	*m/s*
A1	0.62	0.49	0.17	7	0.05	1.7	-1	$3.4\ 10^{-5}$
C1	0.67	0.61	0.198	7	0.015	1.7	-2.7	$1.7\ 10^{-6}$

Where

- n* is the porosity of the material
- $\boldsymbol{\theta_{suc=0}}$ is the volumetric water content at zero suction. This is to enhance the concept that the complete saturation of the material in field is not associate with a null value of the suction.

2.3.1.2 Pumices

The pumices layer present in the two sites of the Sorrento Peninsula originated during the eruption of Vesuvius in 79AD; these pumices appear to have a grain size distribution similar to that of soil layer 5 at the Monteforte Irpino site as shown by the comparison between the grain size distributions in Figure 2-10. However, soil layer 5 has been identified as a fall deposit produced by a more ancient eruption of Vesuvius (i.e. Avellino eruption 3760 b.p.). Evangelista et al., (2005) tested in the laboratory on reconstituted samples, along a main drying path, the water retention behaviour of Avellino pumices; in particular two tests were carried out, by considering the pumice particles initially dry or water-soaked.

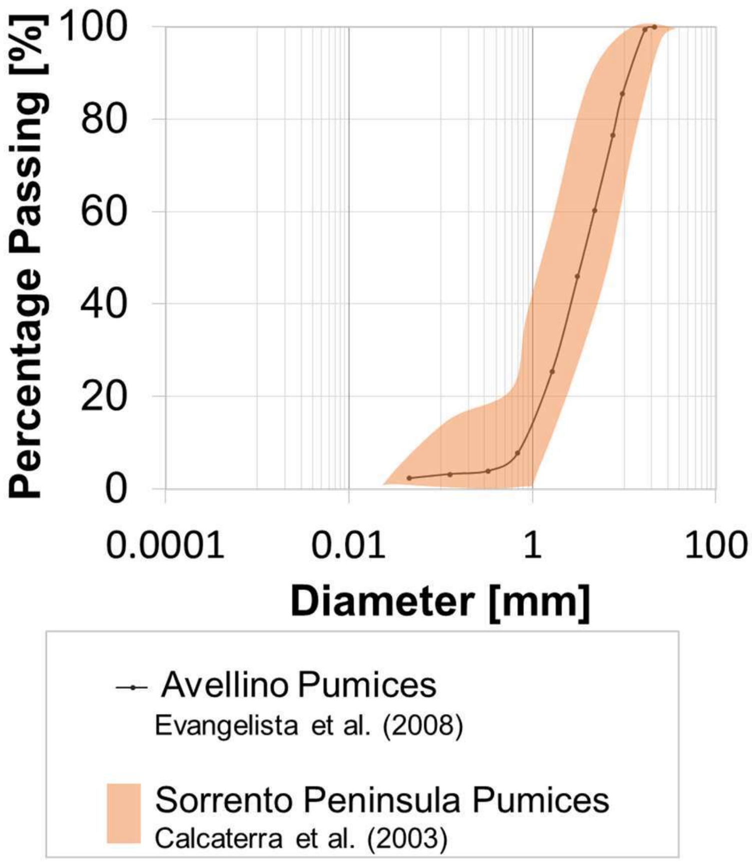

Figure 2-9. Comparison Grain size distribution of Sorrento Pumice (Calcaterra et al. 2003) and Avellino Pumice (Evangelista et al., 2008).

Water retention appears to be bi-modal and was therefore modelled by considering the superposition of two Van Genuchten-type functions:

$$\vartheta = \vartheta_{res,l} + \frac{\left(\vartheta_{sat,l} - \vartheta_{res,l}\right)}{\left(1+\left(\alpha_l \cdot s\right)^{n_l}\right)^{m_l}} + \vartheta_{res,h} + \frac{\left(\vartheta_{sat,h} - \vartheta_{res,h}\right)}{\left(1+\left(\alpha_h \cdot s\right)^{n_h}\right)^{m_h}} \quad \textbf{[2-4]}$$

Two sets of parameters should be assigned for the functions in the high and low range of suction respectively. In particular, α_l, n_l, m_l and $\theta_{sat,l}$, $\theta_{res,l}$ are the fitting parameters for the low range of suction and α_h, n_h, m_h and $\theta_{sat,h}$, $\theta_{res,h}$ are the fitting parameters for the high range of suction. The following constraints have to be imposed to liaise the parameters of the two functions with the overall volumetric water contents at saturation and at the residual state:

$$\vartheta_{sat,low} = \vartheta_{sat} - \vartheta_{res,low} \quad \textbf{[2-5]}$$

$$\vartheta_{sat,high} = \vartheta_{res,low} \quad \textbf{[2-6]}$$

$$\vartheta_{res,high} = \vartheta_{res} - \vartheta_{res,low} \quad \textbf{[2-7]}$$

The best-fitting parameters for the low and high suction range are reported in Table 2-2 and Table 2-3 respectively.

Table 2-2. Hydraulic parameters for the pumices in the low suction range.

$\vartheta_{sat,low}$	$\vartheta_{res,low}$	α_l	n_l	m_l
-	-	*1/kPa*	-	-
0.63	0.12	0.63	3	0.67

Table 2-3. Hydraulic parameters for the pumices in the high suction range.

$\vartheta_{sat,high}$	$\vartheta_{res,high}$	α_h	n_h	m_h
-	-	*1/kPa*	-	-
0.12	-0.12	0.02	2	0.5

For the same reasons mentioned in regards to the soils A1 and C1, the porosity n* of the pumiced is assumed higher than the volumetric water content at zero suction (n*=0.8).

The saturated hydraulic conductivity of the Avellino pumice was available from laboratory measurements and found to be equal to 0.1 m/s.

Unfortunately, no experimental tests have been carried out to investigate the hydraulic conductivity in the unsaturated range. A very classical model was then considered for the hydraulic conductivity derived by combining the Mualem’s model (Mualem, 1974) and the Brooks & Corey’s model (Brooks & Corey’s, 1964)

$$K[m/sec] = K_{sat} \cdot \left(\frac{\vartheta}{n^*}\right)^{\frac{(2+2.5\lambda)}{\lambda}} \quad [2\text{-}8]$$

where θ is the volumetric water content, n^* is the porosity, and λ is the slope of the water retention curve in a log-log plot. The parameter λ was tentatively derived by linearizing the bi-modal water retention curve as shown in Figure 2-10(λ=0.273).

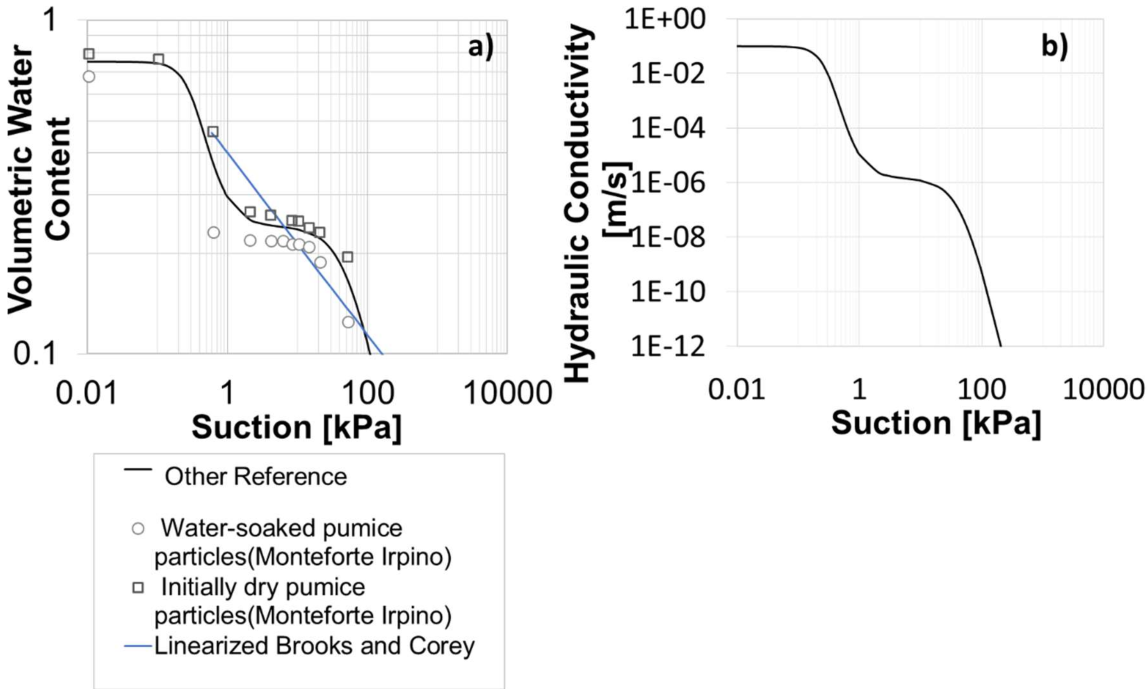

Figure 2-10. Water retention and Hydraulic conductivity curves for the pumices.

2.3.1.3 Soil C2

The soil C2 could not be compared to any soil present at the Monteforte Irpino experimental site. For this layer, a single water retention test was performed on a single undisturbed sample taken from a site close to the landslides events. The water retention and hydraulic conductivity function were determined by inverse analysis of an evaporation process according to the approach presented by Nicotera et al., 2010. The curve determined experimentally was associated with a main drying path. According to Figure 2-12, a scanning path is likely to represent the water retention behaviour in the field more realistically than a main drying path. As a first approximation, the scanning path was derived by shifting the main drying water retention curve in order to have a degree of saturation at zero suction equal to 80% (rather than 100%) as shown in Figure 2-11a, similarly to what has been observed in soil A1 at the Monteforte Irpino site (Figure 2-6).

The hydraulic conductivity function was derived experimentally as a function of the degree of saturation according to Eq. 2.2. The hydraulic conductivity function is shown in Figure 2-11b as a function of suction based on the 'scanning' water retention curve shown in Figure 2-11a.

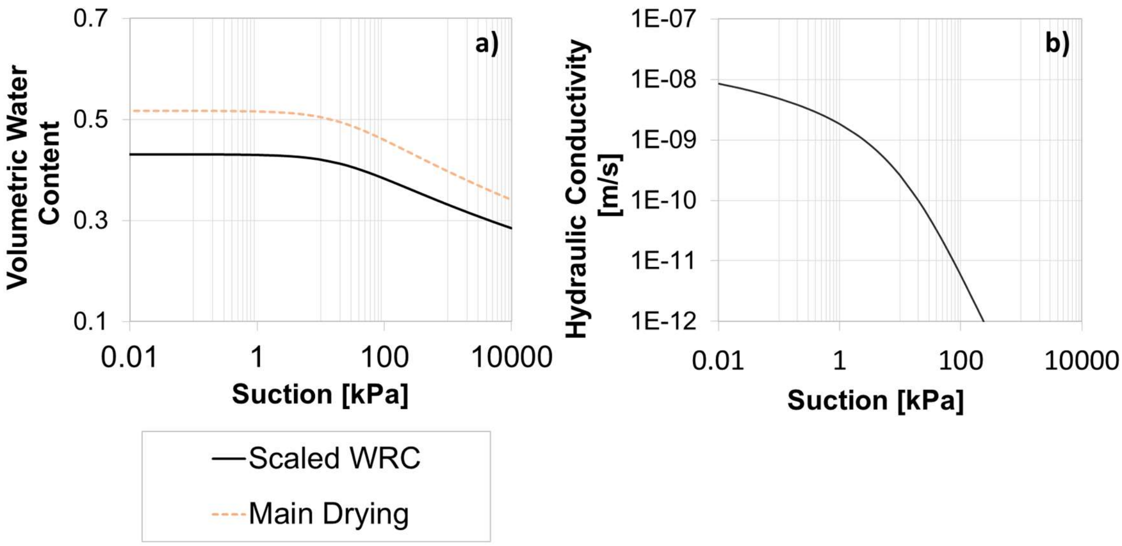

Figure 2-11. Water retention curve (a) and hydraulic conductivity (b) of the soil C2.

Table 2-4. Hydraulic properties for the soil C2.

n^*	$\theta_{s=0}$	θ_r	α	n	λ	k_s
	-	-	*1/kPa*	-	-	*m/s*
0.57	0.517	0.018	0.005	1.07	0.273	$5\ 10^{-8}$

2.3.2 Mechanical Properties

The shear strength properties for the soils A1, P, and C1, were again borrowed from the soils present at the Monteforte Irpino experimental site (associated with soils 1, 3, and 4 respectively). Critical state values of friction angle reported in Table 2-5 have been characterised by Papa (2008) and discussed by Sorbino and Nicotera (2013). For the soil C2, none of the soils present at the Monteforte Irpino experimental site have ‘identical’ grain-size distribution (as occurring for soils A1, P, and C1). The soil at Monteforte Irpino experimental site closest to C2 in terms of grain-size distribution and plasticity index is the Soil 8 in Figure 2-5. The friction angle was therefore borrowed from this Soil 8 according to Papa (2008).

Finally, it was assumed that the saturated failure envelope is characterised by zero effective cohesion with the only exception of Soil A1 where a cohesion of 5 kPa was tentatively assigned to simulate root mechanical reinforcing.

The shear strength in the unsaturated range was formulated as follows according to Nicotera et al. (2015) as follows:

$$\tau = c' + (\sigma - u_w \cdot S_r) \cdot tan\phi' \quad \textbf{[2-9]}$$

where σ is the normal total stress, c’ is the cohesion, u_w is the pore water pressure, S_r is the degree of saturation, and ϕ’ is the critical state friction angle. The use of the critical state friction angle is justified by the ductile behaviour shown by the soils object of this study.

Table 2-5. Mechanical properties for the soils.

	γ_{dry} *kN/m³*	ϕ' °	c’ *kPa*	Gs -
A1	8.06	37	5	2.65
C1	7.09	37	0	2.64
C2	10.64	37	0	2.49
P	4.8	40	0	2.55

2.4 HYDRO-MECHANICAL MODEL

The two landslides events have been modelled numerically in order to reproduce the failure occurred on the 10th of January 1997 following heavy rainfall. Rain-water infiltration has been modelled assuming a rigid soil-skeleton (i.e. without considering any coupling with mechanical deformation). The onset of failure was modelled by assuming the soils to have a rigid-perfectly plastic behaviour

2.4.1 Hydraulic Model

Rainwater infiltration within the slope was modelled using Darcy's law, extended to the case of unsaturated soils:

$$\vec{v} = -K grad(\Psi) = -K grad(z + \frac{u_w}{\gamma_w}) \quad \textbf{[2-10]}$$

where $\vec{v}$ = flow velocity vector; Ψ = piezometric head; K = hydraulic conductivity; u_w = pore water pressure; γ_w = density of water; and z = vertical coordinate increasing upward. The hydraulic conductivity K depends on the degree of saturation, which in turn depends on pore water pressure.

The mass balance equation for liquid water can be written as follows:

$$\mathrm{div}\,\vec{v} + \frac{\partial \theta}{\partial t} = 0 \quad \textbf{[2-11]}$$

where θ = volumetric water content (ratio of water volume to total volume); and t = time. By substituting Equation 2-10 in Equation 2-11, the Richard’s equation in terms of piezometric head is obtained:

$$C\frac{\partial\psi}{\partial t} = \mathrm{div}\left[K\ \mathrm{grad}(\psi)\right] \qquad \textbf{[2-12]}$$

where $C = \gamma_w(\partial\theta/\partial u_w)$, referred to as water capacity of the soil.

The water flow Equation 2-12 was solved numerically via the FEM using the module SEEP/W of the software Geostudio.

2.4.1.1 Geometry

Rain-water infiltration has been modelled by tentatively assuming infinite slope ‘one-dimensional’ water flow. This assumption has then been tested as explained later in the paper. It will be shown that the 1-D model is appropriate for the slopes in question. However, if the test had been negative, a 2-D numerical model would have been considered in a second iteration. The soil profiles have been modelled accordingly to the stratigraphy reported in Figure 2-12.

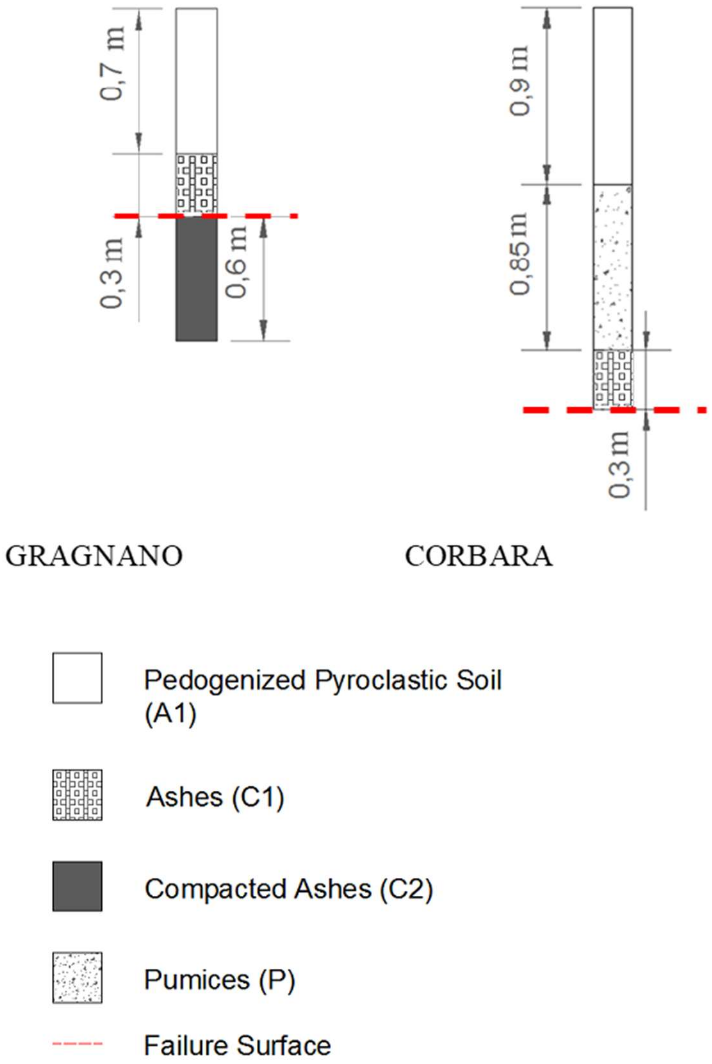

Figure 2-12. Soil profiles adopted in the analyses.

2.4.1.2 Boundary Conditions

The boundary conditions for the numerical model are schematized in Figure 2-13 and consist of:

- Water inflow imposed at the top boundary (to simulate rainfall)
- Water outflow at 10 cm below the ground surface (to simulate evapotranspiration from the root system)

- Impermeable bottom boundary (to simulate the bedrock)

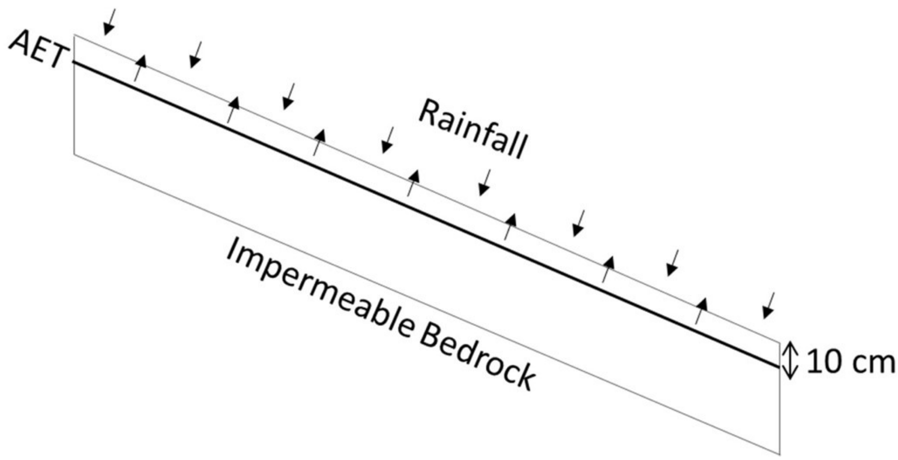

Figure 2-13. Scheme of the Boundary Conditions considered for the model.

2.4.1.2.1 Rainfall Data

Rainfall data were taken from rain gauges as close as possible to the landslide areas. Figure 2-14a-b show the rainfall registered from the 1st of January 1994 until the 31st of January 1997 for Gragnano and Corbara respectively.

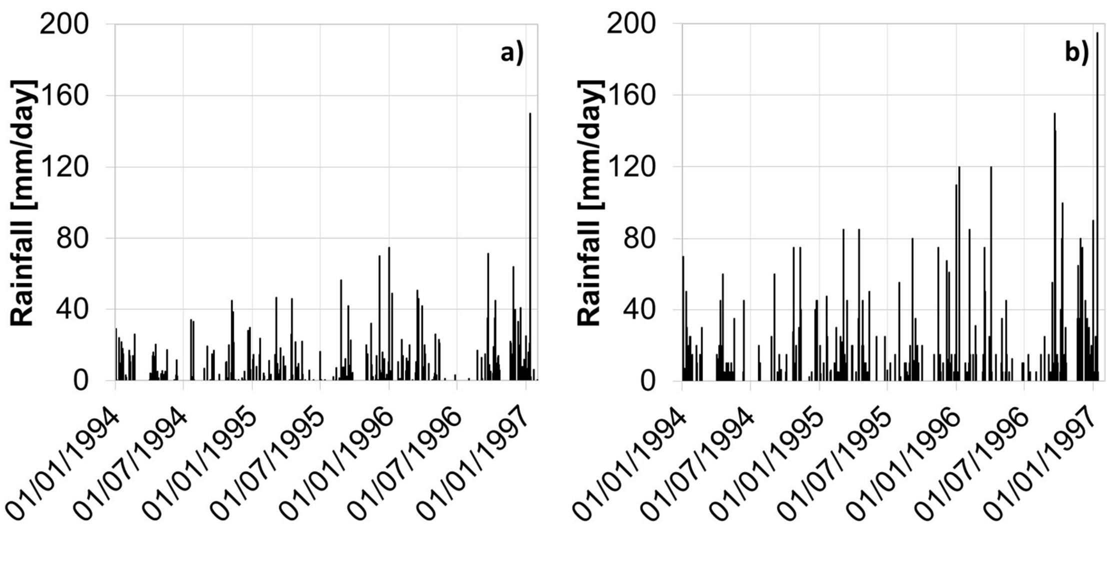

Figure 2-14. Rainfall from 1994 to 1997 registered by the pluviometer in Castellammare di Stabia (a) and Tramonti (b).

2.4.1.2.2 Potential Evapotranspiration

The evapo-transpiration fluxes in the energy-limited regime (potential evapo-transpiration) were calculated using the Penmann-Monteith equation (Monteith 1965)

$$ET_0 = \frac{\Delta(1-\alpha)R + \rho_a c_p e_s \dfrac{(1-RH)}{r_a}}{\Delta + \gamma(1+\frac{r_s}{r_a})}$$

[2-13]

where

- Δ is the slope of the saturated vapour pressure curve ($\delta e_o/\ \delta T$, where e_o = saturated vapour pressure (kPa) and T_{mean} = daily mean temperature (°C))
- R is the (short wave) radiation flux
- α is the albedo assumed to be equal to 0.23 according to Allen et al. (1998)
- γ is the psychrometric constant (kPa ° C^{-1}) given by 0.665 10^{-3} P where P is the atmospheric pressure (kPa)
- ρ_a is the air density
- c_p is the specific heat of dry air, assumed 1.013 10^{-3} (MJ kg^{-1} °C^{-1}),
- e_s is the mean saturated vapour pressure
- r_a is the bulk surface aerodynamic resistance for water vapour
- RH is the ambient relative humidity
- r_s is the canopy surface resistance

The aerodynamic resistance r_a was in turn modelled according to Allen et al. (1998)

$$r_a = \frac{ln\left[\frac{z_m - d}{z_{om}}\right] ln\left[\frac{z_h - d}{z_{oh}}\right]}{k^2 u_z}$$

[2-14]

where

- z_m height of wind measurements (m),
- z_h height of humidity measurements (m),

- d zero plane displacement height (m),
- z_{om} roughness length governing momentum transfer (m),
- z_{oh} roughness length governing transfer of heat and vapour (m),
- k von Karman's constant, 0.41 (-),
- u_z wind speed at height z (m s^{-1}).

and the canopy resistance r_c was assumed equal to 50 s m^{-1} according to the value suggested by Abtew et al. (1995) for the family of chestnuts.

The radiation *R*, the relative humidity *RH*, the temperature *T*, and wind speed *u* were taken from an open access database (www.ilmeteo.it for temperature, relative humidity, and wind speed and www.solaritaly.enea.it for solar radiation). The albedo α was assumed equal to 0.15 according to Oke (1992). The monthly evapo-transpiration fluxes calculated using Eq. 2-13 are shown in Figure 2-15 for both the sites of Gragnano and Corbara.

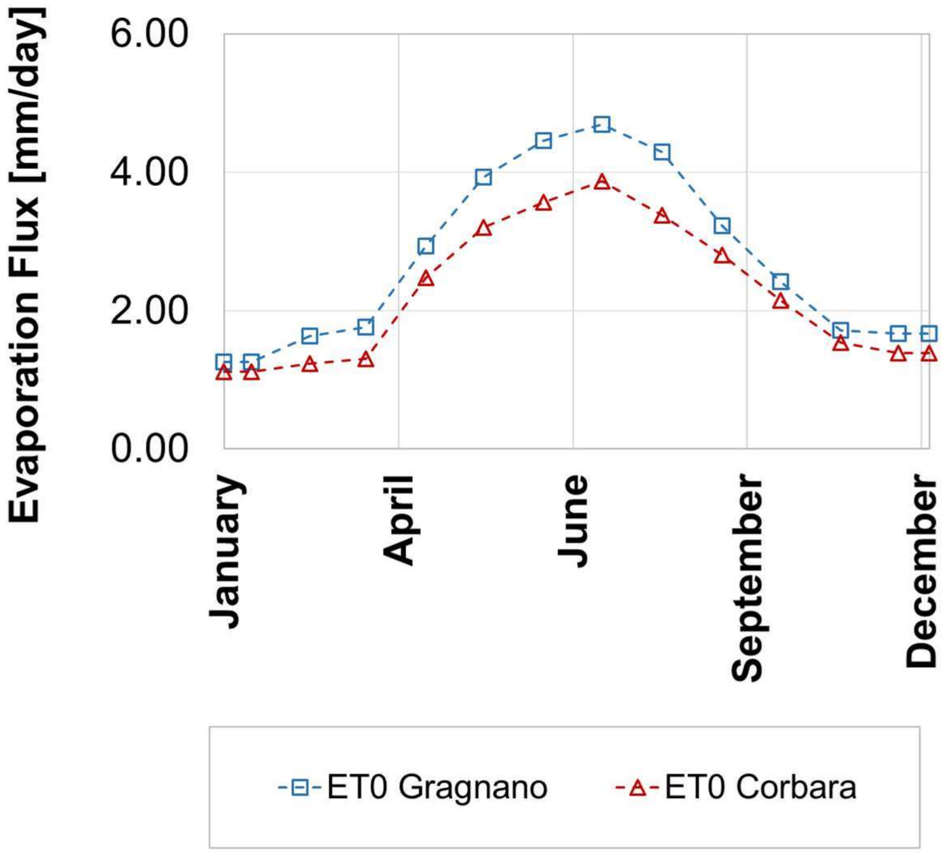

Figure 2-15. Monthly evaporation fluxes for Gragnano and Corbara.

2.4.1.2.3 Water limited Evapotranspiration

Potential evapotranspiration only occurs if the soil-plant system can deliver the water flow demanded by the atmosphere. For the case of high potential evapotranspiration rate and/or low soil moisture content, this condition cannot be met and the actual water outflow is dictated by soil-plant system rather than the meteorological conditions (water-limited regime).

The reduction of water outflow in the water limited regime can be modelled via a reduction function that relates the ratio between actual and potential evapotranspiration to the suction at the water extraction. Figure 2-16 shows a typical reduction function as suggested by Feddes, et al.(1978). As shown, as long as the suction values stay lower than s0, the system is able to accommodate the atmospheric demand (actual evaporation = potential evaporation). When the suction reaches the value s0, the system’s water storage is not sufficient to accommodate the potential evapotranspiration any more. Therefore, for $s>s_0$, the actual evaporative flux decreases until the system is completely dry ($s=s_1$).

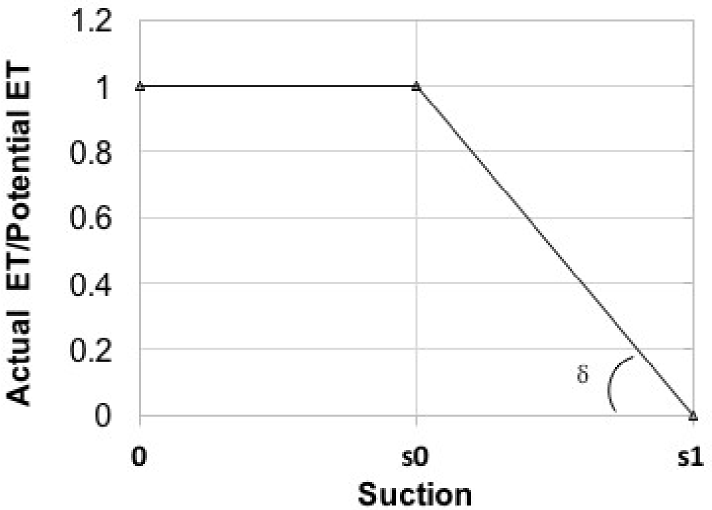

Figure 2-16. Generic reduction function.

An approach was developed in this work to calibrate the parameters of the reduction function: the suction value s_0 and the slope of the reduction function δ. A soil column 1.6 m high characterised by the same soil profile at the Gragnano landslide site (Figure 2-12a) was considered. The column was subjected to the boundary condition derived from Eq. 2-13 for the period starting 01/01/1995.

Two different initial hydrostatic conditions, associated with suction at the base of the column equal to 0 and 10 kPa respectively, were considered. Figure 2-17a shows the evolution of suction at the top of the column over time. It can be seen that suction tends to increase very rapidly after a period of time, which depends on the initial condition. The very rapid increase of suction is associated with the attainment of the water-limited regime; the soil column is no longer able to deliver the evaporation rate imposed at the boundary.

Figure 2-18b shows the time derivative of suction with respect to suction. It can be observed that i) time derivative is now independent of the initial condition and ii) the suction marking the transition to the water-limited regime can be clearly identified. The suction of 1000 kPa has been chosen for s_0.

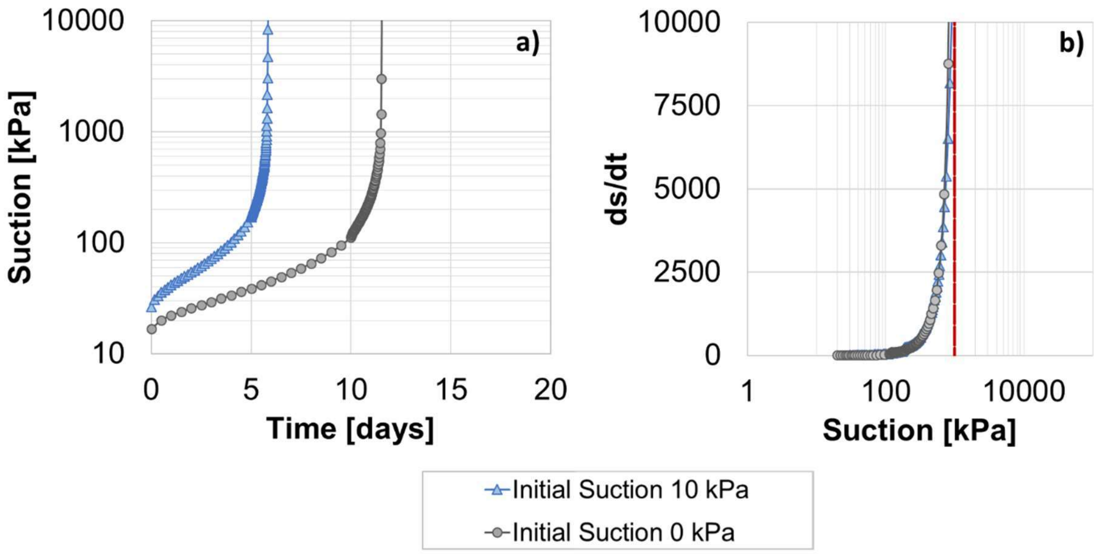

Figure 2-17. Identification of the limit suction value.

To characterise the water limited regime, the assumption has been made that suction at the extraction point remains constant in the water limited regime. This assumption is built upon the observation that suction in the leaves tends to remain constant in the water-limited regime (Duursma et al. 2008). The parameter δ was then selected by trial and error in order to reproduce a constant value of suction in the water limited regime as shown in Figure 2-18. The reduction function calibrated on the Gragnano soil profile is shown in Figure 2-19.

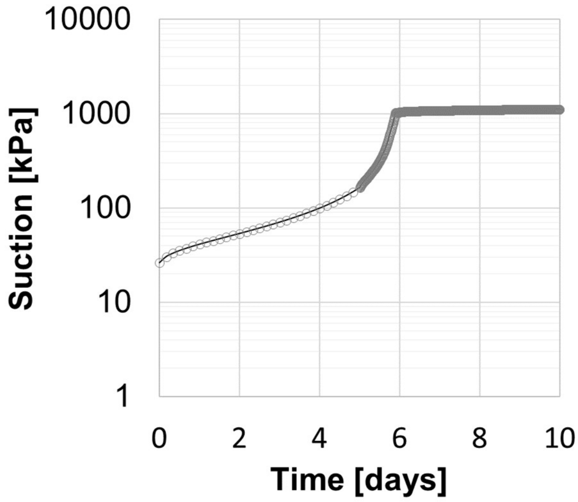

Figure 2-18. dentification of the value of suction at which the Actual Evapotranspiration goes to zero.

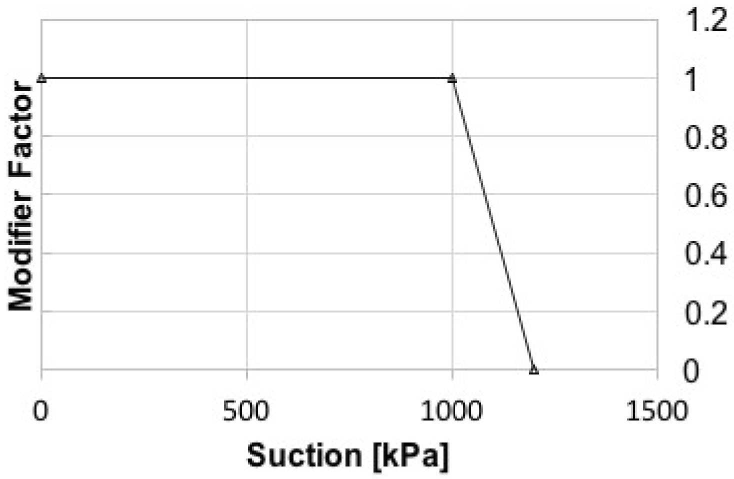

Figure 2-19. Reduction function calibrated on the Gragnano soil profile.

2.4.1.3 Initial Condition for the transient analysis

The landslide events occurred on the 10 January 1997. The numerical analysis of water flow was then carried out between 1 January 1996 and 28 February 1997. The numerical analysis requires an assumption about the initial condition in terms of pore-water pressure profile at the start of the analysis (1 January 1996). This initial condition is unknown and cannot be assumed a priori due to its significant influence on the numerical results, i.e. the slope may or may not experience failure in the numerical simulation depending on the (arbitrary) choice of the initial hydraulic condition.

An approach was then developed in this work to derive the initial hydraulic condition. Since the same approach is also used to test and validate the hydraulic model, it is discussed separately in the following section.

2.4.1.4 Validation of the hydraulic model

A distinct numerical analysis was carried out by considering rainfall and evapotranspiration occurring in 1994 and 1995 and repeating the same rainfall and evapotranspiration pattern for three times for Gragnano (for a total of 6 years) and for 1 time for Corbara (for a total of 2 years). Three steady-state ‘infinite slope’ initial conditions were selected, assuming that suction at the bottom of the soil profile was equal to 10 kPa, 40 kPa and 100 kPa respectively.

The results from this analysis are shown in Figure 2-20 in terms of suction at the bottom boundary versus time. It can be observed that:

i) The effect of the (arbitrary) initial condition is eventually cancelled if the water flow analysis is carried out for a time sufficiently long (after about 4 years for Gragnano and 0.2 years for Corbara).

ii) Once the suctions generated by the three different initial conditions converge, suction tends to fluctuate around an average value that tends to remain constant over time.

Condition i) allows selecting the initial condition in an unambiguous way. Once convergence has occurred, the time evolution of suction over 1995 can be assumed to be the actual one. As a result, the suction profile at 31/12/1995 can be assumed as the initial condition for the analysis to be carried out for the period 01/01/1996 to 28/02/1997.

The condition ii) can be taken as an evidence of the robustness of the hydraulic model assumed in terms of boundary conditions. In fact, one would expect that a hydrological balance is accomplished over a relatively long period. If the hydraulic model (including its boundary conditions) is not set properly, it may occur that the slope becomes either fully-saturated or entirely dry over time. In this case, it appears that the 1-D ‘infinite slope’ hydraulic model is appropriate for the slopes of Corbara and Gragnano. Should the test on hydrological balance have failed, a different model should have been selected (e.g. 2-D) and the iteration started again.

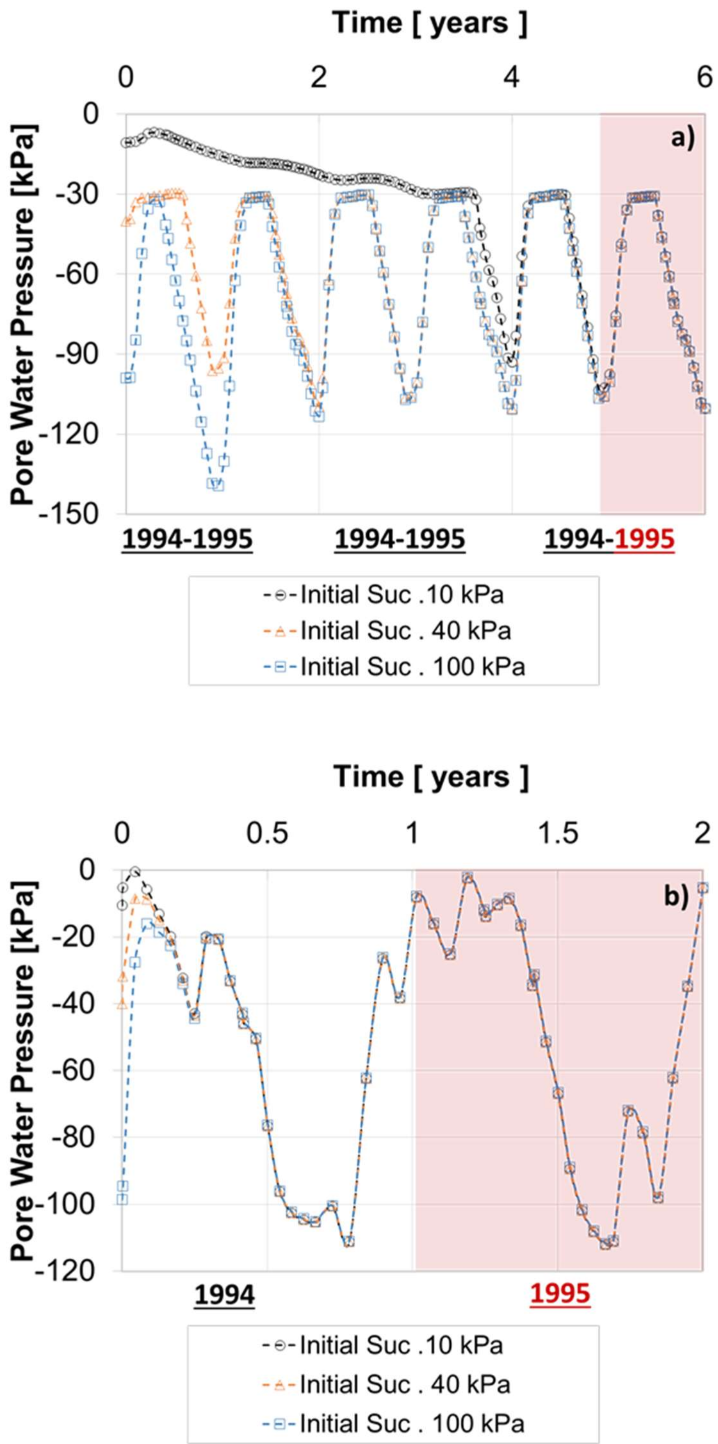

Figure 2-20. Cancellation of the initial condition at the bedrock for a) Gragnano’s model and b) Corbara’s model.

2.4.2 Mechanical Model

2.4.2.1 Geometry

The length L and depth D of the landslides at the release zone measured during the geomorphological survey after the landslide event are reported in Table 2-6. It can be observed that the ratio D/L is less than 1/10 and the onset of failure was therefore modelled by assuming an ‘infinite slope’ failure mechanism.

Location	**Length** *m*	**Depth** *m*	**D/L**	**β** °
Gragnano	18	1.6	0.09	33
Corbara	24	2.3	0.096	35

Table 2-6. Geometric characteristics of the landslides under study.

2.4.2.2 Factor of Safety

The factor of safety at any depth can be derived via the limit equilibrium method. By considering the shear strength criterion given by Equation 2-9, the following equation can be derived

$$\mathrm{FoS} = \frac{\tan\phi'}{\tan\beta} + \frac{-u_w S_r \cdot \tan\phi'}{(\bar{\gamma} H) \cdot \sin\beta \cdot \cos\beta} \tag{2-15}$$

where H is the depth of the failure surface, β is the inclination of the slope, and $\bar{\gamma}$ is the average unit weight given by:

$$\bar{\gamma} = \frac{1}{H}\int_0^H [\gamma_s(1 - n^*) + \gamma_w n^* S_r]dz \tag{2-16}$$

where γ_s and γ_w are the unit weight of solids and water respectively, and n^* is the porosity.

2.5 RESULTS

To derive the factor of safety versus time, the water flow equation (Eq. 2-12) was first solved numerically considering the hydraulic properties, initial condition, and boundary conditions discussed in the previous section. In particular, the water retention and hydraulic conductivity functions shown in Figure 2-7, Figure 2-8, Figure 2-10 and Figure 2-11 were considered for the materials forming the slope as shown in Figure 2-12. The boundary conditions shown in Figure 13 and discussed in the "Hydro-mechanical Model" Section were considered.

Figure 2-21 shows the evolution of the Factor of Safety (FoS) for the case studies analysed from 1 January 1996 until the day where a FoS equal to unity was attained at one depth at least.

To highlight the evolution of the FoS, Figure 2-22 shows the evolution of the minimum FoS from January 1996 to the 10th of January 1997 when the landslide events occurred.

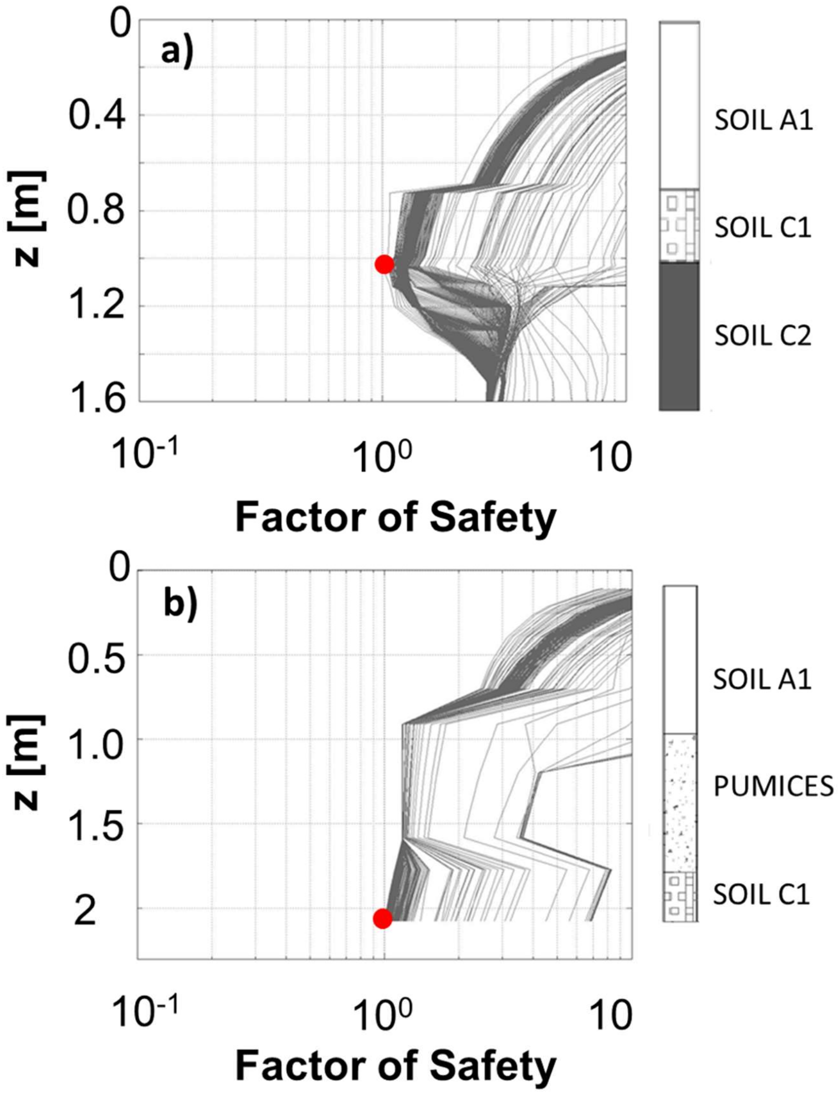

Figure 2-21. Evolution of the Factor of safety profile from January 1996 to the 10th of January 1997 when the Landslide events occurred in Gragnano(a) and Corbara(b).

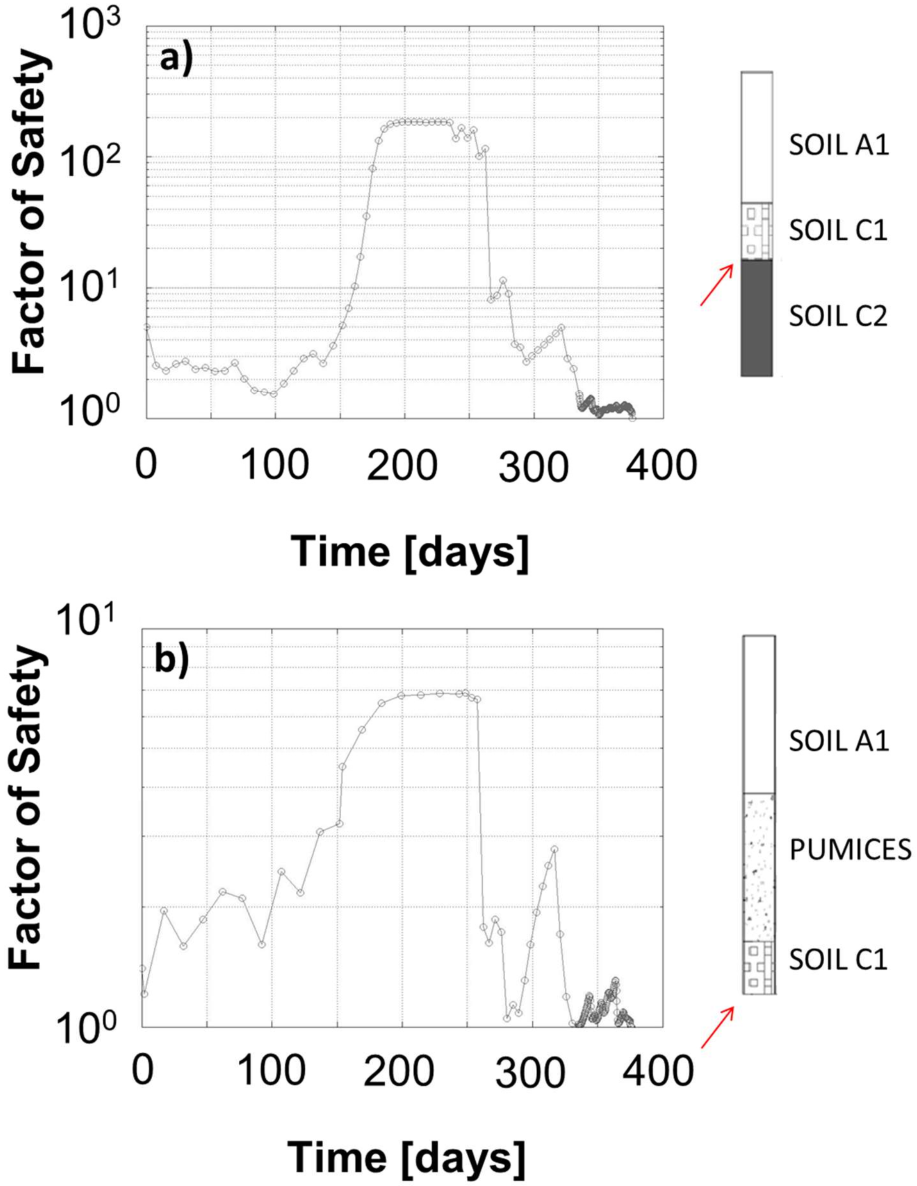

Figure 2-22. Evolution of the minimum Factor of safety profile from January 1996 to the 10th of January 1997 when the Landslide events occurred in Gragnano (a) and Corbara (b).

The numerical simulation returned failure conditions on the 12 January 1997 for the case of Corbara (progressive day no. 377) and 11 January 1997 (progressive day no. 376) for the case of Gragnano. These times compare favourably well with the date of 10 January 2017 where landslides occurred. It is also worth observing that the numerical simulation returns a failure surface developing at the interface between C1 and C2 for Gragnano and at the interface between C1 and the bedrock for Corbara. Again, this is consistent with the field observation following the survey after the landslide event. Overall, these results returned by the numerical simulation corroborate the approach adopted to formulate the physically-based hydro-mechanical model for the two landslides.

To have a better insight into the hydrological mechanisms triggering the landslides in the Sorrento Peninsula, it is worth exploring the pore-water profiles at the time of failure as shown in Figure 2-23. A sharp change in hydraulic conductivity occurs at the interface between the ashes (C1) and the compacted ashes (C2) for the case of Gragnano (Figure 2-23a) and at the interface between the ashes (C1) and the bedrock for the case of Corbara (Figure2-23b). This causes the formation of a perched water table as inferred from the positive pressure generated above the C1-C2 interface for Gragnano and C1-Bedrock for Corbara. Positive pore-water pressures then cause a drop in normal effective stress and, hence, shear strength until failure is eventually triggered.

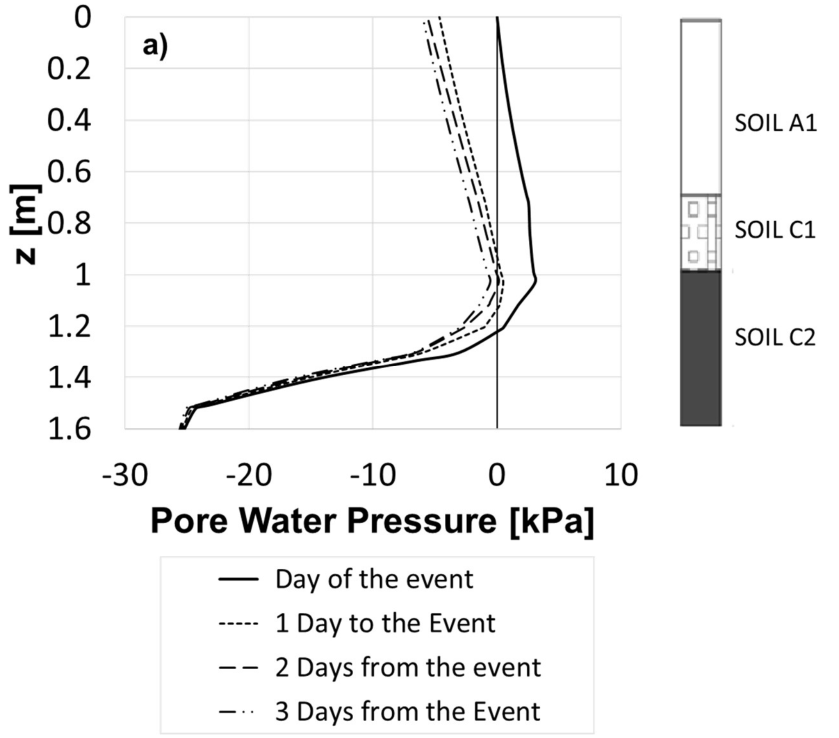

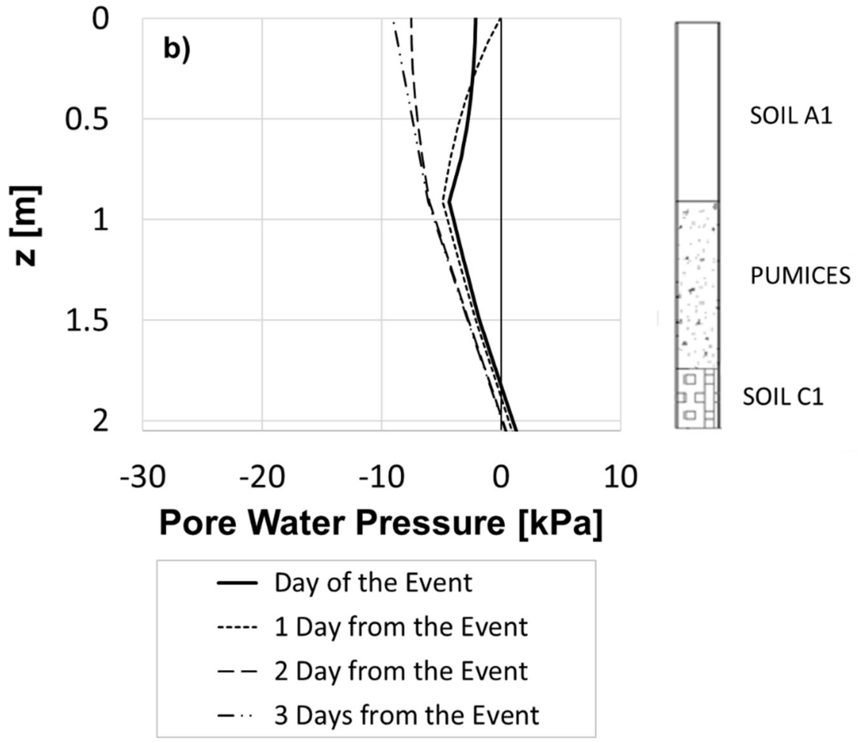

Figure 2-23. Pore water pressure profile at the time of the failure in Gragnano (a) and Corbara (b).

2.6 CONCLUSIONS

This paper has presented an approach to formulate physically-based models for shallow landslides. The model was built in a ‘bottom-up’ fashion based on geological, geomorphological, and geotechnical investigation of historic landslides.

These investigations allowed designing typical soil profiles and characterising mechanically and hydraulically the materials forming the different geological layers present in the area. The hydraulic model was then tentatively set as one-dimensional and tested against i) its ability to reproduce a satisfactory hydrologic balance over a relatively long period with the slope subjected to real rainfall and evapotranspiration pattern and ii) its capability of losing memory of the initial condition inevitably set up in an arbitrary fashion. The hydrological balance was considered as a ‘hypothesis test’ for the hydraulic model. If the test is positive, which was the case for the shallow slopes considered in this study, there will be no need to develop more sophisticated (and computationally expensive) hydraulic models in two or three dimensions. This clearly simplifies the numerical modelling of the landslide initiation at the catchment scale. At the same time, the use of a hydraulic 1-D model can be corroborated by numerical evidence and not cast a-priori as often the case in numerical studies of shallow landslide initiation at the catchment scale reported in the literature.

The hydraulic model (including its boundary and initial conditions) was then coupled with a simple mechanical model and tested against its capability of reproducing the time of failure and the location of the slip surface identified by the geological survey following the landslide events. Again, this was taken as ‘hypothesis test’ for the hydro-mechanical physically-based model for the Sorrento Peninsula catchment.

The model has shown to adequately capture time and location of failure for the two historical landslide events considered. This makes it possible to generalise the physically-based model to the entire catchment with fair confidence and use is as a basis to develop hazard maps and/or hydrological triggering thresholds used in early-warning systems.

3 THE HYDRAULIC CONTROL OF THE RHIZOSPHERE ON RAINFALL-INDUCED SHALLOW LANDSLIDES: THE LESSON LEARNED FROM A CASE STUDY IN SCOTLAND.

To be Submitted for publication to Landslides

Brunella Balzano[(1)], Alessandro Tarantino[(2)]

POSITION AND AFFILIATION:
[(7)] Phd Student, University of Strathclyde, Department of Civil and Environmental Engineering
[(8)] Professor, University of Strathclyde, Department of Civil and Environmental Engineering

Candidate’s contribution: All the job carried out for the purpose of this study has to be attributed to my personal contribution to the research. I carried myself all the laboratory experiments and I have been helped in the site surveying by my supervisor, Professor Alessandro Tarantino.

The rainfall data used as boundary conditions for the analyses have been kindly offered by Transport Scotland Database.

ABSTRACT

The paper presents a case study of shallow landslide where the rhizosphere is shown to play a major role in controlling slope instability. Field investigation and laboratory testing were

carried out to characterise the hydraulic conductivity of the rhizosphere and deeper horizons. This characterisation formed the basis for the development of a physically-based model for shallow landslides. This model was first validated against its capability of simulating two historical landslide events and then exploited to demonstrate the beneficial effects of the rhizosphere on slope stability. The lesson learned from this study is that shallow landslide hazard can be mitigated by enhancing the capacity the rhizosphere to act as a natural lateral drainage. This implies that plants with root-system architecture that enhances lateral subsurface flow should be privileged when designing vegetation-based remedial measures.

ACKNOWLEDGMENTS

The authors wish to thank Transport Scotland and its Operating Company, BEAR Scotland, for the rainfall data at Rest and Be Thankful. The authors also wish to thank Prof Mike Winter for the helpful discussions. The financial contribution of the European Commission to this research through the Marie Curie Industry-Academia Partnership and Pathways Network MAGIC (Monitoring systems to Assess Geotechnical Infrastructure subjected to Climatic hazards) – PIAPP-GA-2012-324426 – is gratefully acknowledged.

3.1 INTRODUCTION

Rainfall is a major triggering factor of shallow landslides. When heavy and/or prolonged rainfall events occur, water infiltrates into the slope and pore-water pressures build-up. In turn, this reduces the soil shear strength eventually triggering slope instability. Rainfall-induced shallow landslides may evolve into flow slides and debris flows. These are characterised by high velocities and long travel distance and are a main cause of property and infrastructure damage, injury, and death.

It is widely acknowledged that the presence of vegetation can influence landslide occurrence. Plants can significantly enhance slope stability by reinforcing the soil due to root anchoring effects and/or increasing its shear strength via the particle bonding associated with root exudates and microbiological activity (Ali et al. 2008; Fan et al., 2008; Zhang et al., 2010). On the other hand, vegetation promotes soil water extraction via the transpiration process (soil water is driven from the soil through the plant to the atmosphere), which contributes in keeping the soil in an unsaturated state thus enhancing its shear strength (Gerten et al., 2004; Ting, Hao, and HuaDe, 2012).

There is indeed a third effect that has thus far been little explored. The root system can promote subsurface lateral flow in the rhizosphere by creating networks of preferential flow. It has been suggested that this hydrological mechanism may help ‘preserve’ low pore-water pressures in potentially unstable layers thus reducing the susceptibility of slopes to landsliding (Ghestem et al., 2011). However, there are no studies assessing quantitatively the actual impact of the hydraulic ‘diversion’ promoted by the rhizosphere on landslide occurrence.

This paper presents a case study of shallow landslide where the rhizosphere is shown to play a major role in controlling slope instability. Field investigation and laboratory testing were carried out to characterise the hydraulic conductivity of the rhizosphere and the deeper horizons. This characterisation formed the basis for the development of a physically-based model for the shallow landslide, which was first validated against its capability of simulating two historical landslide events and then exploited to demonstrate the beneficial effects of the rhizosphere.

The lesson learned from this study is that shallow landslide hazard can be mitigated by enhancing the capacity the rhizosphere to act as a natural lateral drainage. This implies that plants with root-system architecture that enhances lateral subsurface flow should be privileged when designing vegetation-based remedial measures.

3.2 BACKGROUND

The rhizosphere is a region with a high concentration of biological and non-biological activities; it is highly influenced by the presence of the roots and, therefore, exhibits characteristics that differ from bare soil.

Roots grow into the rhizosphere during their life and, together with other natural activities (i.e. presence of worm, insects and other animals, freeze–thaw and wetting–drying cycles, erosion), they contribute to the formation of a network of interconnected macropores with diameters ranging from a few tenths of micrometres (Marshall, 1959) to many centimetres (Pierson, 1983). Aubertin (1971) largely studied the nature of the macropores in forested soils and observed their capability to alter subsurface flow, providing pathways or conduits for the rapid movement of free water into and through the soil profile. In particular, the experimental campaign carried out revealed a close correlation between the presence of old root channels and overall conductivity of the soil. Thanks to this hydrological mechanism, roots are capable of influence water pressures in soils and have therefore a major control on the occurrence of shallow landslides.

There are few but significant examples in the literature about the interplay between root architecture, preferential subsurface flow, and landslide occurrence. Gaiser (1952) has pioneered the concept that root channels may serve as large openings for rapid water flow. He mapped the presence of channels formed from decayed roots through the upper horizons of a temperate forest soil and concluded that the effect of root-induced macroporosity in the soil profile is an aspect that should not be neglected in the natural slope stability analysis.

Whipkey (1969) measured subsurface flow after rainfall simulations. Through observations in trenches, Whipkey (1969) observed water leaking from root channels, with the greatest flow from channels just beneath or at an angle to the area where the rainfall simulations were carried out. Noguchi et al. (1997) also highlighted the similarity between the direction of subsurface flow and the direction of root growth in the upper layers of a semitropical forest.

Because of their specific properties, root channels need to be considered with reference to their influence on preferential flow. Rhizosphere is therefore an important factor in addressing the complex nature of preferential flow at the hillslope scale, which has been assumed to influence landslide initiation (Sidle et al., 2001).

Nonetheless, no quantitative studies have been carried out to demonstrate the key role of the rhizosphere on hillslope subsurface flow and, hence, landslide initiation.

3.3 CASE STUDY: REST AND BE THANKFUL (SCOTLAND)

3.3.1 Site Geology

The slopes of the A83 Rest & Be Thankful are located approximately 34 miles North West of Glasgow (Figure 3-1). The study section of the A83 between Ardgartan and The Rest & Be Thankful has a long and well documented history of slope instability and landslide occurrence. The A83 forms part of the important trunk road network in Scotland and is vital for quick and easy access between the Western region of the country and the Central Belt and Highlands.

The site is underlain by a bedrock layer of steeply sloping metamorphic rocks from the

Beinn Bheula Schist Formation (BGS, 2012). The formation is composed of pelites, semipelites and a mixture of coarse to fine psammites. The rocks were formed roughly 542 million years ago in the Neoproterozoic where a period of regional metamorphism altered the original sedimentary rocks and caused large scale folds and faults which can be seen throughout the present-day landscape (BGS, 2012).

The superficial deposits on the slopes and the valley floor include mainly glacial till of quaternary age. The valley floor itself is composed of river terrace deposits including gravels silts and clays of quaternary age. The bedrock plays little part in the landslide activity on these slopes. The recent landslides here have largely been associated with slope deposits, including peat and topsoil as well as the underlying layers of colluvium. The colluvium comprises sandy to gravelly silts and clays, with varying amounts of cobbles and boulders. The colluvium deposits on this slope represent earlier phases of slope instability (BGS, 2012).

Figure 3-1. Site location within Scotland. (BGS)

3.3.2 Field survey

A number of field surveys were conducted between 2015 and 2017. Soil profile was examined by inspection of a number of landslide scarps still visible at the site. Figure 3-2a shows one of these scarps where three soil horizons can be identified: topsoil, transition soil, and subsoil. Overall, the layers overlying the bedrock form a cover that is approximately 1 m.

The soil horizons were also inspected using an open-end sampler as shown in Figure 3-2b. It is interesting to notice that the penetration depth does not coincide with the length of the soil column in the sampler. When forcing the sampler into the ground, the top soil reduced in volume significantly due to its very open structure and, hence, high compressibility.

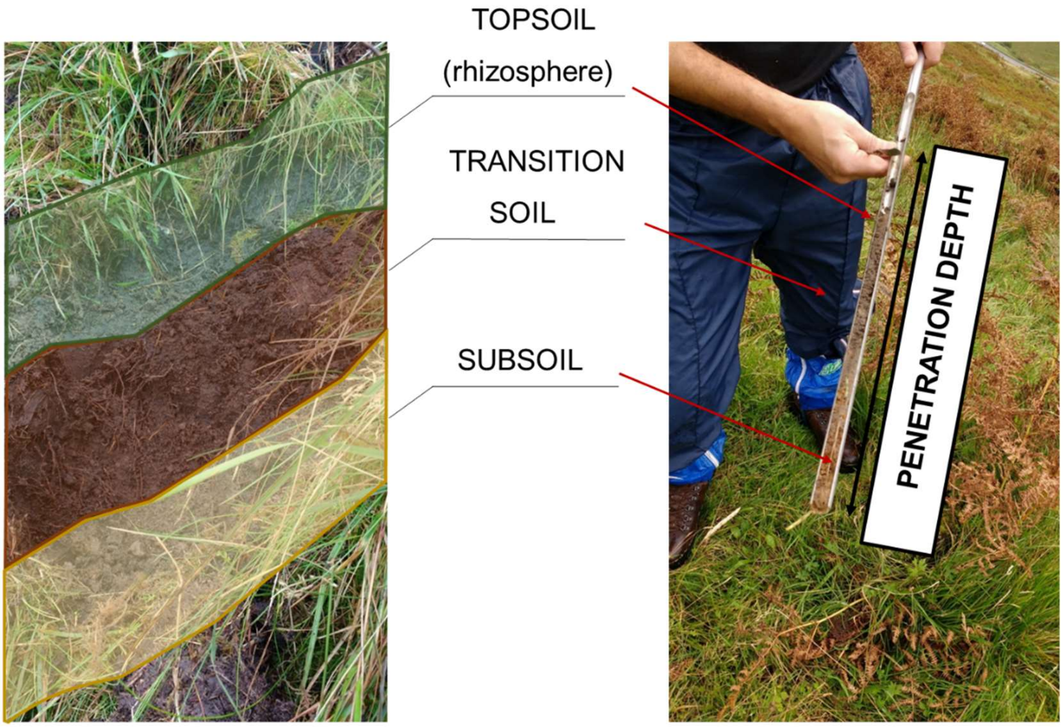

Figure 3-2. Identification of the soil horizons at Rest and Be Thankful. (Field Campaign 2017)

The top soil is associated with the rhizosphere, the narrow region of soil that is directly influenced by root secretions and activity of soil microorganisms. The topsoil extends for approximately 25-30 cm as shown in Figure 3-3 where the depth of the rooting zone can be clearly detected.

Figure 3-3. Observation of the Topsoil Depth. (Field Campaign 2017)

In terms of grain size distribution, the three horizons are very similar as shown in Figure 3-4, suggesting that the three horizons have the same geological origin (glacial till). The biological activities taking place in the rhizosphere have just promoted soil aggregation giving rise to more open (lower density) texture.

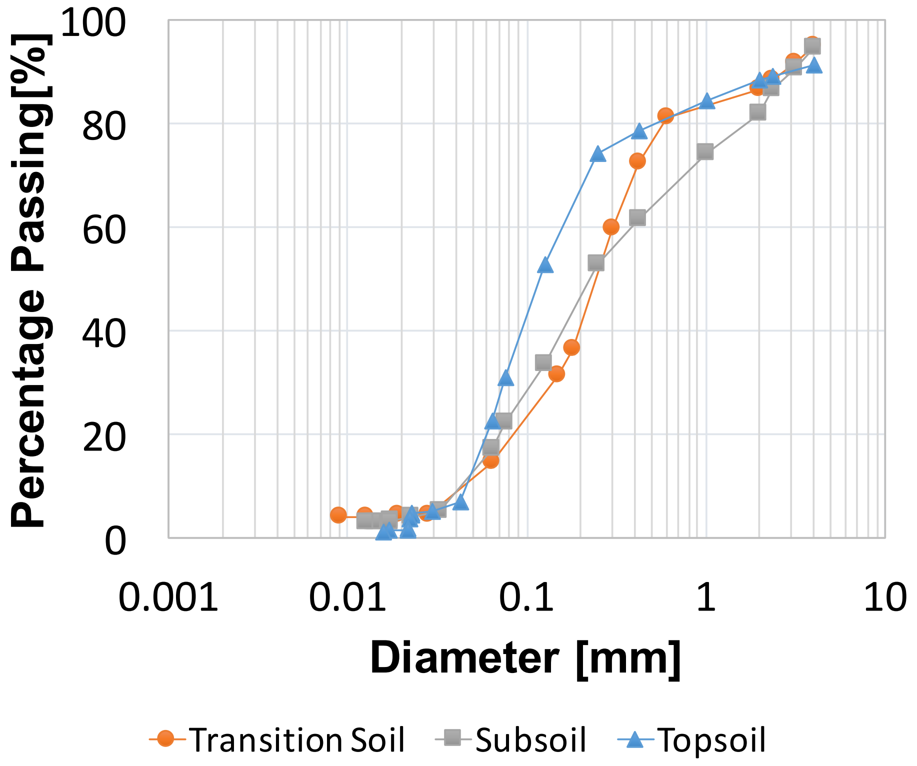

Figure 3-4 Grain Size distribution of Transition soil, Subsoil and Topsoil.

A distinctive feature of the slope morphology is the presence of gullies cutting the planar slope parallel to the dip direction. These gullies are spaced between 30 and 50 m. The gullies are characterised by a relatively thin soil cover and appears to be always saturated. Figure 3-5 shows the saturated nature of the soil cover in the gully as observed after several days without rain.

Figure 3-5. Evidence of the saturation state of the soil in the gullies.

3.3.3 The landslide case studies

Rest and Be Thankful has been a source of problem for mobility in Scotland for years. The A83, which runs along the perimeter of the Rest and Be Thankful slopes, has been closed on a several occasions due to rainfall-induced landslides, causing significant disruption to local traffic. Only in the past 4 years, the A83 has been closed 5 times due to the instability of the slopes and the falling of landslides material on the road.

The two events analysed in the present work are the landslides events of the 1st of December 2011 and 1st of August 2012 (Figure 3-6). Those events have been chosen because the rainfall data available covered only the period going from January 2011 to January 2013. Both the events happened after a period of heavy rainfall, which triggered the movement of up to hundreds of tons of soil.

The December 2011 landslide occurred after 65.8mm of rain, a quarter of the December's expected average for the area, fell in 48 hours. The road was subsequently closed in both directions resulting in a 26-mile diversion. The road was kept closed for several days, as it was not safe for the engineers to stay on field.

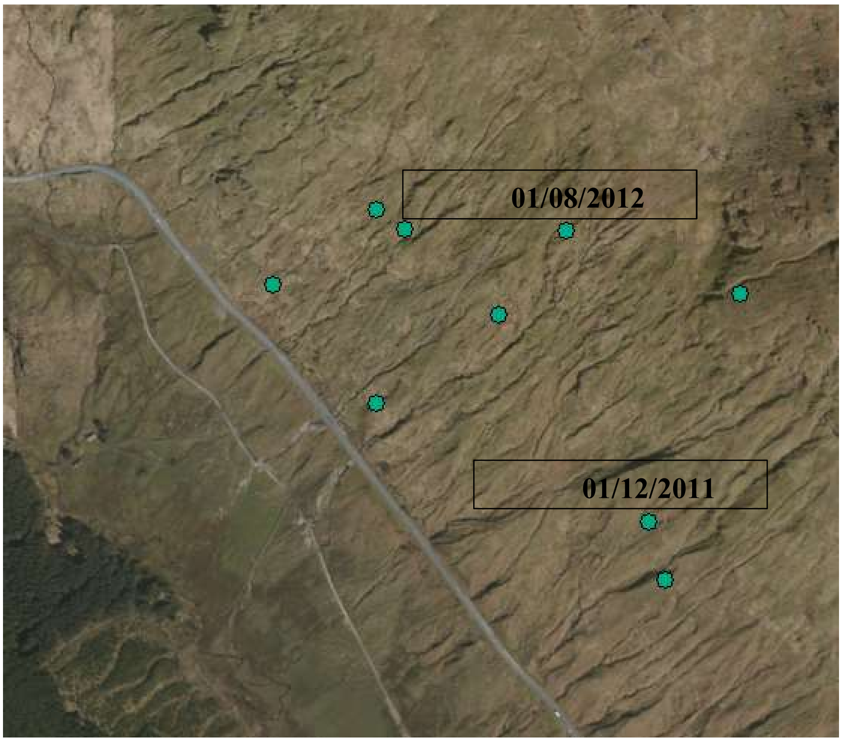

Figure 3-6. Areal Picture of the Rest and Be Thankful site. Relative position of the two landslides events analysed in the present work. (BGS; Google Earth)

The landslide is a translational slide that has degraded into a flow as it has passed over a local break of slope, moving approximately 100 tonnes of material. In the lower section of the slope it was exploited a small gully (Figure 3-7).

Figure 3-7. December 2011 Landslide. BGS (c) NERC [2011].

Figure 3-8 shows the debris flow of August 2012 blocking the road. This event happened following a period of heavy rainfall. The clean-up operation took more days than expected as it was not safe for the engineers to stay too long on site.

Figure 3-8. August 2012 Landslide. 'BGS (c) NERC [2012].

3.3.4 Laboratory investigation of hydraulic conductivity of soil horizons

The saturated hydraulic conductivity of the three soil horizons was measured in the laboratory on samples collected in the field.

The saturated hydraulic conductivity of the topsoil was measured on a specimen 80 mm diameter and 20 mm high cut in the laboratory from a block taken from the field. The specimen was placed in an oedometer cell and subjected to 3 kPa vertical stress. A steady-state water flow was established with a hydraulic head differential of 14 cm. Water flow was measured by monitoring the change in water mass of the upstream reservoir using a balance.

The saturated hydraulic conductivity of the transition soil and the subsoil were measured on samples still in the sampling tubes used to collect the soil from the field. The sampling tubes were placed on the pedestal of a triaxial cell and filled with water up their top. The pedestal of the triaxial cell was then connected to a water reservoir to establish a hydraulic head differential of 10 cm. Water flow was measured by monitoring the change in water mass of the downstream reservoir using a balance.

The saturated hydraulic conductivity tests were carried out at low pore-water pressures (up to 1-1.5 kPa) to achieve conditions of ‘field-saturation’, i.e. the maximum level of saturation practically achieved in the field due to pressure heads developed by ponding water.

The reason for the two different procedures used to measure the hydraulic conductivity (oedometer cutting ring for the top soil and sampling tube for transition soil and subsoil) lies on the different texture of the soils. The topsoil is very compressible and any sampler/cutting ring should have a very low height to diameter ratio to minimise the disturbance of the shear stresses developing at the inner surface of the sampler/ring during insertion into the soil. A large oedometer cutting ring cannot be used in the field as the soil sample is difficult to withdraw.

On the other hand, the sample can be easily cut and trimmed from a block sample transported to the laboratory. Block samples could not be easily taken from the lower horizons (transition soil and subsoil) due to the cohesionless nature of these soils and the large excavation that would be required to extract block samples from greater depths.

The field-saturated hydraulic conductivity measurements are summarised in Table 3-1. It is clearly shown that the topsoil (rhizosphere) has hydraulic conductivity significantly higher than transition soil and the subsoil.

3.4 DEVELOPMENT OF A PHYSICALLY-BASED MODEL FOR THE CASE STUDY

3.4.1 Hydraulic model

3.4.1.1 Geometry

Figure 3-9 shows a 3D schematic view of a portion of the hillslope. The hillslope is crossed by gullies (schematised as vertical wall channels in the figure) and it can be therefore subdivided into a main hillslope, a side slope, and a gully. The soil formation overlies a bedrock formation.

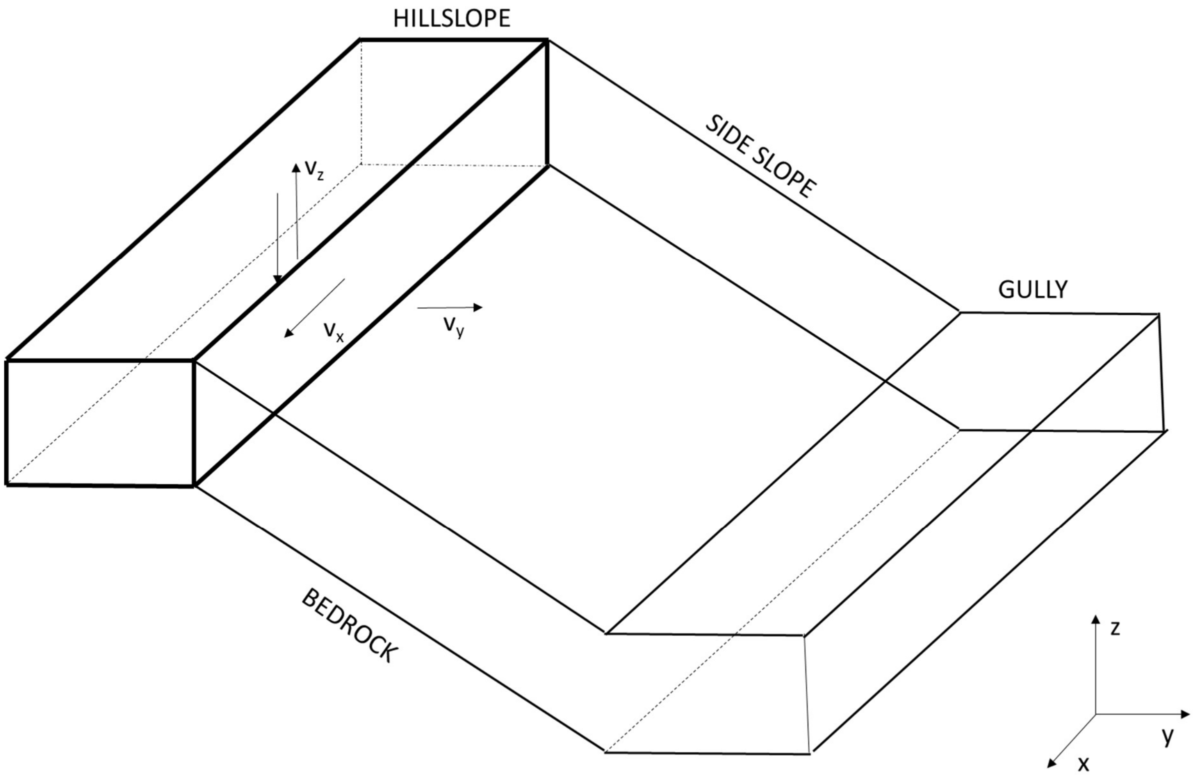

Figure 3-9. Schematic layout of the hillslope.

Although the problem is 3-D, a full 3D hydraulic model would be difficult to implement because of the computational burden and the uncertainties associated with the geotechnical characterisation of the slope (geometry and hydro-mechanical parameters). Simplifications in the hydraulic model were therefore pursued.

It was assumed that flow in x-direction could be neglected since the length of the slope in x-direction is significantly larger than the dimensions in the cross section (y- and z- directions). As a result, flow was assumed to occur only in z-direction (associated with rainfall and evapotranspiration at the ground surface) and y-direction (associated with lateral drainage into the gully) as shown in Figure 3-10.

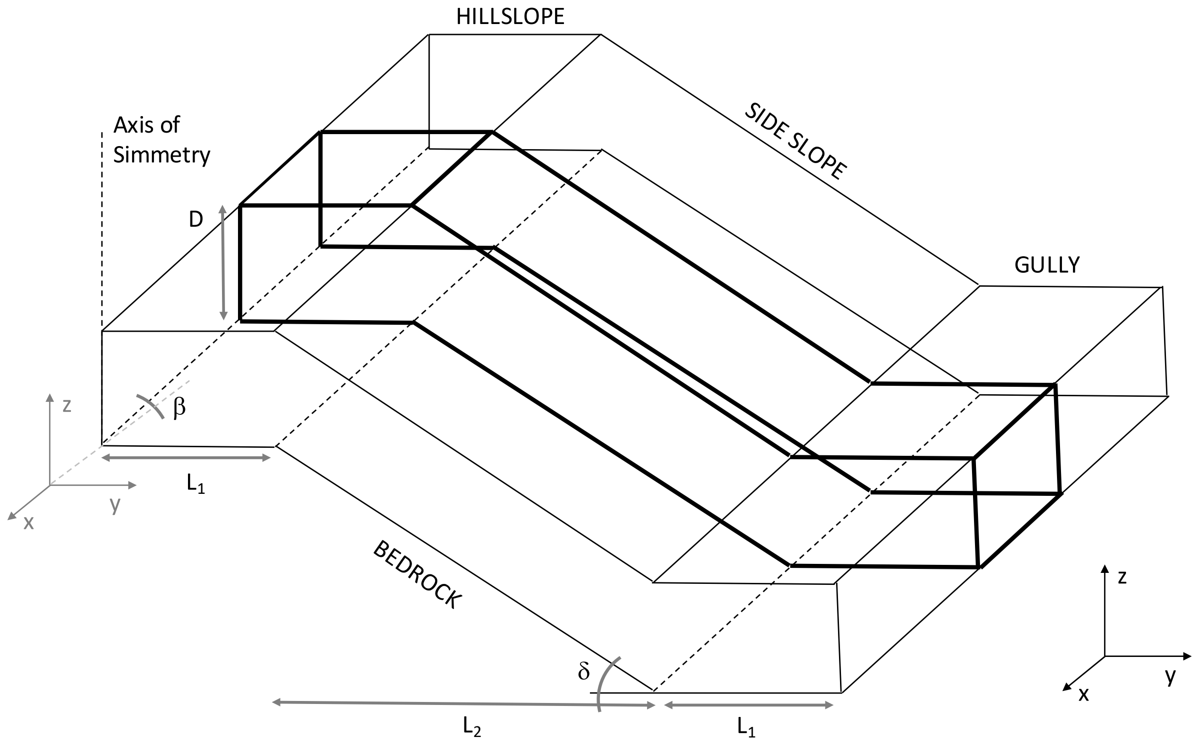

Figure 3-10. Two- dimensional hydraulic model.

The geometrical parameters of the two slopes analysed in this work are summarised in Table 3-1. The angle β is defined as the inclination of the hillslope with reference to the horizontal plane x-y.

Table 3-1. The geometrical parameters of the two slopes analysed.

Landslide Event	β °	δ °	**D** *m*	L_1 *m*	L_2 *m*
December 2011	35	25	0.9	5	12
August 2012	35	30	0.9	5	12

3.4.1.2 Water flow equation

Rainwater infiltration within the slope was modelled using Darcy's law, extended to the case of unsaturated soils:

$$\vec{v} = -K \text{ grad } (\psi) = -K \text{ grad} \left(z + \frac{u_w}{\gamma_w} \right) \quad \textbf{[3-1]}$$

where v = flow velocity vector; ψ = piezometric head; K = hydraulic conductivity; u_w = pore water pressure; γ_w = density of soil water; and z = vertical coordinate increasing upward. The hydraulic conductivity K depends on the degree of saturation, which in turn depends on pore water pressure.

The mass balance equation for liquid water can be written as follows:

$$\text{div}\vec{v} + \frac{\partial \theta}{\partial t} = 0 \quad \textbf{[3-2]}$$

where θ = volumetric water content (ratio of water volume to total volume); and t = time. By substituting Equation 3-1 in Equation 3-2, the Richard's equation in terms of piezometric head is obtained:

$$C \frac{\partial \psi}{\partial t} = \text{div}[K \text{ grad}(\psi)] \quad \textbf{[3-3]}$$

where $C = \gamma_w(\partial\theta/\partial u_w)$, referred to as water capacity of the soil.

The water flow Equation 3-3 was solved numerically via the FEM using the module SEEP/W of the software Geostudio. The soil constitutive functions required to solve Equation 3-3 include the water retention function $\theta=\theta(uw)$ and the hydraulic conductivity function $K=K(u_w)$.

3.4.1.3 Water retention functions

A 2-parameter Van Genuchten function (1990) was selected to simulate water retention behaviour of the three soil horizons:

$$S_r = (1 + \alpha(s)^{n})^{-\left(1-\frac{1}{n}\right)} \quad \text{[3-4]}$$

where α and *n* are empirical soil parameters.

The parameter n controls the slope of the tangent to the water retention curve at the inflection point. To derive this parameter, the water retention data-points for the three horizons were first derived from the Arya and Paris (1981) pedo-transfer approach. Each set of data-points were fitted using a Van Genuchten function and the average value of the parameter n was used for all water retention curves of the three soil horizons (n=1.5).

The parameter α was then estimated by constraining the water retention function to pass through a single water retention data points derived from field measurement. At given depth, suction was measured with a high-capacity tensiometer (Tarantino et al., 2003) inserted at the bottom of a 22-mm diameter borehole.

Degree of saturation was determined on sub-samples withdrawn using the open-end sampler. To this end, a soil segment was isolated in the tube sampler and trimmed to make it level with the rim of the open-end sampler. The measurement of the length of the segment together with the geometry of the cross-section of the open-end sampler made it possible to estimate the volume of the sub-sample (Figure 3-11). The sub-sample was then cleared away from the sampler, stored in a self-sealed plastic bag, and its wet and dry mass measured once back to the laboratory.

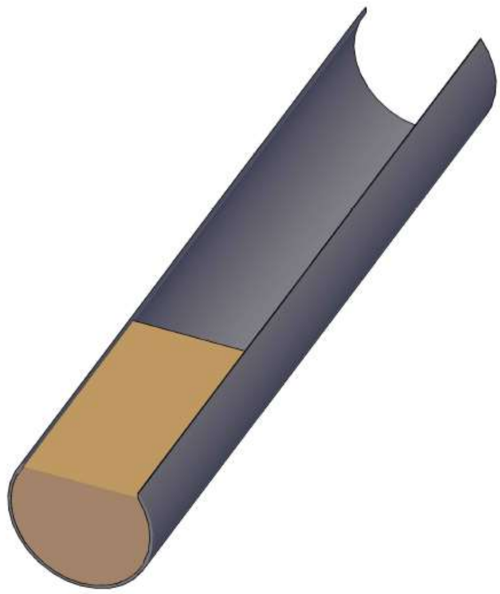

Figure 3-11 Cross Section of the open-end sampler.

The three water retention curves passing through the single experimentally determined water retention data point are shown in Figure 3-12a. It is worth noticing that the degree of saturation at zero suction was set equal to 85%, which is a reasonable value for the degree of saturation attained at zero suction along a wetting path.

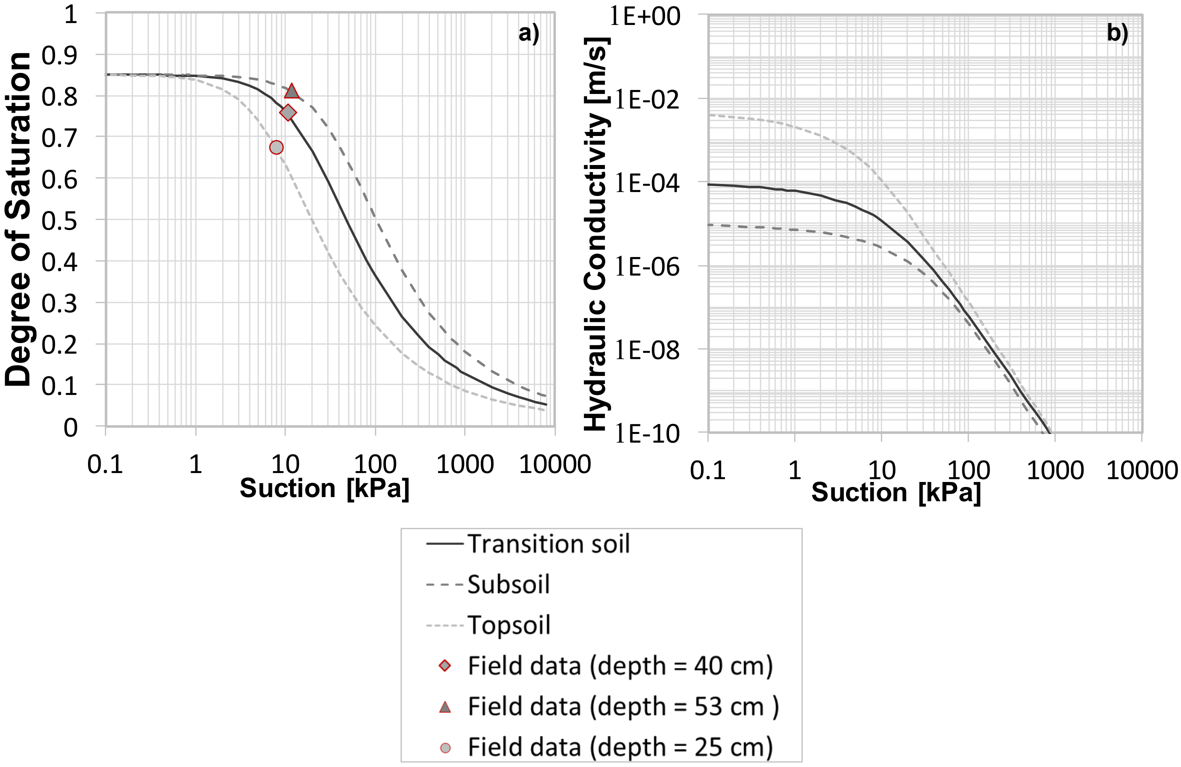

Figure 3-12. (a)Water retention curves for the materials used in the analysis. (b) Hydraulic conductivity curves.

3.4.1.4 Hydraulic conductivity functions

The hydraulic conductivity functions for the three soil horizons were determined by combining the field-saturated hydraulic conductivity k_{sat} measured from laboratory testing (Table 3-1) and the relative hydraulic conductivity k_r estimated from the water retention parameters. The unsaturated hydraulic conductivity was modelled via a Mualem-Van Genuchten function (Mualem 1976).

$$k = k_s S_r^{0.5}[1 - \left(1 - S_r^{n/n-1}\right)^{1-\frac{1}{n}}]^2 \quad [3\text{-}5]$$

where k_s is the saturated hydraulic conductivity, S_r is the degree of saturation and n is an empirical parameter reported in Table 3-2 for all the horizons.

Table 3-2. Hydraulic Parameters for the soil horizons.

	n*	$\theta_{suc=0}$	θ_r	α	n	m	k_s
		-	-	*1/cm*	-	-	*m/s*
Topsoil	0.78	0.663	0.01	0.013	1.5	0.333	0.005
Intermediate	0.75	0.63	0.01	0.0054	1.5	0.333	0.0001
Sub Soil	0.72	0.612	0.01	0.0025	1.5	0.333	0.00001

3.4.1.5 Hydraulic boundary conditions

The boundary conditions for the numerical model consist of:

- Water inflow imposed at the top boundary (to simulate rainfall)
- Water outflow at 10 cm below the ground surface (to simulate evapotranspiration from the root system)
- Impermeable bottom boundary (to simulate the bedrock)

The first two boundary conditions are discussed in more detail hereafter.

3.4.1.5.1 Rainfall

Rainfall data were made available by Transport Scotland, which has given a considerable contribution to this research by sharing the data collected by their instruments. Figure 3.13 shows the rainfall data from the 1st of January 2011 until the 1st of January 2013.

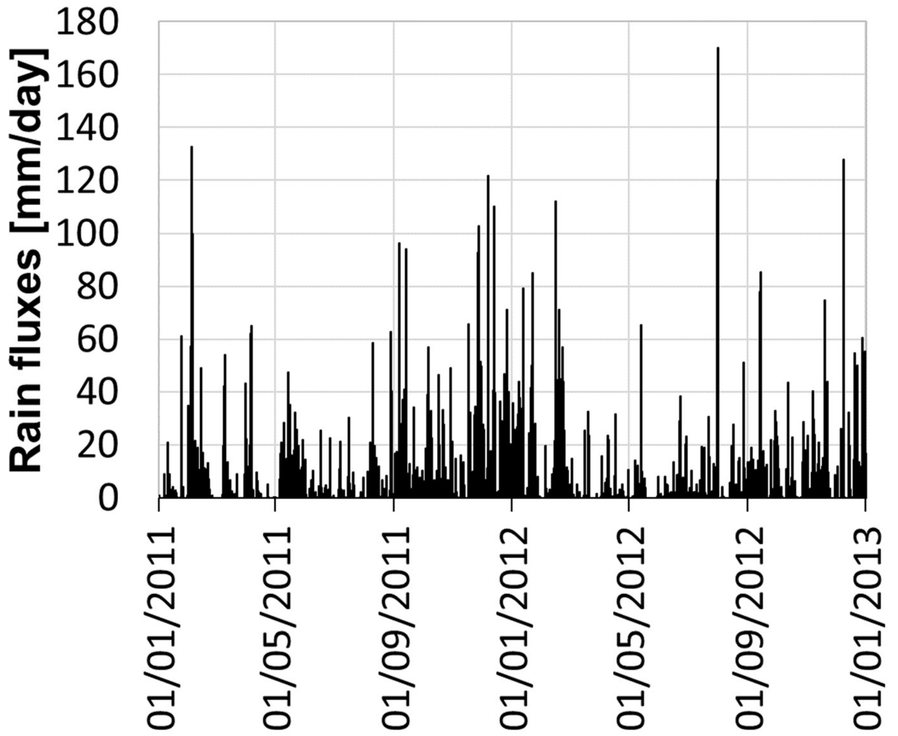

Figure 3-13. Rain fluxes from 01/01/2011 to 01/01/2013 used as boundary condition for the analysis.

3.4.1.5.2 Potential Evapo-Transpiration

The evapo-transpiration fluxes in the energy-limited regime (potential evapo-transpiration) were calculated using the Penmann-Monteith equation (Monteith 1965)

$$ET_0 = \frac{\Delta(1-\alpha)R + \rho_a c_p e_s \dfrac{(1-RH)}{r_a}}{\Delta + \gamma(1 + \frac{r_s}{r_a})} \qquad \textbf{\textit{[3-6]}}$$

For details regarding the variables involved in the equation the reader can be refer to Chapter 2. The *canopy resistance* r_s was assumed equal to 45 s m^{-1} as suggested from Allen 1998, by assuming a crop height of 0.50 m.

The *solar radiation R*, the *relative humidity RH*, the *temperature T*, and *wind speed u* were taken from an open access database (www.worldweatheronline.com for temperature, relative humidity, and wind speed and re.jrc.ec.europa.eu for solar radiation) by considering the weather station as close as possible to the landslide areas. The monthly evapo-transpiration flux calculated using Equation 3-6 is shown in Figure 3-14.

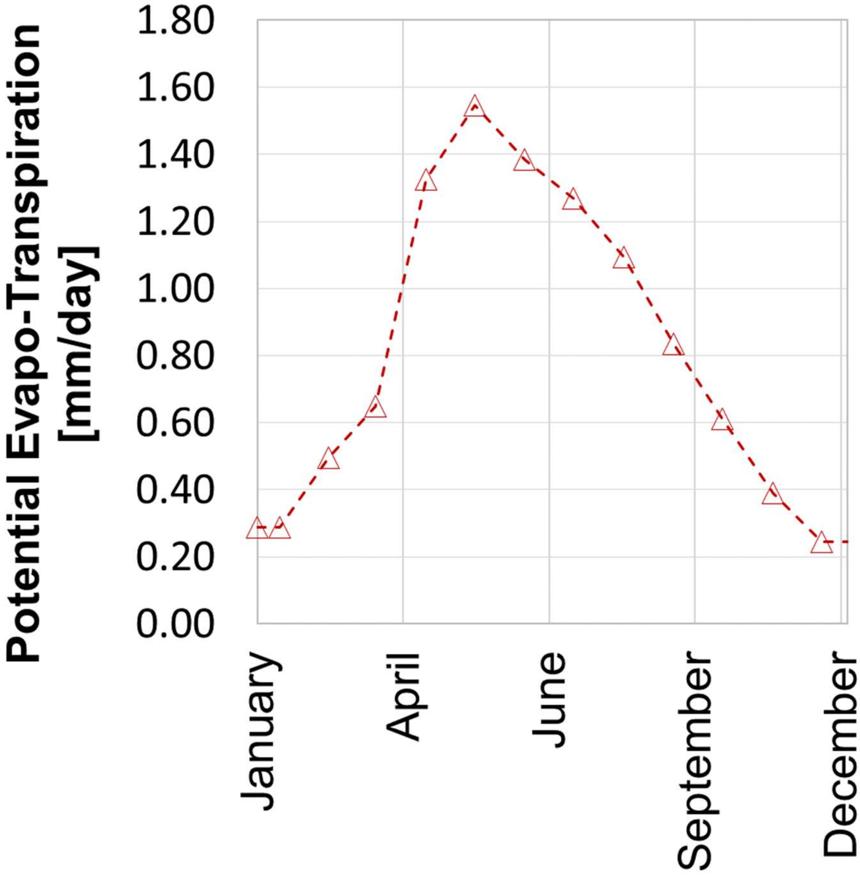

Figure 3-14. Potential Evapo-Transpiration deriving from the Penmann-Monteith formula.

3.4.1.5.3 Water limited evapotranspiration

Potential evapo-transpiration is defined as the atmospheric demand of water from the soil-plant system. If the water availability of the system is enough to accommodate the atmospheric demand, then the water outflow will happen to be coincident with the potential evapo-transpiration.

However, very often there are cases where the atmospheric demand may overcome the availability of the soil-plant system or it may be found in low moisture conditions. If this is the case the soil-plant system will control the actual evapo-transpiration rate, as it won’t be able to accommodate the atmospheric demand any more (water- limited regime).

The reduction of water outflow in the water limited regime can be modelled via a reduction function that relates the ratio between actual and potential evapotranspiration to the suction at the water extraction.

The approach developed in Section 2.4.1.2.3 has been adopted to calibrate the two parameters of the reduction function. A soil column 0.9 m high was considered, and two different hydrostatic initial conditions have been applied. The first one is associated with a suction of 0 kPa at the base of the column while the second is associated with a suction of 10 kPa at the base of the column. Figure 3-15a show the evolution of suction at the top of the column over time. Figure 3-15b shows the time derivative of suction with respect to suction. The suction of 3000 kPa has been chosen for s0 (see Figure2-17).

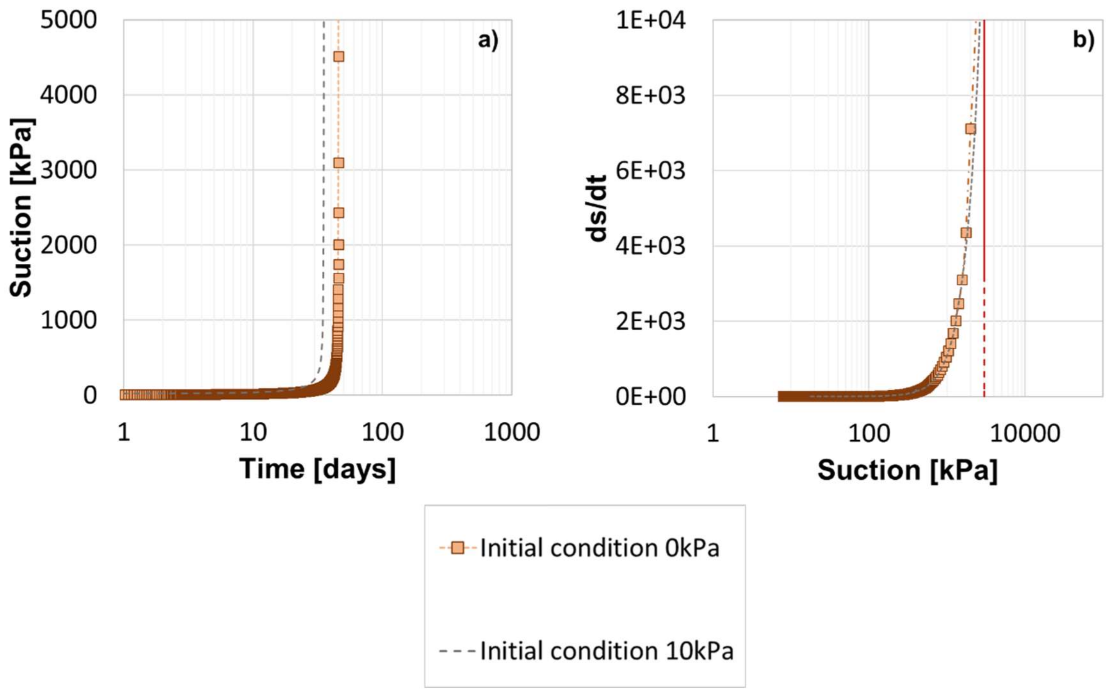

Figure 3-15. Evolution Identification of the limit suction value.

Figure 3-16 shows the result of the analyses made to identify the second parameter characterising the reduction function (Ref. Section 2.4.1.2.3).

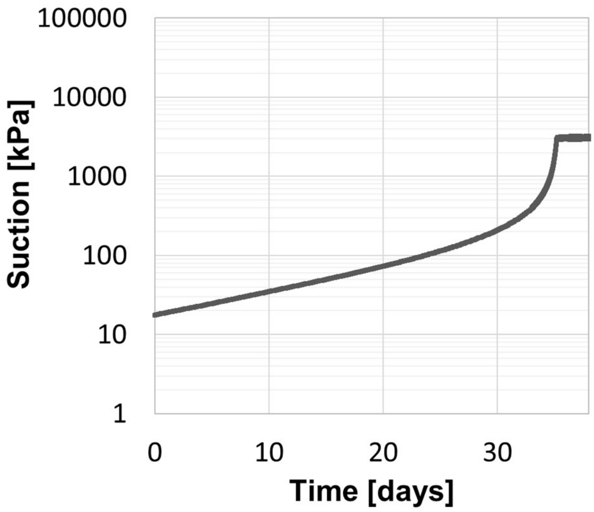

Figure 3-16. Identification of the value of suction at which the Actual Evapotranspiration goes to zero.

Finally, the reduction function adopted for the purpose of this study is shown in Figure 3.17.

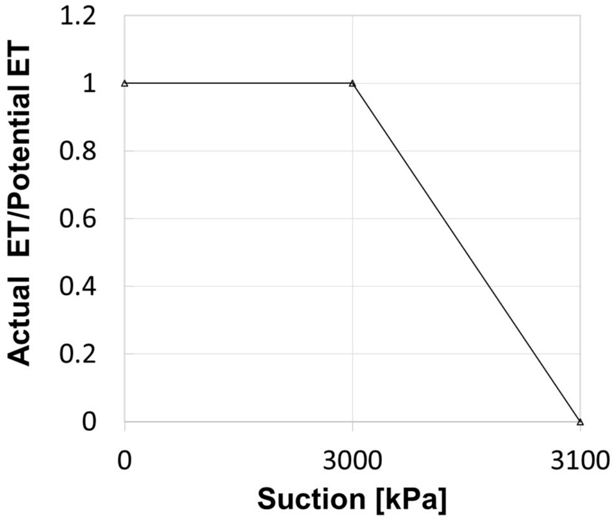

Figure 3-17. Final reduction function.

3.4.1.6 Initial condition and validation of the hydraulic model

The approach suggested in the Sections 2.4.1.3 and 2.4.1.4 has been used to identify the right initial condition for the transient numerical analyses and to validate the hydro-mechanical model built for the Rest and be Thankful case study.

The period from 1 January 2011 to 1 January 2013 was analysed (encompassing the two landslide events occurred on 1 December 2011 and 1 August 2012). Figure 3-18 shows the three initial ‘arbitrary’ hydrostatic conditions.

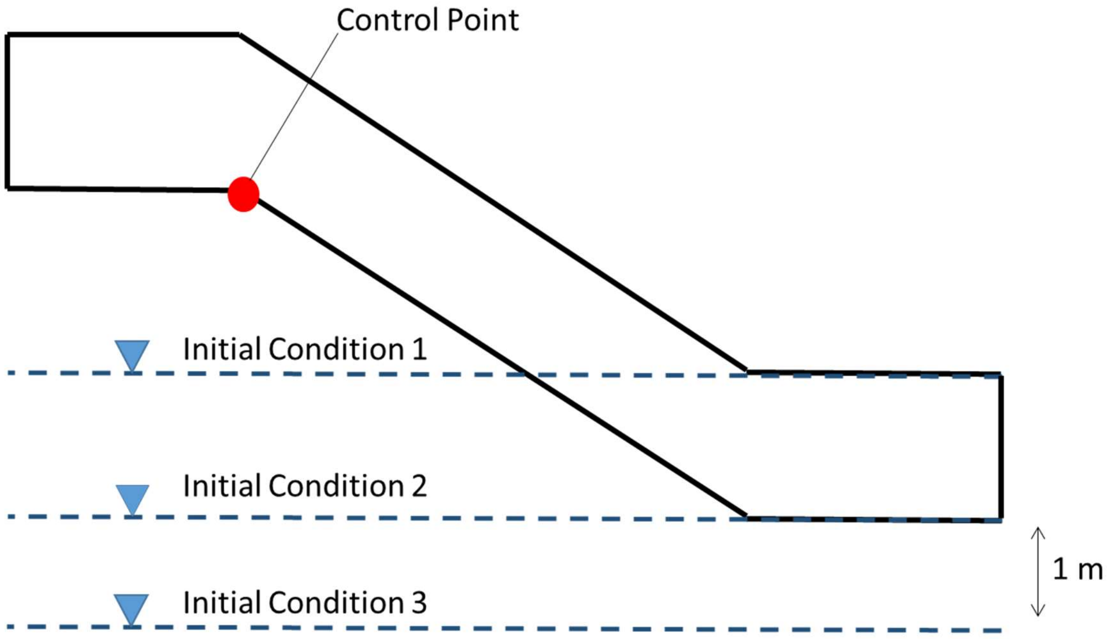

Figure 3-18. Arbitrary initial conditions chosen for the analysis.

The results from these analyses are shown in Figure 3-19 in terms of suction at the bottom boundary of the hillslope versus time.

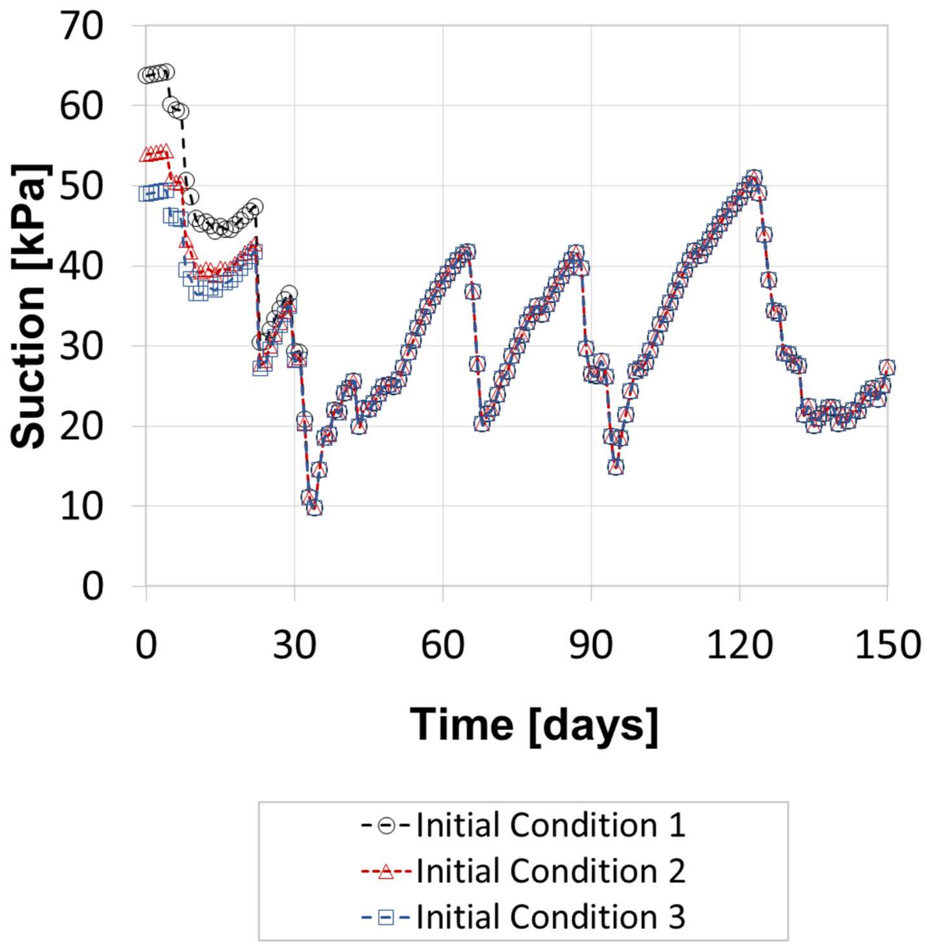

Figure 3-19. Cancellation of the initial condition and validation of the hydro-mechanical model.

Once again, it can be observed that:

i) The track of the (arbitrary) initial condition is eventually lost after about 1 month.

ii) After the convergence, suction tends to fluctuate around an average value that tends to remain constant over time.

Condition ii) was taken as an evidence of the robustness of the hydraulic model assumed in terms of boundary conditions and 2-D geometry.

3.4.2 Mechanical model

3.4.2.1 Shear strength

The saturated shear strength for the top and the transition soils was determined experimentally in the laboratory on samples collected in the field using a square cutter 60 mm side. Samples were transferred to the shear box frame using a wooden piston and saturated overnight by flooding the shear box container. Specimens were then loaded in steps to 100kPa and 200 kPa and sheared at the shearing displacement rate of 0.033 mm/min.

The topsoil showed it to have friction angle ϕ' = 12° and an effective cohesion c'=50 kPa. The high cohesion c' is generated by the fine root system in the specimen. The transition soil exhibited a failure envelope in the Mohr-Coulomb plane (normal stress σ' versus tangential stress τ) passing though the origin. Shear strength parameters were therefore characterised by an effective by cohesion c'=0 kPa and a friction angle ϕ' = 36°. This strength was also associated with the subsoil due to the very similar grain size distribution.

The shear strength τ in the unsaturated range was modelled according to Tarantino and El Mountassir (2013):

$$\tau = c' + (\sigma - u_w S_r) \cdot \tan\phi' \quad \textbf{[3-7]}$$

where σ is the total normal stress, c' is the cohesion, u_w is the pore-water pressure, S_r is the degree of saturation, and ϕ' is the friction angle.

3.4.2.2 Geometry

The stability problem is 3-D in principle. However, failures in the -transverse direction (plane y-z) were not considered due to the lower slope inclination compared to the slope dip direction.

Instabilities were therefore assumed to occur only in the direction of the maximum slope (hillslope) as corroborated by experimental observations of historical landslides. Considering that the thickness of the soli cover (less than 1m) is much lower that the length of the slope (a few hundredths of meters), an infinite slope model seemed appropriate to interpret hillslope movements. As a result, failure was modelled as a translational movement in the x-z plane Figure 3-20.

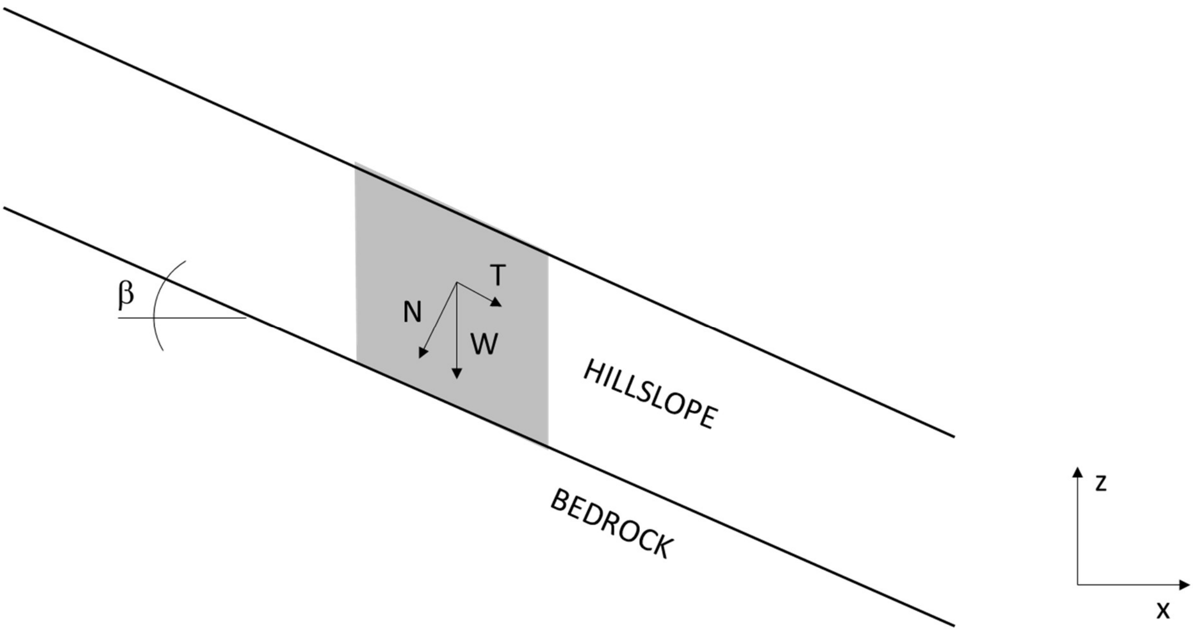

Figure 3-20. Mechanical model infinite slope.

3.4.2.3 Factor of Safety

The factor of safety at any depth can be derived via the limit equilibrium method. By considering the shear strength criterion given by Equation 24 the following equation can be derived

$$\mathrm{FoS} = \frac{\tan\phi'}{\tan\beta} + \frac{-u_w S_r \cdot \tan\phi'}{(\bar{\gamma}H) \cdot \sin\beta \cdot \cos\beta} \tag{3-8}$$

where H is the depth of the failure surface, β is the inclination of the slope, and $\bar{\gamma}$ is the average unit weight given by:

$$\bar{\gamma} = \frac{1}{H}\int_0^H [\gamma_s(1-n^*) + \gamma_w n^* S_r]dz \tag{3-9}$$

where γ_s and γ_w are the unit weight of solids and water respectively, and n^* is the porosity.

Table 3-3. Mechanical properties for the soils.

	γ_{dry} *kN/m³*	ϕ' °	c’ *kPa*	G_s -
TOPSOIL	2.88	12	50	1.31
INTERMIDIATE	7.12	36	0	2.85
SUB SOIL	6.84	36	0	2.44

3.5 THE ROLE OF THE RHIZOSPHERE ON THE OCCURRENCE OF SHALLOW LANDSLIDES.

3.5.1 Validation of the physically-based model for the shallow landslide

The physically-based numerical model was first challenged to reproduce failure of the two historical landslides analysed in this work. The evolution of the profile of Factor of Safety (FoS) over time at the centre of the hillslope (axis of symmetry in Figure 3-10) is shown Figure 3-21a and Figure 3-22a for the Landslide ‘December 2011’ and the Landslide ‘August 2012’ respectively. It can be observed that the minimum factor of safety always occurs at the base of the hillslope at the interface with the bedrock.

The evolution of the Factor of Safety (FoS) at the base of the slope over time is shown in Figure 3.21b and Figure 3-22b for the December 2011 and August 2012 landslides respectively. The failure condition simulated by the physically-based model is associated with the FoS becoming slightly less than unity. It can be observed that the time of failure predicted by the physically-based model matches the time of failure satisfactorily with a discrepancy of 4 days for the December 2011 landslide and 2 days for the August 2012 landslide respectively.

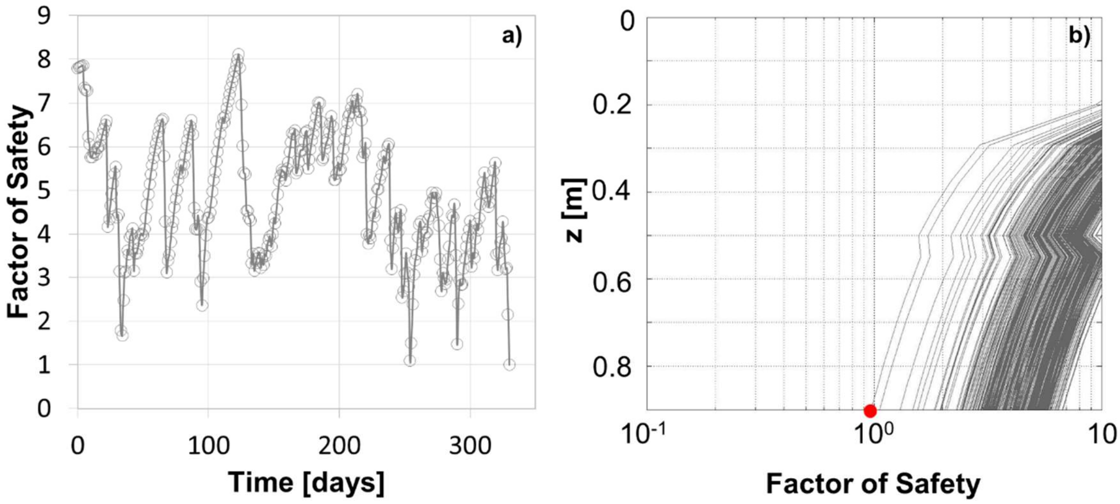

Figure 3-21. Landslide Event: 01/12/2011 (a) Evolution of the minimum Factor of Safety until the time of failure. (b) Evolution of the Factor of Safety profile and highlight of the failure surface.

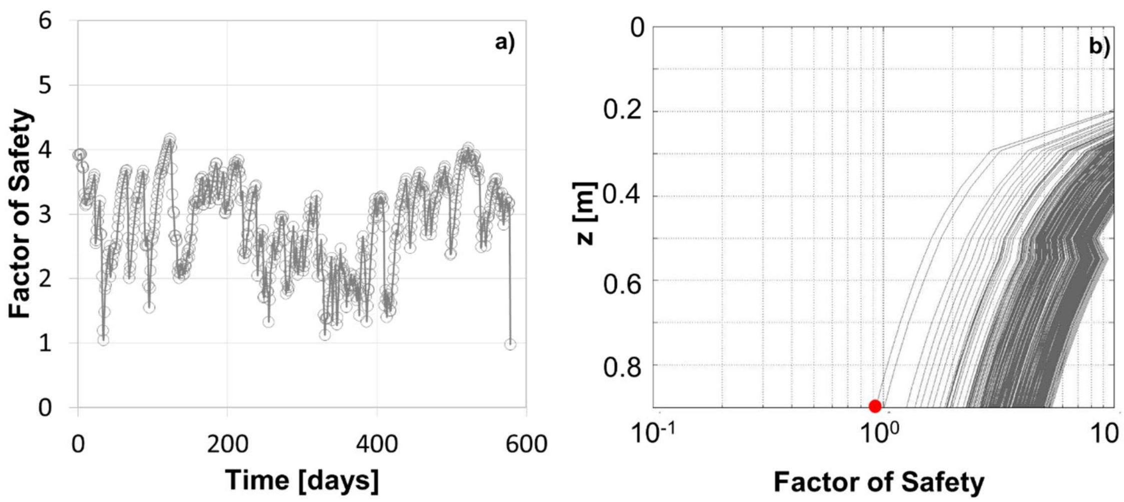

Figure 3-22. Landslide Event: 01/08/2012 (a) Evolution of the minimum Factor of Safety until the time of failure. (b) Evolution of the Factor of Safety profile and highlight of the failure surface.

The two failures are associated with heavy rainfall occurring over a period of a few days preceding the landslide event (Figure 3-13). It is interesting to observe that a heavy rainfall event also occurred in February 2011 without triggering slope failures (in both the numerical simulation and the real world). It is also interesting to observe that the same rainfall event on December 2011 triggered failure at one location only (Landslide ‘December 2011’).

It appears evident that the amount of rainfall cumulated over a few days is not the only triggering factor and other aspects control the landslide mechanism. It is interesting to interrogate the physically-based numerical model to explore the hydro-mechanical processes leading to failure initiation.

Figure 3-23 shows that pore water pressure contours and the flux vectors for the Landslide ‘December 2011’ at two distinct times, February 2011 (heavy rainfall not causing failure) and December 2011 (heavy rainfall causing failure) respectively.

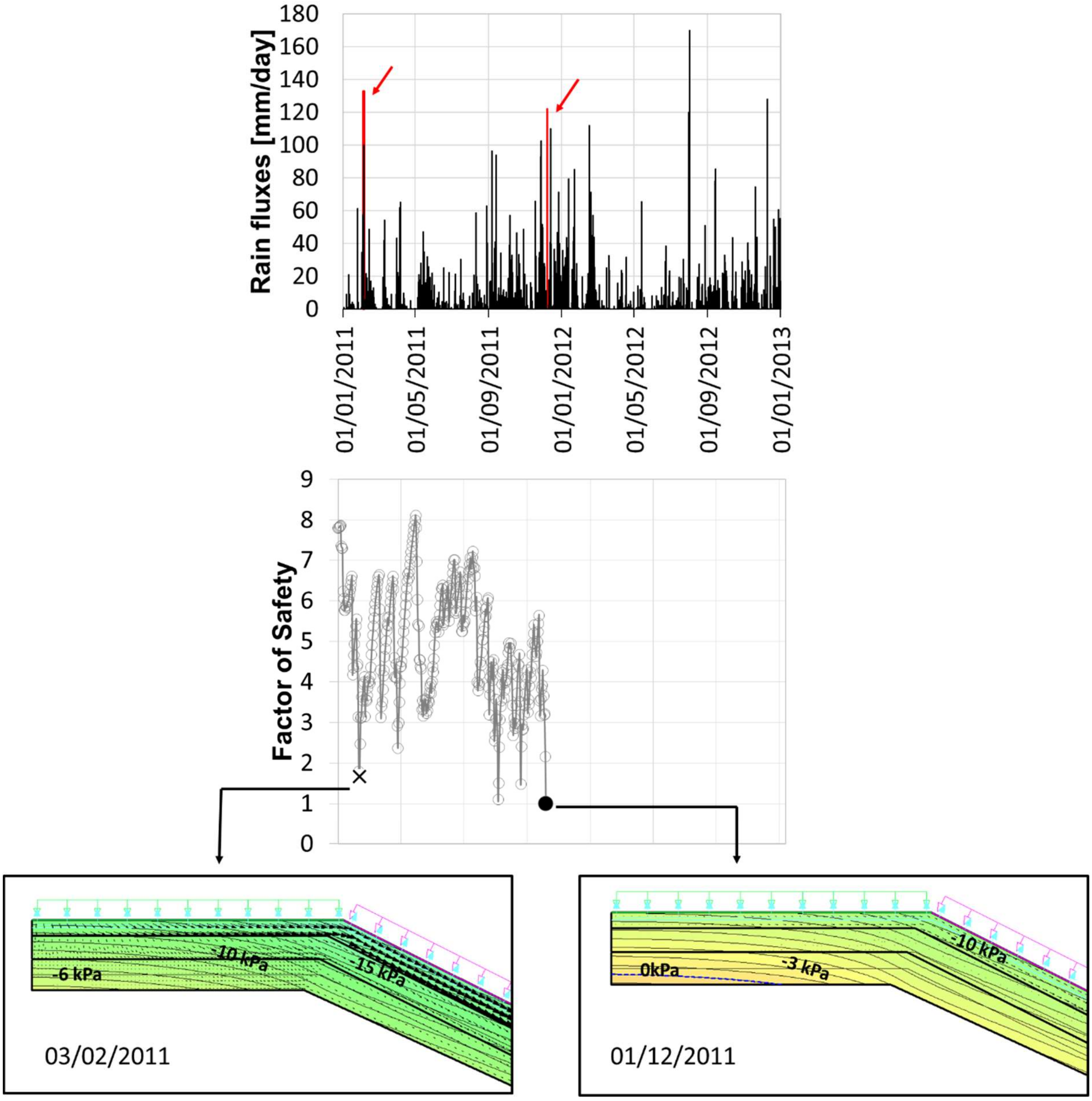

Figure 3-23. Pore water pressure contours and the flux vectors for the Landslide 'December 2011' at two distinct times, February 2011 (heavy rainfall not causing failure) and December 2011 (heavy rainfall causing failure).

It can be observed that pore-water pressures on February 2011 (not causing failure) are lower (more negative) than the pore-water pressures on December 2011, where pore-water pressure becomes positive at the base of the slope as shown by the formation of a phreatic surface (Figure 3-23). At the same time, it can be observed that flux vectors on February 2011 highlight a predominance of lateral flow in the rhizosphere whereas flux vectors on December 2011 shows a significant component of downward flow, which led eventually to the formation of a phreatic surface at the base of the slope.

This different hydrological response of the slope is controlled by the antecedent rainfall, which is significantly lower on February 2011. The lower antecedent rainfall maintains low the degree of saturation and, hence, the hydraulic conductivity of the transition soil and subsoil. This promotes the diversion of rainwater ‘channelled’ by the topsoil (rhizosphere) on the main rainfall event and preserves the pore-water pressure in the bottom layers.

It is also interesting to compare the pore water pressure contours and the flux vectors on December 2011 for the two landslides, Landslide ‘December 2011’ (heavy rainfall causing failure) and Landslide ‘August 2012’ (heavy rainfall not causing failure) respectively (Figure 3-24 and Figure 3-25).

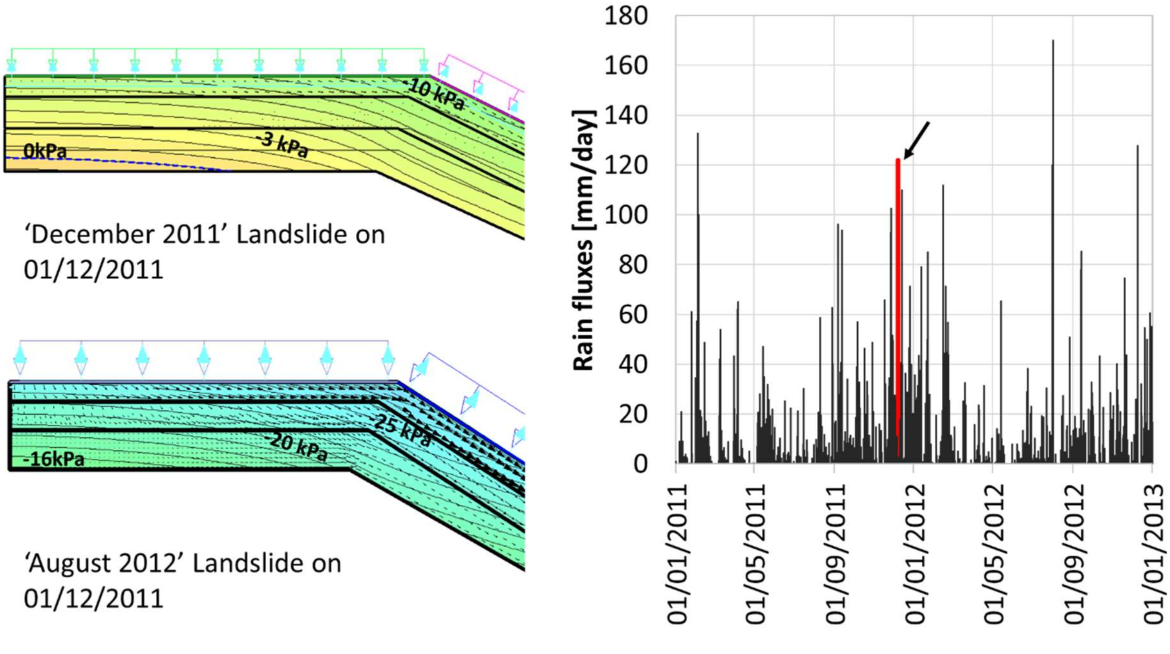

Figure 3-24. Pore water pressure contours and the flux vectors on December 2011 for the two landslides, Landslide ‘December 2011’ (heavy rainfall causing failure) and Landslide ‘August 2012’ (heavy rainfall not causing failure).

It can be observed that the of pore water pressure distribution and the flow direction pattern is very similar. However, a phreatic surface only forms for the Landslide 'December 2011'. This is associated with the slightly lower 'drainage' capacity of the side-slope for the Landslide 'December 2011', in turn associated with the lower inclination of the side-slope (25° for the Landslide 'December 2011' against 30° for the Landslide 'August 2012').

3.5.2 Effect of the rhizosphere

To highlight the role of the rhizosphere in creating a subsurface lateral drainage, an exercise was developed for comparison by considering the case where rhizosphere is not present. The slope was assumed to be formed by a homogenous soil profile with hydraulic properties equal to the ones of the subsoil.

The comparison of the pore water pressure contours and the flux vectors for the two cases is shown in Figure 3-25 (by considering antecedent and incident rainfall on February 2011). It can be clearly observed that the rhizosphere diverts the incident rainfall thus preserving low water pressures in the deeper horizons. On the other hand, flux vectors are nearly vertical in the rhizosphere-less soil. This accelerates the formation of a phreatic surface at the bottom of the slope triggering premature failure of the slope.

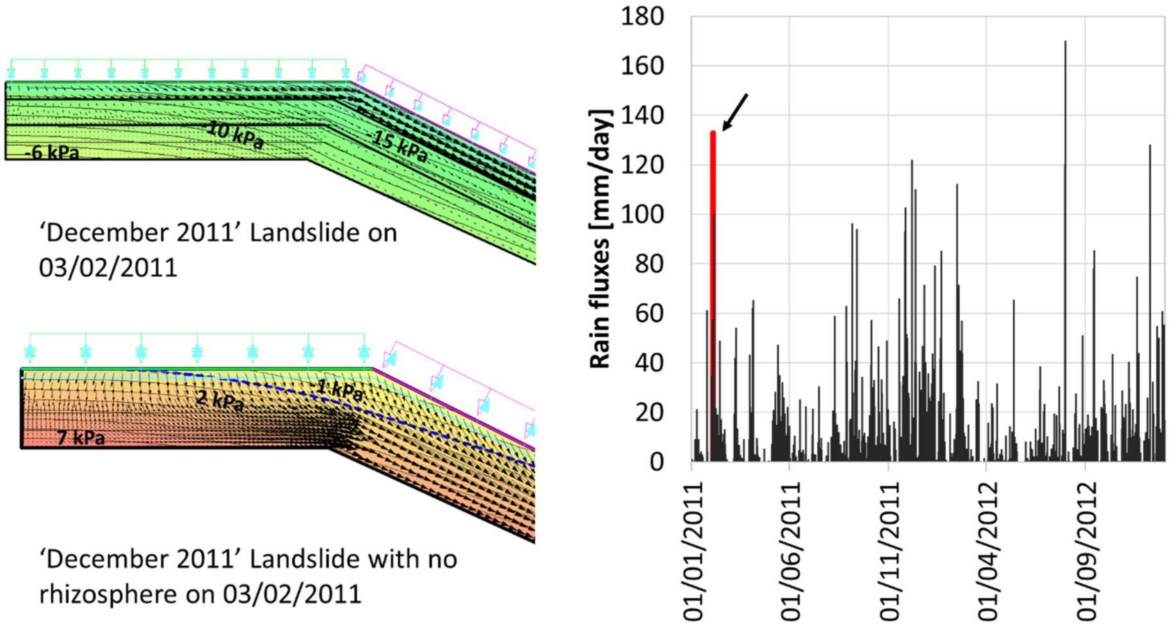

Figure 3-25. Comparison of the pore water pressure contours and the flux vectors on February 2011 for the case with rhizosphere and in absence of rhizosphere.

If one compares the evolution of the FoS versus time for the rhizosphere profile and the rhizosphere-less profile, it is observed that rhizosphere-less profile fails on the first significant rainfall event. In other words, if the rhizosphere at Rest and Be Thankful had not acted as a lateral subsurface drainage, the soil cover would have been already swept away and one would observe the bedrock entirely exposed.

3.6 DISCUSSIONS

The lesson learned from this study is that the rhizosphere ‘protects’ the slopes by hampering downward rainwater infiltration through the promotion of subsurface lateral flow towards the gullies. As a result, shallow landslide hazard can be potentially mitigated by enhancing the capacity the rhizosphere to act as a natural lateral drainage.

Diffuse landslides require ‘diffuse’ mitigation measures and, for this reason, vegetation is often seen as one of the few practicable solutions. This is also the case of R&BT where a few preliminary studies have been carried out to examine ecological mitigation measures, i.e. tree-planting and other forms of re-vegetation (Winter and Corby, 2012). In particular, the authors suggested a mix of native broadleaf tree and shrub species. This would give a mix of root spread and depth, including potentially to bedrock, maximising the root reinforcement effect.

The final design of the vegetation-based engineered slope would likely require further studies (including the development of a field trial) to clearly identify the hydro-mechanical processes to be ‘engineered’ by vegetation. In turn, this should stem from the understanding of the hillslope hydrology and its interplay with failure mechanisms.

The study presented in this paper potentially suggests that one of the criteria to be considered in the selection of the vegetation to be re-planted should stem from the role played by the rhizosphere in diverting rainwater from the deeper soil horizons. This would imply that plants with root-system architecture that enhances lateral subsurface flow should be privileged.

Ghestem et al. (2011) have discussed the influence of plant root systems on subsurface flow and their implication on slope stability. In particular, they proposed a classification of plant root architecture with respect of the mode of subsurface flow they generate. Figure 3-27 shows the different scenarios of the effects of root architecture on preferential flow according to Ghestem et al. (2011).

For example, roots oriented perpendicular to the slope gradient are able to capture downward water flow (Figure 3-27k) and would be ideal for plantation on the hillslope. On the other hand, tuft-root systems (Figure 3-27i) allow water infiltrating into upper soil layers and would be ideal for plantation on the side-slope.

On the other hand, taproot systems conveying water to deeper soil layers (Figure 3-27h) should be avoided as these will short-circuit water flow towards the interface between the soil cover and the bedrock cancelling any beneficial effect of the rhizosphere. It is therefore possible that remedial measures based on tree planting might have a detrimental effect on slope stability.

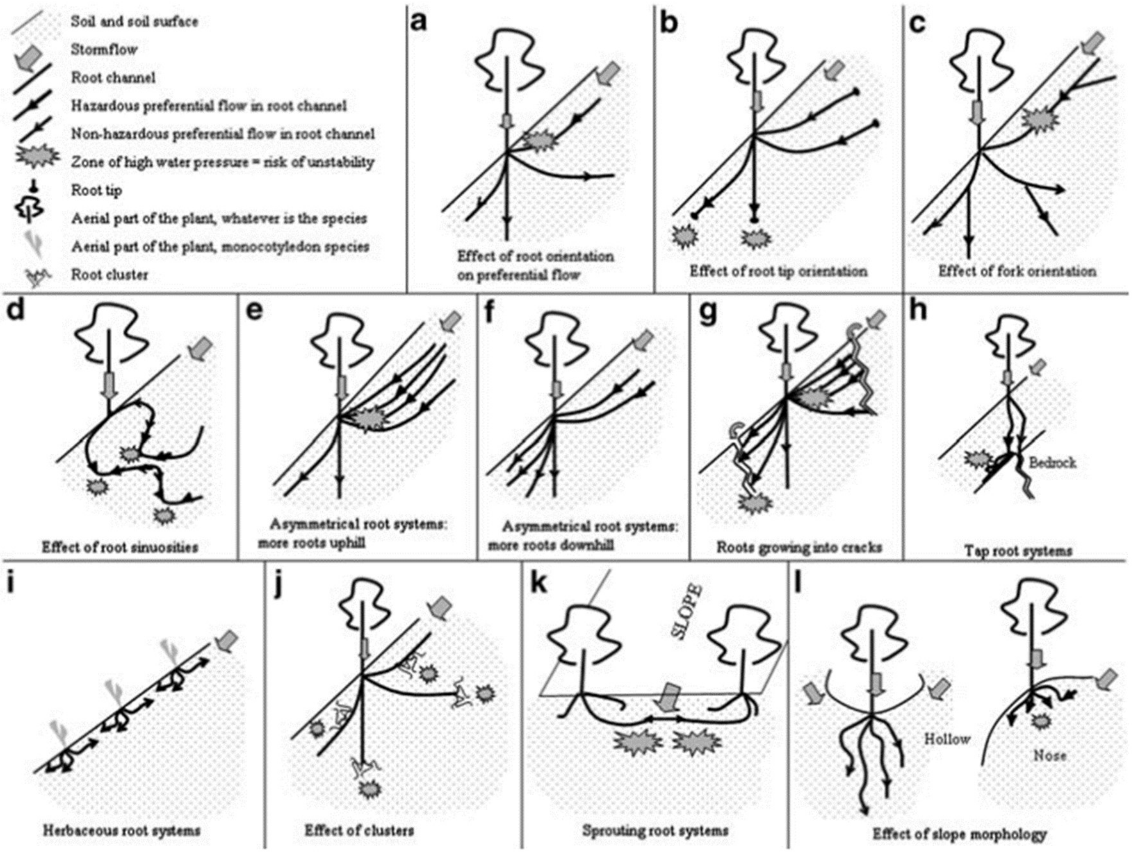

Figure 3-26. Illustrations of different scenarios of the effects of root architecture on preferential flow. (a) Downslope root orientation is more efficient for transporting excess water. (b) Root extremities can represent dead-end paths for water flow. (c) Root branching may divide or concentrate flow. (d) Sinuous roots divert or concentrate water fluxes, depending on their orientation. (e) When the majority of roots grow upslope, there is a potential for pore-water accretion at shallow depths to occur near the plant stem. (f) When more roots grow downslope, drainage of water is facilitated. (g) Roots growing toward cracks enhance the risk of water accretion. (h) Taproot systems convey water to deeper soil, where it can drain into cracks in the bedrock if cracks are present. However, if the soil–bedrock limit is impermeable, zones of high water pressures can be created. (i) Tuft-root systems allow water to infiltrate into upper soil layers. (j) Clusters of roots act as sponge-like structures and concentrate high water pressures. (k) Roots oriented perpendicular to the slope gradient capture downward water flow. (l) Topographic situations can combine various water-flow and root-distribution patterns. (Ghestem , Sidle , & Stokes, The Influence of Plant Root Systems on Subsurface Flow: Implications for Slope Stability, 2011)

3.7 CONCLUSIONS

Vegetation is often seen as one of the few practicable solutions to mitigate landslide hazard at the catchment scale. Vegetation may reinforce slopes via the anchoring of root system to deeper stable layers (mechanical effect) or by promoting the increase in suction via the transpiration process (hydrological effect). This paper has investigated a third effect thus far little explored, i.e. the role played by the high hydraulic conductivity of the rhizosphere on hillslope hydrological processes and, hence, on the occurrence of shallow landslides.

The case study of Rest and Be Thankful in Scotland has been the object of this study. Soil profile of shallow landslides has been reconstructed by inspecting scarps at the upper edge of recent landslides and hydraulic and mechanical properties of the rhizosphere and the underlying horizons have been characterised via a combination of laboratory testing and field measurements. A physically-based hydro-mechanical model has been derived thereof and validated against its capability of reproducing time of occurrence of two historical landslides.

The physically-based model has been then exploited to highlight the role of the rhizosphere on slope hydrology. For comparison, the case of a soil profile where rhizosphere is not present has also been considered and water flow was simulated for the case of bare and vegetated soil. Numerical simulations clearly show that the rhizosphere hamper vertical infiltration of rainwater. This allows the pore-water pressures to remain generally negative in the deeper layers at the interface with the bedrock. When prolonged rainfalls exceed the ‘drainage’ capacity of the rhizosphere in diverting water flow laterally towards the gullies, downward infiltration of rainwater is promoted potentially triggering slope instability.

The lesson learned from this study is that the rhizosphere has beneficial effects on slope stability by preventing downward rainwater infiltration. As a result, shallow landslide hazard can be potentially mitigated by enhancing the capacity the rhizosphere to act as a natural lateral drainage. In turn, this implies that plants with root-system architecture that enhances lateral subsurface flow should be privileged when designing vegetation-based remedial measures.

4 CRITERIA TO IDENTIFY RAINFALL THRESHOLDS FOR THE TRIGGERING OF RAINFALL-INDUCED SHALLOW LANDSLIDES

To be Submitted to Canadian Geotechnical Journal

Brunella Balzano[(1)], Alessandro Tarantino[(2)], Marco Valerio Nicotera[(3)]

POSITION AND AFFILIATION:
[(9)] Phd Student, University of Strathclyde, Department of Civil and Environmental Engineering
[(10)] Professor, University of Strathclyde, Department of Civil and Environmental Engineering
[(11)] Lecturer, Università degli Studi di Napoli Federico II, Department of Civil Engineering

Candidate’s contribution: As per Chapter 2.

ABSTRACT

Early warning systems are a well established practice for rainfall-induced landslides risk mitigation. They are usually based on rainfall threshold curves, with the aim to highlight the rainfall events more likely to trigger a slope failure. Antecedent Rainfall Models are one of the possible approaches to develop rainfall threshold curves. They result from the correlation between the amount of rain cumulated in a period prior the landslides event and the daily rainfall which has been recorded on the day of the failure. This paper proposes an approach for selecting

the “right” antecedent period for the ARM threshold curves. The approach is based on the physically-based model developed and validated in Chapter 2 and is tested against the case study of the Sorrento Peninsula catchment. Empirical data of the triggering rainfall events on the Sorrento Peninsula catchment collected by De Vita et al 2001 are used to validate the results of the proposed approach.

4.1 INTRODUCTION

Rainfall-induced shallow landslides are one of the most dangerous natural hazards with a significant impact on society and economy. They affect very often extensive areas and they frequently intersect human activities (Lu and Godt, 2013), posing a significant hazard to people, public and private property, lifelines, and utilities.

An early warning system is often the only practical approach to mitigate risk via reducing the vulnerability of landslide affected areas. They are usually based on threshold values of rainfall, which is the most ‘accessible’ and the most frequently used landslide precursor (Guzzetti et al., 2007).

Antecedent Daily Rainfall (ADR) models (De Vita et al., 2001; Govi et al., 1980; Crozier, 1986; Govi et al, 1985; Kim et al., 1991; Aleotti, 2004) are generally used when it is recognised that cumulative rainfall prior to the main triggering event plays a critical role in contrast to the Intensity-Dration (ID) models where only the rainfall associated with the main event is considered (Caine, 1980; Crosta, 1989; Calcaterra, 2000; Aleotti, 2004; Arboleda et al., 2006).

A critical aspect in the ADR models is the choice of the appropriate length of antecedent period (Guzzetti et al., 2008). Antecedent rainfall influences groundwater levels and soil moisture, and can be used to determine when landslides are likely to occur (Guzzetti et al., 2007). There appears to be a lack of consistency among the number of approaches proposed in the literature (Terlien, 1998; Kim et al., 1991; Heyerdahl et al., 2003). More in general, there is a lack of objective criteria that can be used to identify the antecedent period.

A second limitation of the ADR models is that the threshold is defined as lower bound of critical rainfalls. However, the lower bound approach often leads to over-conservative thresholds, which cause repeated false alerts and result in a loss of confidence in the early-warning system. Ideally, this limitation can be overcome if different thresholds are identified for sub-areas sharing similar predisposing geomorphological factors.

This work presents an approach for selecting of the ‘antecedent’ period, i.e. the appropriate period over which the cumulative rainfall prior the main triggering even has to be quantified and is based on the use of a physically-based numerical model.

The approach has been tested on a real catchment (Sorrento Peninsula, Southern Italy) well known for its susceptibility to shallow landslides. The slopes of the Sorrento Peninsula are characterized by the presence of pyroclastic covers resulting from intense ancient volcanic activity typical of this area. The occurrence of these landslide events is often associated to highly daily rainfalls preceded by prolonged periods of rainfall. The database used to benchmark the proposed approach was derived from De Vita et al. 2001, who have investigated extensively the hydrological factors triggering debris flows in the Sorrento Peninsula.

4.2 THE CASE STUDY OF SORRENTO PENINSULA

4.2.1 Geological setting

The Sorrento Peninsula is located on the Tyrrhenian coast of Campania Region. This region lies on a major tectonic depression called the Campania graben, generated during the Plio-Quaternary. This graben is bounded by several groups of more than 1500m thick Mesozoic dolomites and limestones Mountains, including the Sorrento Peninsula–Lattari Mountains, the Partenio Mountains, the Caserta Hills, Pizzo D’Alvano mountain, and Maggiore Mountain (Figure 4-1). Due to the past intense volcanic activity, the most recent deposits on the limestone formation are pyroclastic deposits. They can be associated with the Late Pleistocene–Holocene Plinian eruptions of the Campi Flegrei and Somma-Vesuvio volcanic areas.

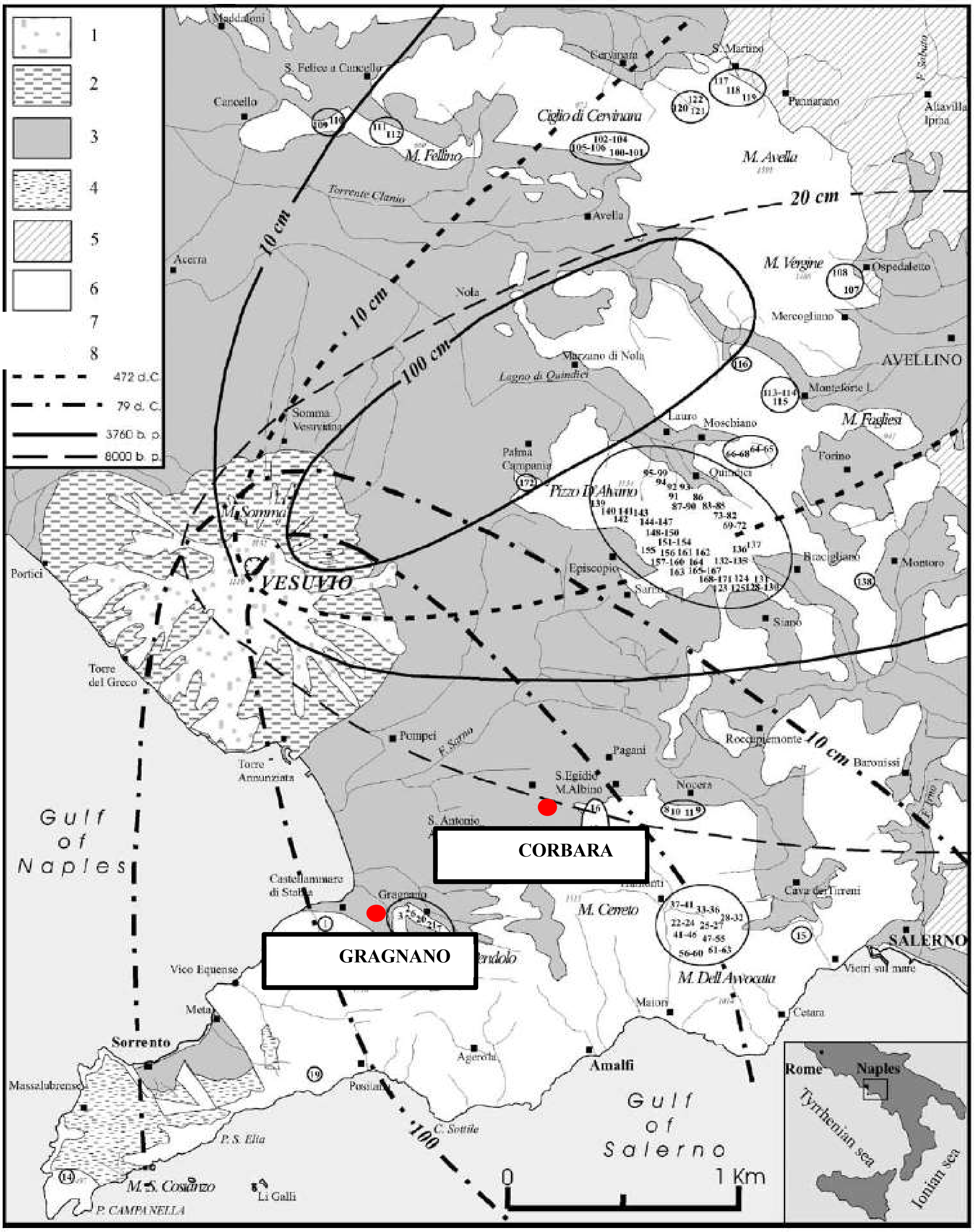

Figure 4-1. Main Somma-Vesuvio pyroclastic fall deposits (AD 472; AD 79; 3760 b.p. “Avellino eruption”; 8000 b.p.”Mercato eruption”.(Di Crescenzo & Santo, Debris slides-rapid earth flows in the carbonate massifs of the Campania region (Southern Italy): morphological and morphometric data for evaluating triggering susceptibility, 2005)

On average, the geomorphology of the catchment is characterized by slopes with inclinations varying from 27° to 50° and thicknesses of the pyroclastic cover varying from 0.8 m to 3 m (Di Crescenzo et al., 2008). The soil profiles are composed by three main class of soils:

- A top layer of pyroclastic soil, which has been affected by bio-chemical processes as a result of the direct and indirect action of microorganism and vegetation (A1). This layer originally formed during the last stage of the 79 AD eruption.
- Pumices (P). This layer was deposited during the early stage of the 79 AD eruption.
- Ashes, deriving from an ancient eruption (130000 years ago ca.) from Campi Flegrei volcanic areas (C1 and C2)

  Geological surveys along the landslides bodies have shown that pumices are not always present in the soil profiles of the Sorrento Peninsula. Therefore, two classes of the landslides event can be identified:

- Landslides events characterized by the presence of pumices
- Landslides events characterized by the absence of pumices

In Chapter 2 an approach to formulate a physically-based model for shallow landslides was developed. The model was based on geological and geotechnical investigation and then tested against two historic case studies of the Sorrento Peninsula, chosen as representatives of the two classes of landslides events. The physically-based model is briefly described in the following paragraph and has been adopted in this work as part of the approach to select an appropriate antecedent period.

4.2.2 Development of physically-based models

The physically based model developed in Chapter 2 is schematized in Figure 4-2. In particular, Figure 4-2a is the model representing the class of landslides with no pumices present in the soil profiles. Typically, the soil profile characterizing this class of landslides is composed by a top layer of pyroclastic soil (A1), a middle layer of ashes (C1) and a sub layer of compacted ashes (C2), as shown in Figure 4-2a. The range of thicknesses of each layer for the no-pumices class is reported in Table 4-1.

Figure 4-2b shows the model representing the class of landslides characterized by the presence of pumices. As shown, the top layer of pyroclastic soil and the bottom layer of ashes are divided by an interposed middle layer of pumices. Table 4-1 shows the range of thicknesses for this class of soil profiles.

Figure 4-2 also shows the boundary conditions adopted for the physically-based models. They consist of:

- Water inflow imposed at the top boundary (to simulate rainfall)
- Water outflow at 10 cm below the ground surface (to simulate evapotranspiration from the root system)
- Impermeable bottom boundary (to simulate the bedrock)

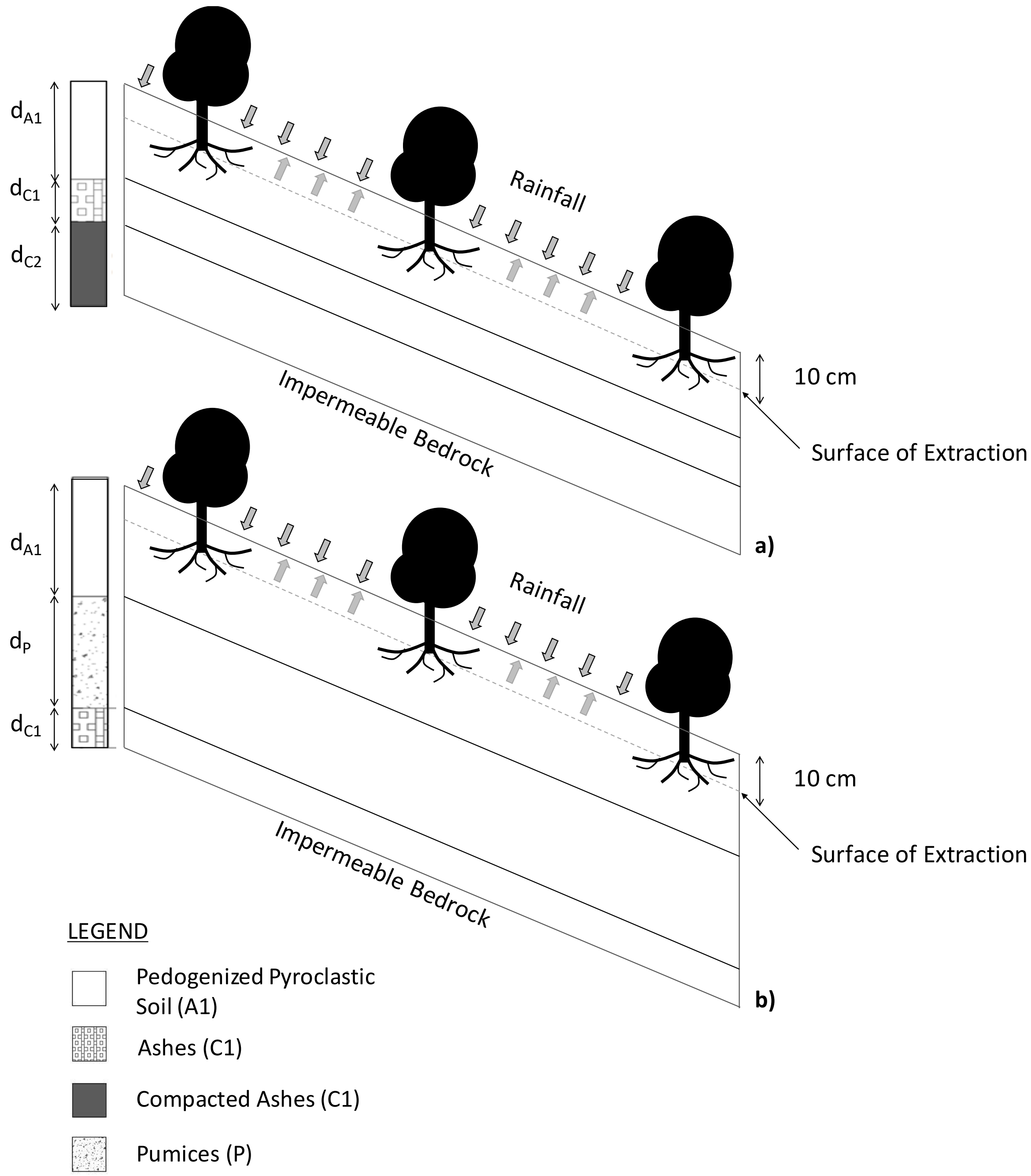

Figure 4-2. Geometries, Soil profiles and Hydro-Mechanical model scheme for the two main classes of slopes of the Sorrento Peninsula. a) No-Pumices Slopes. b) Pumices Slopes.

Table 4-1. Range of thicknesses for the Sorrento Peninsula soil profiles.

Landslides	d_{A1}	d_{C1}	d_P	d_{C2}
	m	*m*	*m*	*m*
No-Pumices	0.55-0.8	0.25-0.4	-	0.45-0.65
Pumices	0.75-0.95	0.25-0.4	0.8-0.9	-

The physically based model was then tested against two specific historic landslides events. In particular, the two events occurred on the 10th of January 1997 in 2 different locations of the Sorrento Penisula: Gragnano and Corbara. The two locations can be considered as representative of the two classes of slopes. In particular, the Gragnano's event has been chosen as representative of the no-pumices slopes class, while the Corbara's is representative of the pumices slopes class. The details related to the two events are briefly reported in the following sections.

The physically-based model was validated by testing its ability to reproduce the the time of failure and the location of the slip surface identified by the geological survey following the landslide events (Chapter 2).

4.2.2.1 Soil profile with pumices (Corbara)

This event was characterised by a total length of 250m. It started as a translational shallow landslide that evolved into a debris flow. The soil profiles was investigated during extended surveys carried out by the Geology Department of University of Naples Federico II. The bedrock is covered by a very thin layer (0.3-0.4 m) of ashes, overlain by a 0.8-0.9 m layer of yellow pumices and a 0.9m layer of pedogenised pyroclastic soil. The values of thicknesses and slope inclinations are reported in Table 4-2.

4.2.2.2 Soil profile without pumices (Gragnano)

The Gragnano (1997) landslide took place in an area characterized by a high grade of susceptibility, mainly due to high values of slope angles (around 35°) and a fair continuity of the pyroclastic material between 0.5 -2.5 m thick. The average length of the landslide is roughly 220 m, involving 4500 m^3 of material. The strongly fracturated carbonate bedrock is covered by an ash-fall layer characterized by a high clay content (C1 and C2). The latter is covered by the products of 79 AD Plinian eruption, i.e. coarse pumices (B), ashes (A2) and soil (A1). The values of thicknesses and slope inclinations specific for the selected two cases are reported in Table 4-2.

Table 4-2. Thicknesses for the soils profiles of the Gragnano and Corbara case studies.

Lanslides class	d_{A1} *m*	d_{C1} *m*	d_P *m*	d_{C2} *m*	Slope °
Gragnano	0.6	0.3	-	0.6	33
Corbara	0.9	0.3	0.85	-	35

4.2.3 Modelling mechanical response of the slope

The infinite slope failure mechanism has been chosen to model the onset of failure Factor of safety.

The factor of safety at any depth can be derived via the limit equilibrium method. By considering the shear strength criterion given by Equation 15, the following equation can be derived

$$\mathrm{FoS} = \frac{\tan\phi'}{\tan\beta} + \frac{-u_w S_r \cdot \tan\phi'}{(\bar{\gamma}H) \cdot \sin\beta \cdot \cos\beta} \qquad \textbf{[4-1]}$$

where H is the depth of the failure surface, β is the inclination of the slope, ϕ’ is the friction angle and $\bar{\gamma}$ is the average unit weight given by:

$$\bar{\gamma} = \frac{1}{H}\int_0^H [\gamma_s(1 - n^*) + \gamma_w n^* S_r]dz \qquad \textbf{[4-2]}$$

where γ_s and γ_w are the unit weight of solids and water respectively, and n^* is the porosity.

4.2.4 Modelling hydraulic response of the slope

The Darcy's law extended to the case of unsaturated soils has been used to model rainwater inflitratin within the slope:

$$\vec{v} = -Kgrad(\Psi) = -Kgrad(z + \frac{u_w}{\gamma_w}) \qquad \textbf{[4-3]}$$

where $\vec{v}$ = flow velocity vector; ψ = piezometric head; K = hydraulic conductivity; u_w = pore water pressure; γ_w = density of soil water; and z = vertical coordinate increasing upward. The hydraulic conductivity K is a function of the degree of saturation, which in turn depends on pore water pressure.

The mass balance equation for liquid water can be written as follows:

$$\text{div}\, v + \frac{\partial\theta}{\partial t} = 0 \qquad \textbf{[4-4]}$$

where θ = volumetric water content (ratio of water volume to total volume); and t = time. By substituting Equation 4-3 in Equation 4-4, the Richard's equation in terms of piezometric head is obtained:

$$C\frac{\partial\psi}{\partial t} = \text{div}[K\ \text{grad}(\psi)] \qquad \textbf{[4-5]}$$

where $C = \gamma_w(\partial\theta/\partial u_w)$, referred to as water capacity of the soil.

The volumetric water content θ appearing in Equation 4-4 is given by:

$$\theta = n^* S_r \qquad \textbf{[4-6]}$$

where n^* = porosity; and Sr = degree of saturation. The water flow Equation 4-6 was solved numerically via the FEM using the module SEEP/W of the software Geostudio.

4.2.5 Hydraulic and mechanical properties of materials

Figure 4-3 shows the water retention and hydraulic conductivity curves for the materials characterizing the soil profiles of the two landslides classes. The curves result from a best fitting of the experimental data.

A Van Genuchten function (Van Genuchten, 1980) has been used to model the water retention behaviour for Soils A1, C1 and C2. The parameters resulting in the best fit of the experimental data and therefore chosen to model the hydraulic behaviour of the soils are reported in Table 4-3.

The water retention curve of the Pumices (P) has been modelled by considering the superposition of two Van Genuchten-type functions, representing the behaviour in the low suction range and high suction range respectively. The hydraulic parameters chosen to model the hydraulic behaviour of the pumices are reported in Table 4-4.

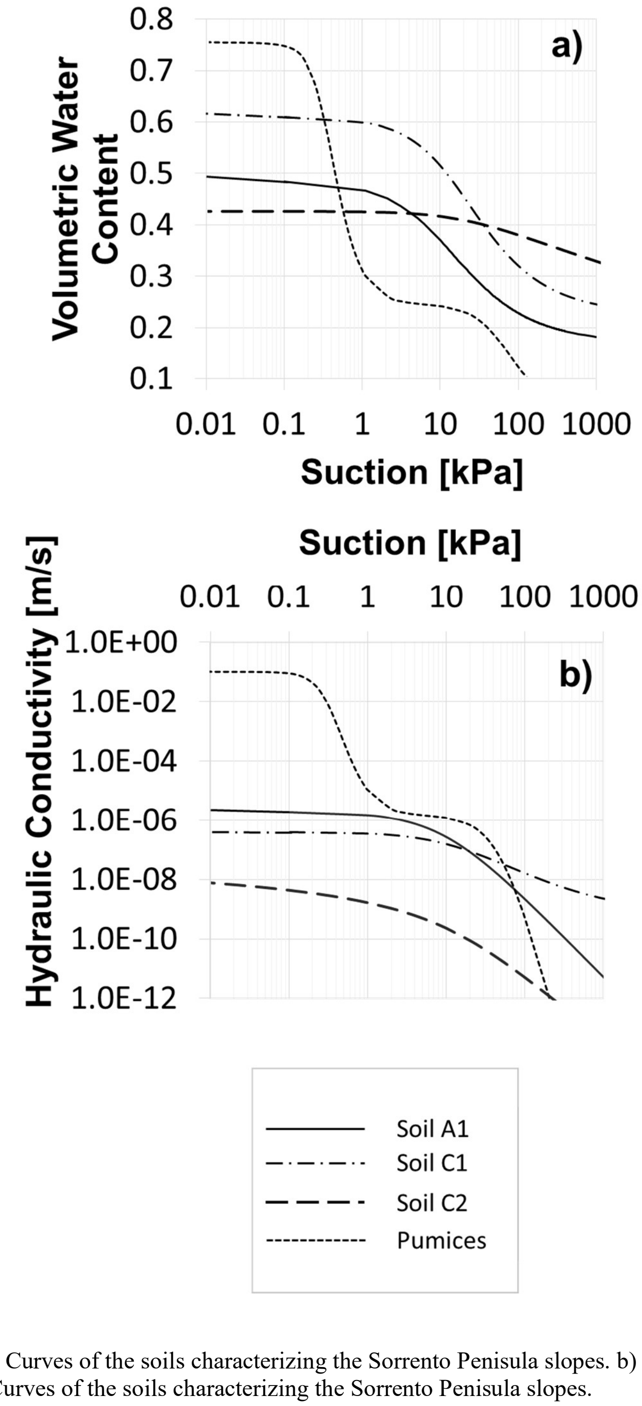

Figure 4-3. a)Water Retention Curves of the soils characterizing the Sorrento Penisula slopes. b) Hydraulic Conductivity Curves of the soils characterizing the Sorrento Penisula slopes.

Table 4-3. Hydraulic properties of the soils A1, C1 and C2.

Soil	$\theta_{s=0}$	θ_r	S_{res}	u_w^*	α	n	l	k_s
	-	-	-	*kPa*	*1/kPa*	-	-	*m/s*
A1	0.49	0.17	0	7	0.05	1.7	-1	$3.4\ 10^{-5}$
C1	0.61	0.198	0.065	7	0.015	1.7	-2.7	$1.7\ 10^{-6}$
C2	0.517	0.018	-	-	0.005	1.07	0.273	$5\ 10^{-8}$

Table 4-4. Hydraulic properties of the Pumices.

Suction Range	θ_s	θ_r	α	n	k_s
			1/kPa		*m/s*
Low	0.63	0.12	0.63	3	$1\ 10^{-2}$
High	0.12	-0.12	0.02	2	

More details about the procedure adopted and the hypothesis made on the hydraulic and mechanical characterization of the materials, the reader can refer to Chapter 2.

Table 4-5 shows, then, the mechanical parameters adopted for the soils.

Table 4-5. Mechanical Properties of the Sorrento Peninsula soils

	γ_{dry}	ϕ'	c'	n*	Gs
	kN/m³	°	*kPa*	-	-
A1	8.06	37	5	0.69	2.65
C1	7.09	37	0	0.72	2.64
C2	10.64	37	0	0.57	2.49
P	4.8	40	0	0.8	2.55

4.3 IDENTIFICATION AND VALIDATION OF RAINFALL THRESHOLD

4.3.1 Criterion for selecting the 'antecedent' period

A daily-antecedent rainfall threshold curve is shown schematically in Figure 4-4. Any combination of daily rainfall and antecedent rainfall resulting in a data point above the threshold curve is assumed to trigger a landslide.

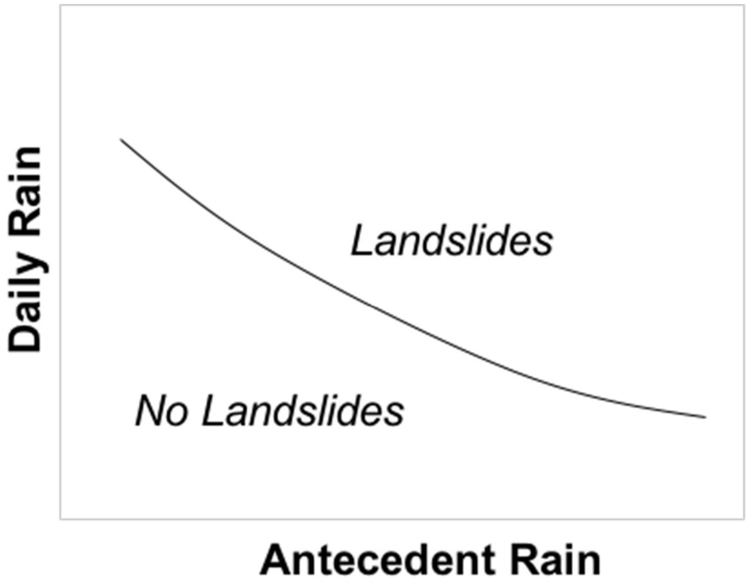

Figure 4-4. Scheme for a general Antecedent Rain- Daily Rain Threshold Curve.

The implicit assumption behind the daily-antecedent rainfall threshold curve is that the total amount of rainfall over the period preceding the triggering event (antecedent rainfall) is the only predisposing factor. In other words, it is assumed that the same amount of rainfall over the antecedent period leads the slope to the same condition at the onset of the triggering daily rainfall, regardless of the conditions at the start of the antecedent period and regardless of the rainfall pattern over the antecedent period.

Let us consider two generic rainfall patterns that cumulate the same volume of water over a preceding period. Let us assume that the pore-water pressures within the slope are different at the start of the preceding period and that pore-water pressures remain different at the end of the preceding period (Figure 4-5d). Despite the same cumulative rainfall volume, the slope is not characterised by the same conditions at the onset of the daily triggering rainfall. Different daily rainfalls would therefore be required to trigger failure. As a result, there is not a one-to-one correspondence between cumulative rainfall volume and daily triggering rainfall.

On the other hand, let us consider the case shown in Figure 4-5c where the pore-water pressure and, hence, the factor of safety converge at the end of the preceding period. The same daily rainfall would trigger the failure and a one-to-one correspondence between cumulative rainfall volume and daily triggering rainfall can be established. The duration of this preceding period therefore characterises the ‘right’ antecedent period, as the initial difference in pore-water pressure and, hence, factor of safety is cancelled.

The antecedent rainfall can therefore be defined as the volume of rainwater cumulated over a period of time sufficiently long to cancel the previous hydrological history of the slope.

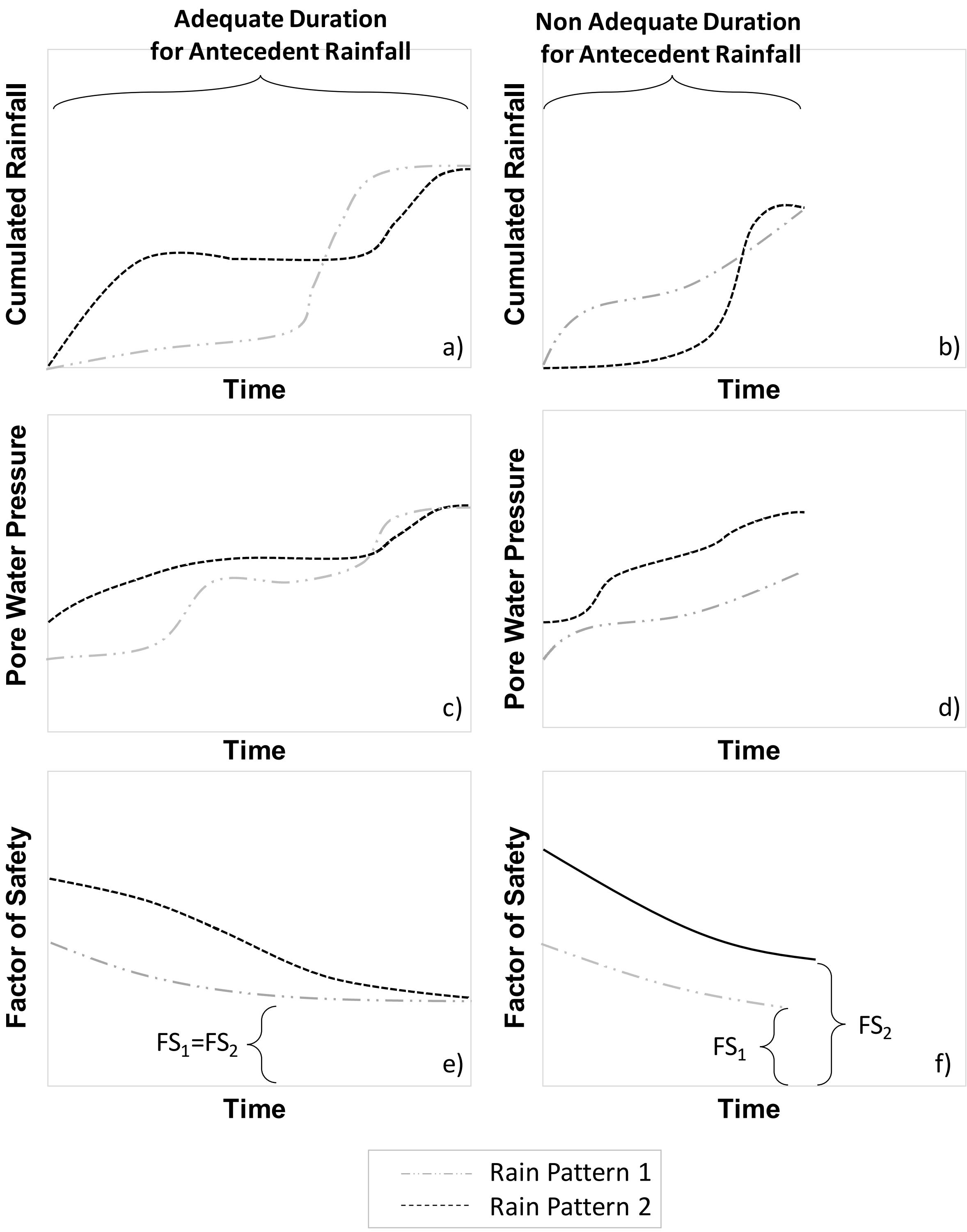

Figure 4-5. Scheme of the criterion to identify the “right” antecedent period.

4.3.2 Identification of antecedent rainfall period

The concept illustrated in Figure 4-5 has been implemented by using real rainfall patterns recorded for the catchment object of this study. Two candidate antecedent periods were explored: 60 days and 90 days.

In the first case, two 60-days rainfall patterns were taken from winter 1994/1995 and autumn 1996 respectively. The correspondent cumulated rainfall for the two rain patterns over the 60 days are:

- CR1-60=206.4 mm (winter 1994/1995)
- CR2-60=330.5 mm (autumn 1996)

In order to explore whether the period of 60 days can be considered as ’antecedent’ rainfall in the sense illustrated above, it is necessary for the two patterns to cumulate the same amount of rain water over the 60 days. For this reason, the second pattern has been scaled of a factor equal to CR1-60/CR2-60. Figure 4-6 shows the pattern taken from winter 1994/1995 and the pattern taken from autumn 1996 before and after scaling. The cumulated rainfalls for the two patterns after the scaling process are now coincident.

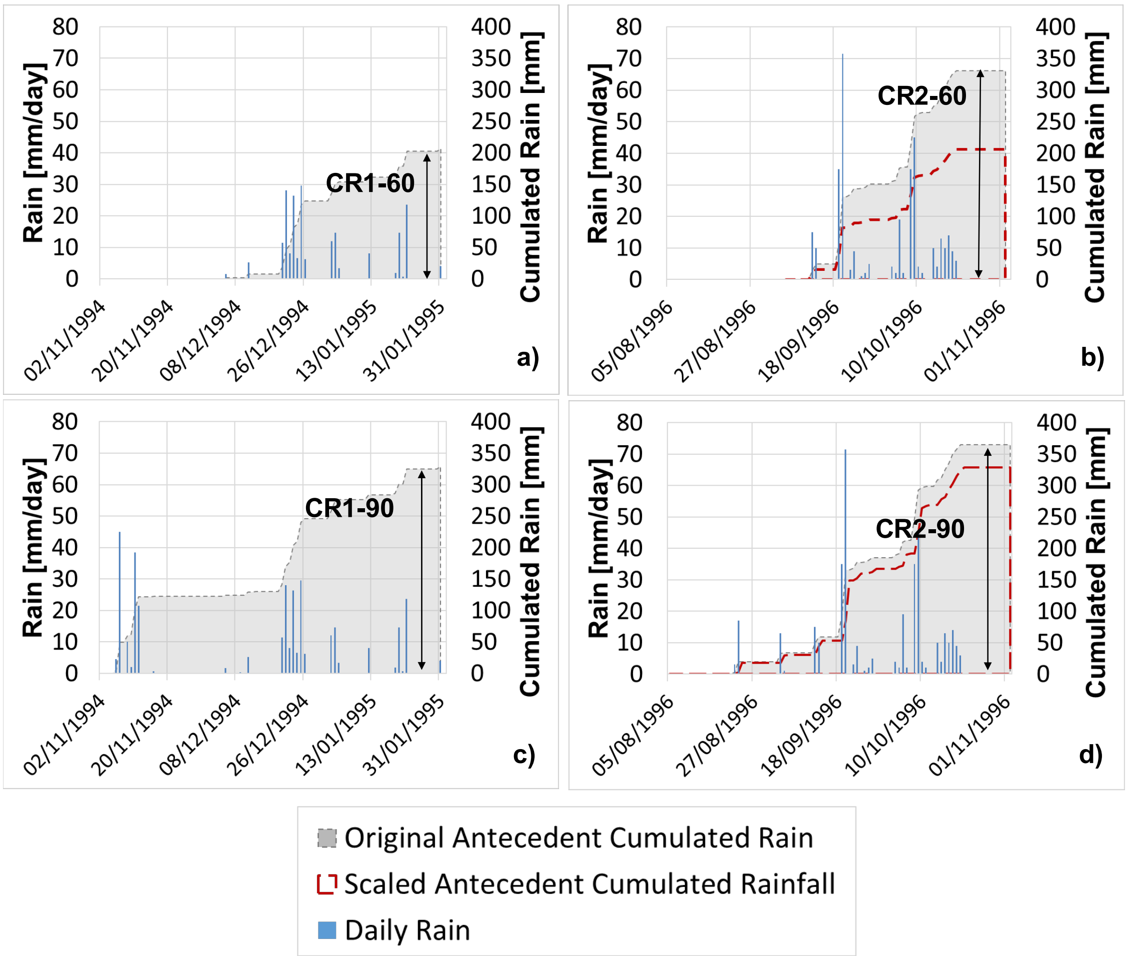

Figure 4-6. a) Winter 1994-1995 60 days Antecedent Rain. b) Scaled Autumn 1996 60 days Antecedent Rain. c) Winter 1994-1995 90 days Antecedent Rain. d) Scaled Autumn 1996 90 days Antecedent Rain.

The physically based model developed for Gragnano has been considered to perform a numerical analysis, in order to study the evolution of pore-water pressures over the 60 days. At the end of the 60 days, a second analysis was carried out by imposing various daily rainfalls for 1 day until identifying the daily rainfall triggering the failure.

Figure 4-7a shows that the two rainfall patterns characterised by the same amount of cumulated rainfall predispose the slope to fail under different daily rainfall. Hence, the period of 60 days cannot be considered as suitable antecedent period.

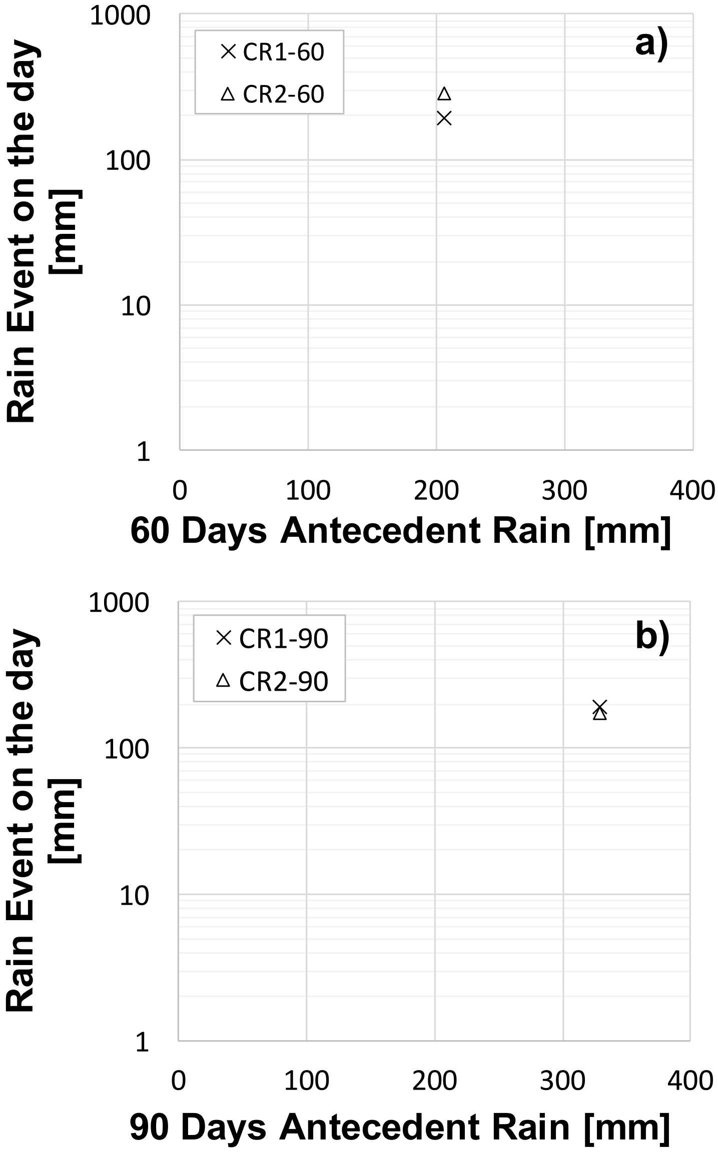

Figure 4-7. Identification of the antecedent rainfall period.

The case of two 90-day rainfall patterns, still taken from winter 1994/1995 and autumn 1996 respectively, was then examined. The correspondent cumulated rainfall for the two rain patterns over the 90 days are:

- CR1-90=328.8 mm (winter 1994/1995)
- CR2-90=364.5 mm (autumn 1996)

Again, the pattern from autumn 1996 was scaled in order to make the cumulated rain coincident over the 90 days (Figure 4-6b). After the 90 days of rainfall, the daily rainfall triggering the failure of the model was explored. Figure 4-7b shows that the two rainfall patterns characterised by the same amount of cumulated rainfall predispose the slope to fail under the same daily rainfall. Hence, the period of 90 days can be considered as suitable antecedent period.

4.3.3 Derivation of rainfall threshold curves

The rainfall threshold curves were derived by considering different cumulated rainfall over 90 days and by determining the corresponding daily rainfall that triggers slope failure. To this end, the two rainfall patterns shown in Figure 4-6 were scaled in order to simulate the effect of various cumulated rainfall over 90 days.

Figure 4-8 shows the result of this analysis. The same cumulated rainfall, although generated by two different rainfall patterns, gives rise to the same triggering daily rainfall. This confirms once again that the period of 90 days can be considered as an appropriate ‘antecedent’ period.

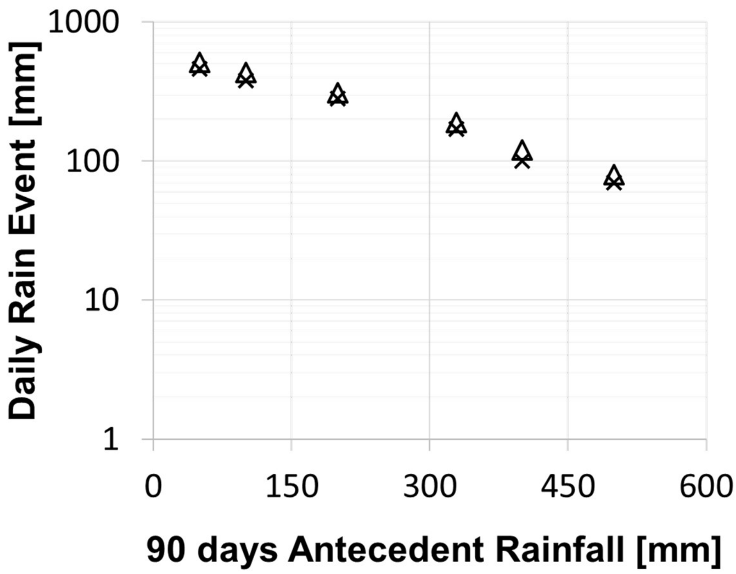

Figure 4-8. Derivation of rainfall threshold curves.

The daily rainfall triggering slope failure tends to decrease as the antecedent rainfall increases. This is intuitive and consistent with field observations as reported in the literature ((De Vita et al., 2002; Guzzetti et al., 2007; Aleotti, 2004). The curve interpolating the critical rainfalls is the rainfall threshold curve. Rainfall data points lying above the threshold curve are associated with slope failure and vice versa.

4.4 VARIABILITY OF HYDROLOGICAL TRIGGERS ACROSS CATCHMENT

4.4.1 Effect of the presence of pumices

The antecedent-daily rainfall threshold curves have been derived for the two soil profiles associated with the landslides of Gragnano and Corbara respectively, which are in turn representing the classes of slopes without pumices and with pumices respectively. These are shown in Figure 4-9. As expected, different soil profiles give rise to different threshold curves.

The presence of pumices shifts the threshold curve upward, i.e. the presence of pumices makes the slope less susceptible to failure. The high permeability of the pumice horizon deviates the rainwater flow in direction parallel to the slope thus preserving the negative pore-water pressures in the underlying layers where the failure surface tends to develop due to the lower friction angle.

Figure 4-9 also shows the antecedent-daily rainfalls that have triggered debris flows in the Sorrento Peninsula according to De Vita et al. (2002). It can be observed that the rainfall threshold curves derived numerically are consistent with the critical rainfalls observed experimentally.

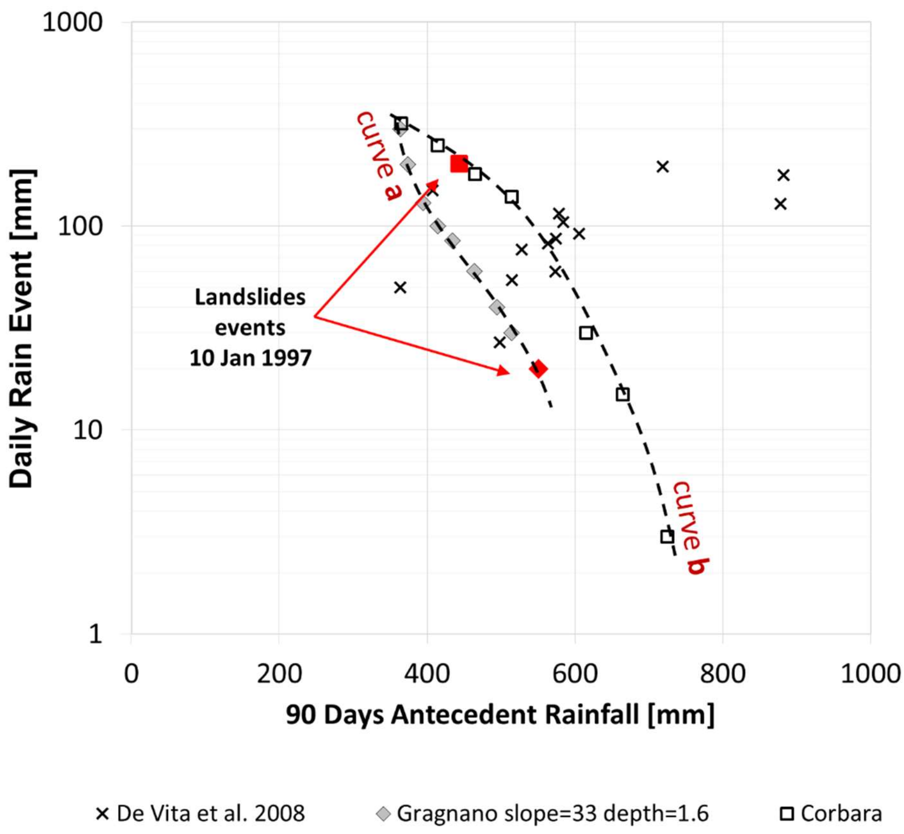

Figure 4-9. Effect of the presence of the pumices on the threshold curves.

4.4.2 Effect of slope inclination within the ‘no-pumice’ class

As an example, the effect of the slope inclination was investigated with reference to the ‘no-pumice’ class of slopes represented by the soil profile of the Gragnano landslide (Chapter 2). The overall depth in vertical direction has been maintained constant while increasing the slope inclination from 33° to 40°. As shown in Figure 4-10 (curve c), the effect of the slope inclination does not appear to play a very critical role. This would lead to the conclusion that rainfall threshold curves across the catchment should not be differentiated based on the inclination of the slope.

4.4.3 Effect of thickness cover within the ‘no-pumice’ class

The effect of the thickness of the pyroclastic cover has also been investigated. Once again, the original geometry of the Gragnano model (Chapter 2) has been considered as a reference. Two cases have been explored:

a) The case where the overall depth of the slope has been increased from 1.6 to 2.5 m by leaving unchanged the ratio between the thicknesses of the layers (Figure 4-10 curve d)
b) the case where the overall depth of the slope has been reduced from 1.6 to 0.8m by leaving unchanged the ratio between the thicknesses of the layers (Figure 4-10 curve e)

Figure 4-10 shows that the threshold curves shift significantly when changing the overall thickness of the cover. In particular, the slopes characterised by a lower thickness appear to be more susceptible to failure. This seems to be consistent with the experiential data. The critical rainfalls highlighted in Figure 4-10 are associated with landslides for which the soil profile could be derived from other sources. The trend inferred from the numerical simulation, i.e. the lower the thickness the higher is the susceptibility to failure, seems to be confirmed by the data observed experimentally.

This would lead to the conclusion that rainfall threshold curves across the catchment should be differentiated based on the thickness of the cover to improve the performance of the early warning system.

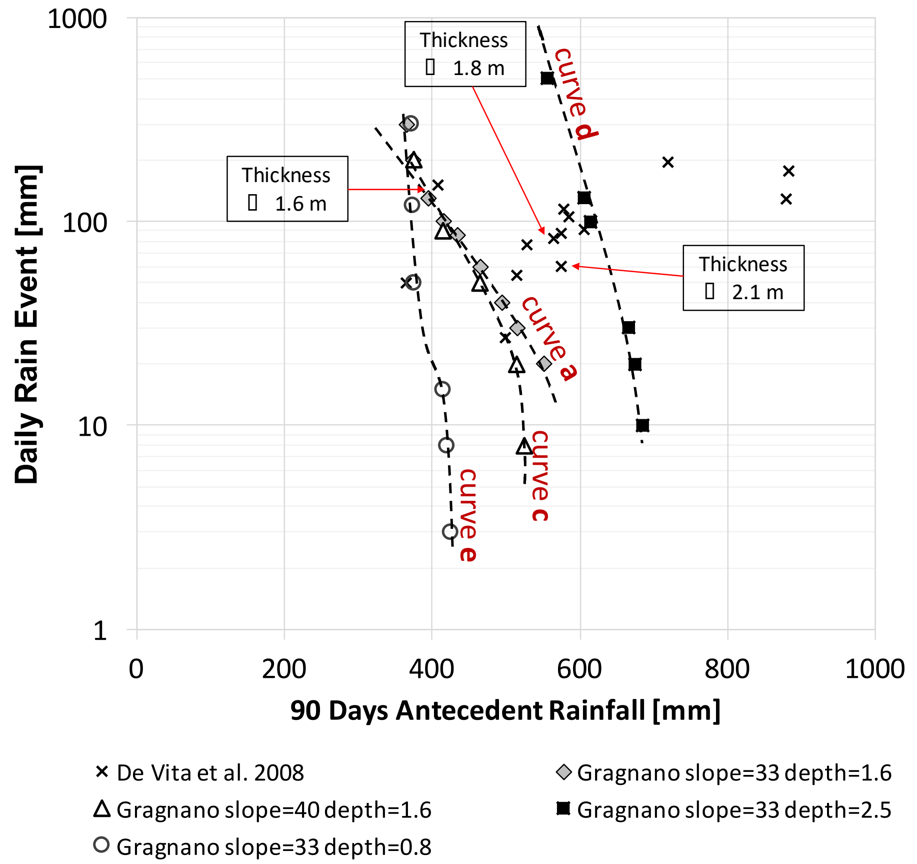

Figure 4-10. Effect of the slope inclination and the thickness cover within the no-pumices class.

4.5 CONCLUSIONS

Antecedent Daily Rainfall (ADR) models are frequently used to define the rainfall thresholds on which early-warning systems for rainfall induced shallow landslides are built. They are used when the cumulated antecedent rainfall is recognized to play a role in triggering the slope failure. However, the choice of the antecedent rainfall period is not always easy to make.

This work proposed a criterion to select the antecedent rainfall. The criterion lies on the assumption that the same amount of cumulated rainfall over the antecedent period leads the slope failure to be triggered by the same daily rainfall. In other words, the rain water cumulated over the antecedent period would be sufficient for the slope to lose memory of its conditions at the start of the antecedent period and regardless of the rainfall pattern over the antecedent period.

The criterion suggested in this work has been tested on the Sorrento Peninsula catchment, which is well known for its susceptibility to debris-flow. In Chapter 2 a physically-based model for the study of the rainfall-induced shallow landslides was developed and then tested on the Sorrento Peninsula case studies. The latter has been used to explore the “right” extension to be considered for the antecedent rainfall. To make sure that the results were not biased towards a specific rainfall event, two different lengths extensions of rainfall patterns have been probed, with the aim to spot the one resulting in a one-to-one correspondence with the triggering daily event. Once that the “right” antecedent period was found, the physically-based model was used to build different threshold curves for the Sorrento Peninsula catchment in order to explore the how the geomorphology of the slopes may influence their susceptibility to landslide. The results appear to be in agreement with the empirical data observed by De Vita et al. (2008).

The analyses showed that the susceptibility of the slopes to fail is reduced by the presence of pumices and by greater thicknesses of the pyroclastic cover. The slope inclination, instead, doesn’t seem to have a relevant influence on the threshold curves.

With the reference to the case of the Sorrento Peninsula, the results lead to the conclusion that the use of sub-threshold curves based on slopes inclinations and thicknesses may help the hazard assessment in the catchment.

More in general, warning systems based on ADR model can be improved with the refining of the interpretation of the rainfall threshold curves taking into account the varying geometry across the catchment. As the geomorphology of the slopes tends to vary across the catchment, the use of unique may lead to over-conservative estimations of the values of rain for which the early warning system would set the alarm.

5 CONCLUSIONS

This thesis work proposed a methodology for the study of rainfall-induced shallow landslides, with the aim to gain a deep understanding of the processes related to the problem. Each chapter shows an approach based on a physically-based model which have been used as a tool to explore several aspects of the landslides triggering mechanisms and how to eventually mitigate the phenomenon.

In Chapter 2 an approach to develop and validate a physically-based model for the study of rainfall-induced landslides was discussed. The model was built in a “bottom-up” fashion; indeed, a key part of the proposed methodology was to start from a hydrological model initially set as simple as possible, test its capability to reproduce the hydrological balance of the catchment and make it more sophisticated only if the test failed. In the case of the Sorrento Peninsula catchment, the 1-D hydraulic model seemed to satisfy the test, hence there was no need to step up to a 2-D model.

Interestingly, the model developed in Chapter 2 resulted in a very satisfactory reproduction of the time and location of two landslides events occurred on the Sorrento Peninsula on the 10th of January 1997 in Gragnano and Corbara respectively. Its remarkable performance allowed the approach to be extended to the whole catchment.

The physically-based model built in Chapter 3 was then used to explore the effect of the rhizosphere on the slope stability. In particular, the case study of Rest and Be Thankful in Scotland was analysed in order to show one singular beneficial effect provided by the presence of the rhizosphere. Ghestem et al 2011 already mentioned the significant influence the vegetation may have on the hydrology of the slopes, focusing on an aspect very little explored in literature so far. It was discussed that several plant species show a singular root architecture that may, interestingly, act as natural lateral drainage, therefore avoiding vertical infiltration of rainwater in the deeper soil horizons.

The physically-based model developed in Chapter 3 was used to explore this theory and validate it against the case study of Rest and Be Thankful catchment. Indeed, the numerical analyses have shown how the lateral drainage promoted by the rhizosphere helped the overall slope stability in the high-intensity rainfall season. Furthermore, the positive effect of the rhizosphere on the hydrology of the slope was also highlighted by comparing with the case where no rhizosphere was present.

Although, the use of vegetation as possible remedial measure to mitigate landslides hazard has been widely explored in literature, the studies carried so far mainly focused on the mechanical effect (root reinforcement) or the positive hydrological contribution given via plant transpiration. Chapter 3 presented a very interesting outcome by exploring the other hydrological contribution given by the root architecture. The study presented may suggest a new criterion to adopt when choosing the vegetation to be re-planted in order to mitigate the landslides hazard. Indeed, the work carried out in Chapter 3 suggests that that plants with root-system architecture that enhances lateral subsurface flow should be privileged.

As previously mentioned, rainfall-induced shallow landslides risk may be mitigated by acting on the hazard or the vulnerability. While the study carried in Chapter 3 suggested a criterion for the hazard mitigation, Chapter 4 explored the second option instead. A common approach often adopted for the vulnerability mitigation is the use of early-warning systems, usually based on threshold values of rainfall events. Indeed, rainfall data are very often the most ‘accessible’ and the most frequently used landslide precursor.

Many models of rainfall-thresholds have been proposed in literature, with the aim to figure out a correlation between possible triggering rainfall scenarios and landslides events. In particular, Chapter 4 explored the Antecedent Rainfall Models (ARM). They are commonly used when cumulative rainfall prior to the main triggering event is recognized to play a critical role in triggering the slope instability.

Very often, the two main challenges associated with ARM models are i) the choice of the antecedent period and ii) the over-conservativeness of the threshold curves, usually drawn as lower boundaries of a collected group of data.

The work carried out in Chapter 4 aimed to introduce an approach to help the selection of the “right” antecedent period. The approach is based on the physically-based model developed in Chapter 2 and was tested against the case study of the Sorrento Peninsula catchment. The latter have been a frequent object of study, seen the susceptibility of its slopes to landslide; therefore, it was possible to validate the results of the work with the threshold data collected by De Vita et al. 2001. Moreover, several analyses have been performed in order to explore the influence of the geomorphology on the threshold curves. The results seemed to suggest that the stratigraphy and the thickness of the slopes may be the most influencing factors.

More in general the outcomes of the analyses performed in Chapter 4 show the potential of the proposed approach in view of an improvement of the ARM models for the vulnerability reduction. Of course, more tests are required as future research works, in order to provide a more complete overview of the method in order to explore the possibility to extend it to other catchments.

6 FUTURE WORKS

As discussed in the previous chapter all the approaches proposed in this thesis work seem to show a great potential in providing a valid tool to assist landslides risk assessment. Although the results presented for each Chapter are very promising, still further studies need to be carried out.

The approach presented in Chapter 2 has been validated against two main landslides events (Gragnano and Corbara) , which have been chosen as representative of the Sorrento Peninsula catchment. Although the physically-based model was perfectly able to reproduce the time and the location of the failure for the selected events, it would be interesting to explore other case studies within the same catchment in order to assure the validity of the 1-D hydraulic model also for other slopes of the catchment.

With regards to the bottom- up method proposed in Chapter 2, it would be also interesting to explore the quality of its performance even on other catchments, with different geomorphology compared to the Sorrento Peninsula. Although the approach shows a great potential, further investigations are, of course, recommended in order to be appointed as a reliable hazard evaluation method.

A similar comment is moved towards the methodology discussed in Chapter 4. The physically-based model built in Chapter 2 has been used in Chapter 4 for the validation and the interpretation ARM threshold curves related to the Sorrento Peninsula catchment. However, the results discussed in Chapter 4 have to be taken as an early stage study which still requires refinements. First of all, not all the events present in the database of De Vita et al (2001) are fully characterized in terms of geomorphological properties; therefore, the validation of the proposed sub-threshold curves with the tendency of the empirical data is only based on few evidences. Moreover, a more detailed sensitivity analysis should be carried out in order to maybe explore the trend of the sub-threshold curves with the varying hydro-mechanic properties of the soils.

With the same spirit, further investigations need to be carried out with regards to the lateral drainage rhizosphere effect explored in Chapter 3. Of the theories presented in this thesis, this is certainly the less explored in literature so far, and therefore it is the one with the greater potential in terms of future research outcomes. Even in this case, the future research should focus in exploring more scenarios where this phenomenon maybe visible. Furthermore, it would be very interesting to carry out an experimental campaign in order to gain a deeper knowledge of the effect that different root architectures may have on the hydrology of the slopes. Although many studies have been carried out on the use of the vegetation to help the slope stability, the aspect related to the contribution given by the rhizosphere still remains quite unknown.

7 LIST OF CAPTIONS FOR FIGURES AND TABLES

8 REFERENCES

Abou Najm, M., Mohtar, R. H., Weiss, J., & Braudeau, E. (2009). Assessing internal stress evolution in unsaturated soils. *Water Resources Research*.

Abtew, W., Newman, S., Pietro, K., & Kosier , T. (1995). Canopy Resistance Studies of Cattalis. *American Society of Agricultural and Biological Engineers, 38*(1), 113-119.

Ahmadi , K., Zarebanadkouki, M., Ahmed , M., Ferrarini, A., Kuzyakov, Y., Kostka, S., & Carminati, A. (2017). Rhizosphere engineering: Innovative improvement of root environment. *Rhizosphere, 3*, 176-184.

Aleotti, P. (2004). A warning system for rainfall-induced shallow failures. *Engineering Geology, 73*, 247-265.

Ali, F. H., & Osman, N. (2008). Shear Strength Of A Soil Containing Vegetation Roots. *Soils and Foundations -Tokyo- 48(4)*, 587-596.

Allen, R. G., Pereira, L. S., Raes, D., & Smith, M. (1998). *Crop evapotranspiration: Guidelines for computing crop waterrequirements. FAO Irrigation and Drainage Paper 56.*

Allen, R., Pereira, L. S., Raes, D., & Smith, M. (1998). *FAO Irrigation and Drainage Paper n.56 Crop Evapotranspiration.*

Amarisiri, A., Shannon, B., & Kodikara, J. (2014). Numerical modelling of desiccation cracking in a restrained. *Canadian Geotechnical Journal*.

Andriola, P., Chirico, G. B., de Falco, M., Di Crescenzo, G., & Santo, A. (2009). A comparison between physically-based models and a semiquantitative methodology for assessing susceptibility to flowsides triggering in pyroclastic deposits of southern Italy. *Geografia Fisica e Dinamica Quaternaria, 32*(2), 213-226.

Arboleda, R. A., & Martinez, M. L. (1996). 1992 lahars in the Pasig- Potrero River system. *Fire and mud: eruptions and lahars of Mount Pinatubo*, 1126.

Aristizabal , E., Velez , J., Martinez , H., & Jaboyedoff , M. (2015). SHIA_Landslide: a distributed conceptual and physically based model to forecast the temporal and spatial occurrence of shallow landslides triggered by rainfall in tropical and mountainous basins. *Landslides, 13*(3), 497-517.

Aristizábal, E. (2013). SHIA _ Landslide: Developing a physically based model to predict shallow landslides triggered by rainfall in tropical environments.

Aubertin , G., Jassogne, L., McNeill, A., & Chittleborough, D. (2007). 3D-visualization and analysis of macro- and meso-porosity of the upper horizons of a sodic, texture-contrast soil. *European Journal of Soil Science, 58*(3), 589-598.

Avila, A. (2004). *Estudio de la retracction y el agrietamiento de arcillas. Aplicacion a la arcilla de Bogota.*

Baroghel-Bouny, V., Mainguy, M., & Coussy, O. (2001). Isothermal drying process in weakly permeable cementitious materials - Assessment of water permeability. *Materials Science of Concrete Special Volume: Ion and Mass Transport in Cement-Based Materials*, 59-80.

Baum, R. L., Godt, J. W., & Savage , W. Z. (2010). Estimating the timing and location of shallow rainfall-induced landslides using a model for transient, unsaturated infiltration. *J. Geophys. Res.- Earth, 115*.

Baum, R. L., Savage, W. Z., & Godt, J. W. (2002). *TRIGRS—A Fortran program for transient rainfall infiltration and gridbased regional slope-stability analysis.* Reston, Virginia: U.S. Geological Survey.

Baum, R., Godt, J., & Savage, W. (2010). Estimating the timing and location of shallow rainfall - induced landslides using a model for transient , unsaturated infiltration. *Journal of Geophysical Research, 118*(3).

Beven, K., & Kirkby, M. (1979). A physically based, variable contributing area model of basin hydrology / Un modèle à base physique de zone d'appel variable de l'hydrologie du bassin versant. *Hydrological Sciences Bulletin, 24*(1), 43-49.

Biot, M. A. (1941). General theory of three-dimensional consoidation. *Journal of Applied Physics, 12*, 155-164.

Bowman, J. (1926). Recent factory experience and experiments in drying terra cotta. *Journal of the American Ceramics Society, 9*(6), 380-91.

Brancaccio L, Cinque A, Russo F, Sgambati D (2000) Le frane del 5–6 maggio 1998 sul gruppo montuoso Pizzo d’Alvano(Campania): osservazioni geomorfologiche sulla loro distribuzione e sulla dinamica delle connesse colate. Quaderni di Geologia Applicata, 1

Caine, N. (1980). The rainfall intensity-duration control of shallow landslides and debris flows. *Geogr Ann A, 62*, 23-27.

Calcaterra, D., Parise, M., Palma, B., & Pelella, L. (2000). The in- fluence of meteoric events in triggering shallow landslides in pyroclastic deposits of Campania, Italy. *Proc. 8th Int. Symp. on Landslides* , *1*, pp. 209-214.

Capparelli, G., & Versace, P. (2014). Analysis of landslide triggering conditions in the Sarno area using a physically based model. *18*(8), 3225-3237.

Clausen, J., & Fish, R. (1994). Successfully drying sanitaryware. Westerville, Ohio: The American CEramic Society.

Clemens, J., Darbyshire, D., & Flinders, J. (2009). Lithos Sources of post-orogenic calcalkaline magmas : The Arrochar and Garabal Hill – Glen Fyne complexes , Scotland. *LITHOS, 112*(3-4), 524-542.

Coussy, O. (2004). *Poromechanics.* West Sussex: Wiley.

Crosta, G. B. (1989). A study of slope movements caused by heavy rainfall in Valtellina (Italy–July 1987). *Proceedings 6th international conference, and field workshop on Landslides ALPS 90*, *79b*, pp. 247-258.

Crozier, M. J. (1986). Landslides: causes, consequences and environment. *London: Croom Helm*, (p. 252).

De Vita, P., & Piscopo, V. (2002). Influences of hydrological and hydrogeological conditions on debris flows in peri-vesuvian hillslopes. *Natural Hazards and Earth System Sciences, 2*, 27-35.

Decagon Devices. (2014). WP4C Dew point Potentiameter.

Di Crescenzo, G., & Santo, A. (1999). Analisi geomorfologica delle frane da scorrimento-colata rapida in depositi piroclastici della penisola sorrentina (Campania). *Geografia Fisica e Dinamica Quaternaria, 22*, 57-72.

Di Crescenzo, G., & Santo, A. (2005). Debris slides-rapid earth flows in the carbonate massifs of the Campania region (Southern Italy): morphological and morphometric data for evaluating triggering susceptibility. *Geomorphology, 66*(1-4), 255-276.

Di Crescenzo, G., De Falco, M., Iervolino, V. E., Rinaldi, S., Santangelo, N., & Santo, A. (2008). Proposal of a new semiquantitative methodology for flowsides triggering susceptibility assessment in the carbonate slope contexts of Campania(Southern Italy). *Italian Journal of Engineering Geology and Environment*, 61-79.

Diamond, S. (1970). Pore size distributions in clay. *Clay and clay minerals, 18*, 7-23.

Duursma, R. A., Kolari , P., Peramaki , M., Nikinmaa, E., Hari, P., Delzon, S., . . . Makela, A. (2008). Predicting the decline in daily maximum transpiration rate of two pine stands during drought based on constant minimum leaf water potential and plant hydraulic conductance. *Tree Physiology, 28*, 265–276.

Evangelista, A., Nicotera, M. V., & Scotto di Santolo, A. (2005). Valutazione del ruolo degli strati pomicei nell'innesco dei fenomeni di colate di fango. *Atti Conegno Nazionale "La mitigazione del rischio di colate di fango a Sarno e negli altri COmuni colpiti dagli eventi del maggio 1998"*, 125-140.

Ewen , B., & Parkin, G. (2000). SHETRAN : DISTRIBUTED RIVER BASIN FLOW MODELING SYSTEM. *JOURNAL OF HYDROLOGIC ENGINEERING* , 250-258.

Fan, C. C., & Su, C. F. (2008). Role of roots in the shear strength of root-reinforced soils with high moisture content. . *Ecological Engineering 33 (2)*, 157-166.

Feddes, R. A., Kowalik, P. J., & Zaradny, H. (1978). Simulation of field water use and crop yield. *Monographs. Pudoc. Wageningen.*, 189.

Ford, R. (1986). *Ceramics drying.* Oxford: Pergamon.

Fraser, H. (1986). *Ceramic faults and their remedies.* London: A & C Black.

Freeze, R.A. and Cherry, J.A. (1979) *Groundwater*. Prentice-Hall, Inc., Englewood Cliffs.

Fredlund, D. G., & Rahardjo, H. (1993). *Soil Mechanics for Unsaturated Soils.* John Wiley & Sons.

Gaiser, R. N. (1952). Root channels and roots in forest soils. *Soil Science Society of America Proceedings, 16*, 62-65.

Ghestem , M., Sidle , R., & Stokes, A. (2011). The Influence of Plant Root Systems on Subsurface Flow: Implications for Slope Stability. *BioScience, 61*(11), 869-879.

Ghestem, M., Cao, K., Ma, W., Rowe, N., Leclerc, R., Gadenne, C., & Stokes, A. (2014). A framework for identifying plant species to be used as 'ecological engineers' for fixing soil on unstable slopes. *PLoS ONE vol: 9 (8)*.

Ghestem, M., Sidle, R., & Stokes, A. (2011). The Influence of Plant Root Systems on Subsurface Flow: Implications for Slope Stability. *BioScience vol: 61 (11)* , 869-879 .

Ghestem, M., Veylon, G., Bernard, A., Vanel, Q., & Stokes, A. (2014). Influence of plant root system morphology and architectural traits on soil shear resistance. *Plant and Soil, 377*(1-2), 43-61.

Godt, J., Baum, R., Savage, W., Salciarini, D., Schulz, W., & Harp, E. (2008). Transient deterministic shallow landslide modeling: Requirements for susceptibility and hazard assessments in a GIS framework. *Engineering Geology, Vol. 102*, 214-226.

Gonzalez-Ollauri , A., & Mickovski , S. (2017). Shallow landslides as drivers for slope ecosystem evolution and biophysical diversity. *Landslides*, 1-16.

Govi, M., & Sorzana, P. (1980). Landslide susceptibility as function of critical rainfall amount in Piedmont basin (Northwestern Italy). *Studia Geomorphologica Carpatho- Balcanica, 14*, 43-60.

Govi, M., Mortara, G., & Sorzana, P. (1985). Eventi idrologici e frane. *Geologia Applicata Ingegneria, 20*(2), 359-375.

Gur'yanov, A. I., & Zakharov, A. I. (2007). Crack formation in a clay semifinished product. *Glass and Ceramics, 64*, 58-62.

Guzzetti, F., Peruccacci, S., Rossi, M., & Stark, C. P. (2007). *Rainfall thresholds for the initiation of landslides in central and southern europe.*

Haigh, S. K., Vardanega, P. J., & Bolton, M. D. (2013). The plastic limit of clays. *Geotechnique, LXIII Number 6*, 435-440.

Heald, A., & Parsons, J. (2005). *Scottish road network landslides study.* Scottish government.

Heyerdahl, H., Harbitz, C. B., Domaas, U., Sandersen, F., Tronstad, K., Nowacki, F., . . . Hernandez, W. (2003). Rainfall induced lahars in volcanic debris in Nicaragua and El Salvador: Practical mitigation. *Proc. Int. Conf. on Fast Slope Movements – Prediction and Prevention for risk Mitigation*, (pp. 275-282).

Kim, S. K., Hong, W. P., & Kim, Y. M. (1991). Prediction of rainfall- triggered landslides in Korea. *Landslides, 2*, 989-994.

Lanni, C., Rigon, R., A., T., & Cordano, A. (2009). Analysis of the effect of normal and lateral subsurface water flow on the triggering of shallow landslides with a distributed hydrological model. *Int. Conf. on Landslide processes: from geomorphologic mapping to dynamic modelling.* Strasbourg, France.

Lu, N., & Likos, W. J. (2004). *Unsaturated soil mechanics.* Hoboken, N.J.: John WIley & Sons.

Marinho, F. A., Take, A., & Tarantino, A. (2008). Tensiometric and axis translation techniques for suction measurement. *Geotechnical and Geological Engineering, 26*(6), 615-631.

Marshall, T. (1959). Relations between water and soil. *Tech. comm. 50. Commonwealth Agricultural Bureau.* Farnham Royal, UK.

Mcmillan, P., Brown, D. J., & Winter, M. (2005). *SCOTTISH ROAD NETWORK LANDSLIDES STUDY.* Scottish Government.

McNear, D. (2013). The Rhizosphere - Roots , Soil and Everything In Between Meeting the Global Challenge of Sustainable Food , Fuel and Fiber Production. *Nature Education Knowledge, 4*(3), 1-15 .

Mitchell, J. K. (1993). *Fundamentals of Soil Behavior.* New York: Wiley Inter-Science.

Montrasio, L., & Valentino, R. (2008). System Sciences A model for triggering mechanisms of shallow landslides. *Natural Hazards and Earth System Sciences, 8*, 1149-1159.

Mualem, Y. (1976). A new model for predicting the hydraulic conductivity of unsaturated porous media. *Water Resources Research, 12*(3), 513-522.

Nicotera, M. V., Papa, R., & Urciuoli, G. (2010). An Experimental Technique for Determining the Hydraulic Properties of Unsaturated Pyroclastic Soils. *Geotechnical Testing Journal, 33*(5), 1-22.

Nicotera, M. V., Papa, R., & Urciuoli, G. (2015). The hydro-mechanical behaviour of unsaturated pyroclastic soils: An experimental investigation. *Engineering Geology, 195*, 70-84.

Noguchi, S., Tsuboyama, Y., Sidle, R., & Hosoda, I. (1997b). Spatially distributed morphological characteristics of macropores in forest soils of Hitachi Ohta experimental watershed, Japan. *Journal of Forest Research, 2*, 207–215.

Pagano, L., Picarelli, L., Rianna, G., & Urciuoli, G. (2010). A simple numerical procedure for timely prediction of precipitation-induced landslides in unsaturated pyroclastic soils. *Landslides, 7*(3), 273-289.

Papa, M. N., Medina, V., Ciervo, F., & Bateman, A. (2013). Derivation of critical rainfall thresholds for shallow landslides as a tool for debris flow early warning systems. *Hydrol. Earth Syst. Sci., 17*, 4095-4107.

Pedrotti, M. (2016). An experimental investigation on the micromechanics of non-active clays in saturated and partially-saturated states. *Ph.D. Thesis, University of Strathclyde, Glasgow, Scotland, UK.*

Pierson, T. C. (1983). Soil pipes and slope stability. *Quarterly Journal of Engineering Geology and Hydrogeology, 16*, 1-11.

Pirone, M., Papa, R., Nicotera, M. V., & Urciuoli, G. (2015). In situ monitoring of the groundwater field in an unsaturated pyroclastic slope for slope stability evaluation. *Landslides, 12*, 259-276.

Pirone, M., Papa, R., Nicotera, M. V., & Urciuoli, G. (2015). Soil water balance in an unsaturated pyroclastic slope for evaluation of soil hydraulic behaviour and bounday conditions. *Journal of Hydrology, 528*, 63-83.

Pirone, M., Papa, R., Nicotera, M. V., & Urciuoli, G. (2016). Hydraulic behaviour of unsaturated pyroclastic soil observed at different scales. *Procedia Engineering, 158*, 182-187.

Qiu, C., Esaki, Æ., Xie , Æ., Mitani, Y., & Wang, Æ. (2007). Spatio-temporal estimation of shallow landslide hazard triggered by rainfall using a three-dimensional model. *Environmental Geology, 52*(8), 1569-1579.

Reed, J. S. (1988). *Introduction to the Principles of Ceramic Processing.* New York: John Wiley & Sons.

Savage, W. Z., Godt, J. W., & Baum, R. L. (2004). Modeling time-dependent areal slope stability. *Landslides: Evaluation and Stabilization*, 27-36.

Scherer, G. W. (1990). Theory of Drying. *Journal of the American Ceramics Society, 73*(1), 3-14.

Shahabi , H., & Hashim, M. (2015). Landslide susceptibility mapping using GIS-based statistical models and Remote sensing data in tropical environment. *Scientific Reports 5*.

Sidle, R. (2015). Understanding hydrogeomorphic controls on landslide initiation. *4th Italian Worksop on Landslides.* Naples, Italy.

Sidle, R., Noguchi , S., Tsuboyama, Y., & Laursen , K. (2001). A conceptual model of preferential flow systems in forested hillslopess: Evidence of selforganization. *Hydrological Processes , 15*, 1675–1692.

Sidle, R., & Bogaard, T. (2016). Dynamic earth system and ecological controls of rainfall-initiated landslides. *Earth-Science Reviews, 159*, 275-291.

Simoni, S., Zanotti, F., Bertoldi, G., & Rigon, R. (2008). Modelling the probability of occurrence of shallow landslides and channelized debris flows using GEOtop-FS . *Hydrological Processes, 22*(4), 532-545.

Sokolov, P. V., & Gak, B. N. (1959). Accelerating the drying of sanitary ware. *Glass Ceramics, 16*(10), 561-565.

Sorbino, G., & Nicotera, M. V. (2013). Unsaturated soil mechanics in rainfall-induced flow landslides. *Engineering Geology, 165*, 105-132.

Take, W. A., & Bolton, M. D. (2003). Tensiometer saturation and the reliable measurement of soil suction. *Geotechnique, 53*(2), 159-172.

Tarafdar, J., & Jungk, A. (1987). Phosphatase activity in the rhizosphere and its relation to the depletion of soil organic phosphorus. *Biology and Fertility of Soils, 3*(4), 199-204.

Tarantino , A., & El Mountassir, G. (2013). Making unsaturated soil mechanics accessible for engineers: Preliminary hydraulic- mechanical characterisatin and stabbility assessment. *Engineering Geology, 165*, 89-104.

Tarantino, A. (2004). Panel report: Direct measurement of soil water tension. *Proceedings 3rd International Conference on Unsaturated Soils*, pp. 1005-1017.

Tarantino, A., & De Col, E. (2008). Compaction behaviour of clay. *Géotechnique, 58*(3), 199-213.

Tarantino, A., & Mongiovi, L. (2002). Design and construction of a tensiometer for direct measurement of matric suction. *Proceedings 3rd International Conference on Unsaturated Soils*, pp. 319-324.

Tarantino, A., & Mongiovi, L. (2003). Calibration of tensiometer for direct measurement of matric suction. *Geotechnique, 53*, 137-141.

Tarantino, A., & Mongiovi', L. (2003). Calibration of tensiometer for direct measurement of matric suction. *Géotechnique, 53*(1), 137-141 .

Tarantino, A., Sacchet, A., Dal Maschio, R., & Francescon, F. (2010). A hydro-mechanical approach to model shrinkage of air-dried green bodies. *Journal of the American Ceramic Society, 93*(3), 662-670.

Terlien, M. T. (1998). The determination of statistical and de- terministic hydrological landslide-triggering thresholds. *Environmental Geology, 35*(2-3), 124-130.

Van Asch, T., Buma, J., & Van Beek, L. (1999). A view on some hydrological triggering systems in landslides. *Geomorphology, 30*(1-2), 25-32.

van Genuchten, M. (1980). A closed-form equation for predicting the hydraulic conductivity of unsaturated soils. *Soil Science Society of America Journal*(44), 892-898.

Varnes, D. (1984). IAEG-Commission on Landslides and Others Mass Movements on Slopes, Landslide hazard zonation: a review of principles and practice. Darantiere, Paris.

Vymazal, J. (2011). Plants used in constructed wetlands with horizontal subsurface flow: A review. *Hydrobiologia, 674*(1), 133-156.

Wang, L.-J., Guo, M., Sawada, K., Lin, J., & Zhang, J. (2015). Landslide susceptibility mapping in Mizunami City, Japan: A comparison between logistic regression, bivariate statistical analysis and multivariate adaptive regression spline models. *Catena, Vol.135*, 271-282.

Whipkey, R. Z. (1969). Storm runoff from forested catchments by subsurface routes. *International Association of Hydrological Sciences Publication , 11*, 773-779.

White, I. D., Mottershead, D. N., & Harrison, J. J. (1996). *Environmental systems, 2nd edn.*, (p. 616). Chapman & Hall, London.

Winter, M., & Corby, A. (2012). *A83 Rest and be Thankful : Ecological and Related Landslide Mitigation Options.* Trasport Scotland.

Winter, M., Macgregor, F., Harrison, M., & Shackman, L. (2013). *Landslide hazard and risk assessment on the Scottish road network.* Trasport Scotland.

Xiao , H., Huang, J., Ma, Q., Wan , J., Li, L., Peng, Q., & Rezaeimalek, S. (2017). Experimental study on the soil mixture to promote vegetation for slope protection and landslide prevention. *Landslides, 14*(1), 287-297.

Yang, X., Varha, T., Liu, C., & Scheibe, T. (2017). What can we learn from in-soil imaging of a live plant: X-ray Computed Tomography and 3D numerical simulation of root-soil system. *Rhizosphere, 3*, 259-262 .

Zhang, C. B., Chen, L., Liu, Y. P., Ji, X. D., & Liu, X. P. (2010). Triaxial Compression Test of Soil Root COmposites to evaluate influence of roots on soil shear strength. *Ecological Engineering 36 (1)*, 19-26.

Zhu, Y., & Leak, N. (2017). *Drying processes - The balance between efficiency and product quality.* Lucideon.